Studies of Added Value Products from Agricultural Wastes through Hydrothermal Method

STUDIES OF ADDED VALUE PRODUCTS FROM AGRICULTURAL WASTES THROUGH HYDROTHERMAL METHOD

Kyushu Institute of Technology

Graduate School of Life Sciences and Systems Engineering

Department of Biological Functions and Engineering

STUDIES OF ADDED VALUE PRODUCTS FROM AGRICULTURAL WASTES THROUGH HYDROTHERMAL METHOD

Name : Izzudin Ibrahim

Student Number : 18899029

Supervisor : Assoc. Prof. Dr. Yoshito Andou

Kyushu Institute of Technology

Graduate School of Life Sciences and Systems Engineering

Department of Biological Functions and Engineering

ACKNOWLEDGEMENT

Alhamdulillah, with the blessings of Allah S.W.T., I manage to complete my doctorate study here at Kyushu Institute of Technology. Here, I would like to thank everyone who had helped me in any way during my study period.

First of all, I would like to thank my main supervisor, Assoc. Prof. Dr. Yoshito Andou for his guidance during the period of my study. His advice, critics, and encouragement throughout the years had pushed me through thick and thin in completing the research and finishing up the thesis presented here.

I would like to express my heartfelt gratitude to my fellow Ando Lab members, especially Dr. Safarul Mustapha, Alvin Lim Teik Zheng, Kawano Tessei for their unending support and help, either in terms of my doctoral studies or in my life personally. Not to forget, Mrs. Fujiwara, Mr. Sakamoto, and Kyutech staff for their assistance in the lab and during my stay here in Japan. Thank you also to the Malaysian community and the Muslim community in Kitakyushu in general for their social support and help. Special thanks to Assoc. Prof Toshiki Tsubota and Prof Dato' Dr. Mohd Ali Hassan for their advice and equipment provided for the analysis of my samples.

Lastly, special thanks to my lovely wife, Ruqayyah Masran for her endless support and help. Thank you very much for being there, from far and in person. Love you 3000.

ABSTRACT

The oil palm industry's steady growth over the past decade has resulted in the increasing production of waste solid and liquid biomass such as oil palm frond (OPF) and palm oil mill effluent (POME). Current disposal practices are not environmentally friendly and undermine the vast potential of biomass as a renewable resource. Due to this problem, research regarding the utilization and valorization of oil palm biomass as raw material for the production of value-added products has gained interest. Many new methods and processes to treat biomass and produce materials such as cellulose-based materials, biochar, activated carbon, and biofuels have been reported, but adoption by the industry has been lackluster. There has been a figurative wall that inhibits implementation and adoption, far beyond bench and pilot scale. Among the factors that inhibit adoption include complicated processes that require specialized equipment and chemicals, multiple pretreatment steps that increase the time required, and waste that needs to be disposed of, besides related increased cost to the industry. The research community must develop simpler, appropriate technology in utilizing oil palm biomass that can be easily adopted by the industry.

This study presents several methods to try to solve the problems stated above. By utilizing the hydrothermal process, biomass (oil palm frond) and its derivative (oil palm empty fruit bunch biochar) were treated using nitric acid as oxidizing agent to remove lignin and in the case of biochar, to improve its performance via additional surface functional groups. For the hydrothermal lignin removal process, treated oil palm frond (OPF) lignin content decreased by 86.5% after 30 min of treatment at 120°C. Cellulose yield was 68.2% which is comparable to other previously reported literature. Further analysis using TGA, FTIR, and XRD concluded that hydrothermally treated OPF has similar thermal stability, surface chemical property, and crystallinity to commercially

available cellulose products (microcrystalline cellulose). The process was also applied to oil palm empty fruit bunch (OPEFB) and Matake bamboo without any modification and pretreatment. Both biomass shows similar lignin reduction and properties such as treated OPF which showed that the process can be applied to other types of biomass without significant parameter modification.

Hydrothermally treated biomass still showed a significant amount of hemicellulose which can be problematic especially in the production of cellulose-based composites and fibers. Removal of hemicellulose via superheated steam (SHS) treatment is proposed due to the excellent hemicellulose removal efficiency reported in the literature. It was found that the process produced biomass that can dissolve in sodium hydroxide (NaOH) solution at room temperature. This property was novel since the dissolution of cellulose in alkali solution usually requires additives such as urea and thiourea, and sub-zero temperature. NaOH-soluble biomass was analyzed via TGA, FTIR, and XRD which showed similar physical and chemical characteristics as normal cellulose fiber (MCC). 13C cross-polarization magic angle spinning (CPMAS) nuclear magnetic resonance (NMR) spectroscopy analysis suggested that the reduction in intra-chain and inter-sheet hydrogen bonding strength is the contributing factor in the increased solubility of cellulose after SHS treatment.

Besides direct biomass treatment, the hydrothermal process was also applied to biochar from oil palm biomass (OPEFB) to improve its performance in adsorbing dye and heavy metals. The process successfully increased the amount of surface functional groups without significant change in the surface morphology based on SEM, BET surface area, FTIR, and EDX analysis. Adsorption isotherm experiments suggested that the adsorption process occurred following the Langmuir isotherm model and pseudo-second-order kinetic model. Intra-particle diffusion model analysis

suggested multiple stages of adsorption. Adsorption performance of functionalized biochar in removing dye and heavy metal from aqueous solution showed improved performance, with almost 7x increase in methylene blue adsorption capacity, and up to 6x increase in removal percentage for heavy metal adsorption. This result suggested that biochar performance can be improved through functionalization, and the process can be done using the hydrothermal method.

The results presented in this thesis provide new methods and processes that can be easily implemented in the industry due to its simplicity, lower usage of chemicals, and utilizing available resources in the palm oil mill industry such as hydrothermal treatment (fresh fruit bunch sterilizer) and steam from the boiler. This result can help promotes better technology for the oil palm industry.

TABLE OF CONTENTS

LIST OF FIGURES

Figure **Page**

LIST OF TABLES

Table **Page**

LIST OF ABBREVIATIONS

CPO	Crude palm oil
POME	Palm oil mill effluent
OPMF	Oil palm mesocarp fiber
OPEFB	Oil palm empty fruit bunch
OPF	Oil palm fronds
OPT	Oil palm trunks
SHS	Superheated steam
MPOB	Malaysian Palm Oil Board
FFA	Free fatty acid
POMFD	Palm oil mill final discharge
PKS	Palm kernel shell
OPDC	Oil palm decanter cake
FFB	Fresh fruit bunch
$NaClO_2$	Sodium chlorite
KOH	Potassium hydroxide
MCC	Microcrystalline cellulose
CNF	Cellulose nanofiber
NaOH	Sodium hydroxide
H_2O_2	Hydrogen peroxide
HCl	Hydrochloric acid
NH_4OH	Ammonium hydroxide
min	minute
SEM	Scanning electron microscopy
FTIR	Fourier transform infrared
XRD	X-ray power diffraction
TGA	Thermogravimetric analysis
hr	hour
TAPPI	Technical Association of Pulp and Paper Industry
ATR	Attenuated total reflectance
CrI	Segal crystallinity index

TG/DTG	Thermogravimetric/differential thermogravimetric
HHV	higher heating value
MB	methylene blue
HNO_3	nitric acid

CHAPTER 1

INTRODUCTION

1.1 Introduction

The use of biomass as raw material for many fields has been purported to be the solution to the ongoing resources crisis faced by humanity. Being inherently renewable and natural, the use of biomass to substitute non-renewable sources such as fossil fuels is its main advantage. Industries such as food, construction, and commodities such as palm oil, corn, and many plant-based products produce an abundant amount of biomass annually. These resources are considered waste for a long time, but new interest by the scientific and industrial research community to use biomass as a new source of raw material in the production of bio-based products has ignited, as the world faces environmental crisis and need a better, more sustainable way of consumption.

Biomass can be used in many ways. Humans have been using biomass in the form of waste material as construction material, source of nutrition, fuel, and many more. But usually, biomass is used directly as it is. While this process is simple and easy to implement, this method of recycling biomass resources directly reduces its potential and possible uses. Lignocellulosic biomass such as straws, fibers, hays, wood chips, fruit seeds and pits, and plant cuttings have been traditionally used as a quick and cheap source of nutrients in agriculture. Resulting waste from harvesting and scheduled maintenance such as pruning was directly recycled into the plantations as crude compost. Excess waste is either piled up in the plantations to decompose slowly or dumped in landfills. Biomass resources are wasted and not use to their full potential due to the lack of appropriate technology to properly utilize them.

One of the major agricultural sectors in Malaysia is the palm oil industry. Malaysia is one of the largest crude palm oil (CPO) producers in the world, second only to Indonesia [1,2]. While palm oil production has a very high production rate and its global production has increased annually, the crop has a bad reputation due to unsustainable practices in the mills and plantations. Reported mass deforestation and other unsustainable practices have stained the industry's reputation and started to reduce palm oil acceptance in the world economy [3]. The palm oil industry needs to improve its operation sustainability via more environmentally friendly practices in its mills and plantation, and also adopting new, more sustainable practices in terms of waste biomass management.

Research related to the oil palm industry sustainability has been the main theme in Malaysia due to the importance of the industry to the Malaysian economy. Popular research interests include the production of biofuels and bioplastics from fermentation using palm oil mill effluent (POME), composting solid biomass such as oil palm mesocarp fiber (OPMF), oil palm empty fruit bunch (OPEFB), oil palm fronds (OPF), and oil palm trunks (OPT), recycling and utilization of biomass into products such as fiberboards and biocomposites and carbonization, pyrolyzation, gasification and other heat treatment on oil palm biomass to produce biochar, activated carbon, bioliquids, and syngas. **Figure 1.1** shows the biomass produced in the palm oil industry and related processes.

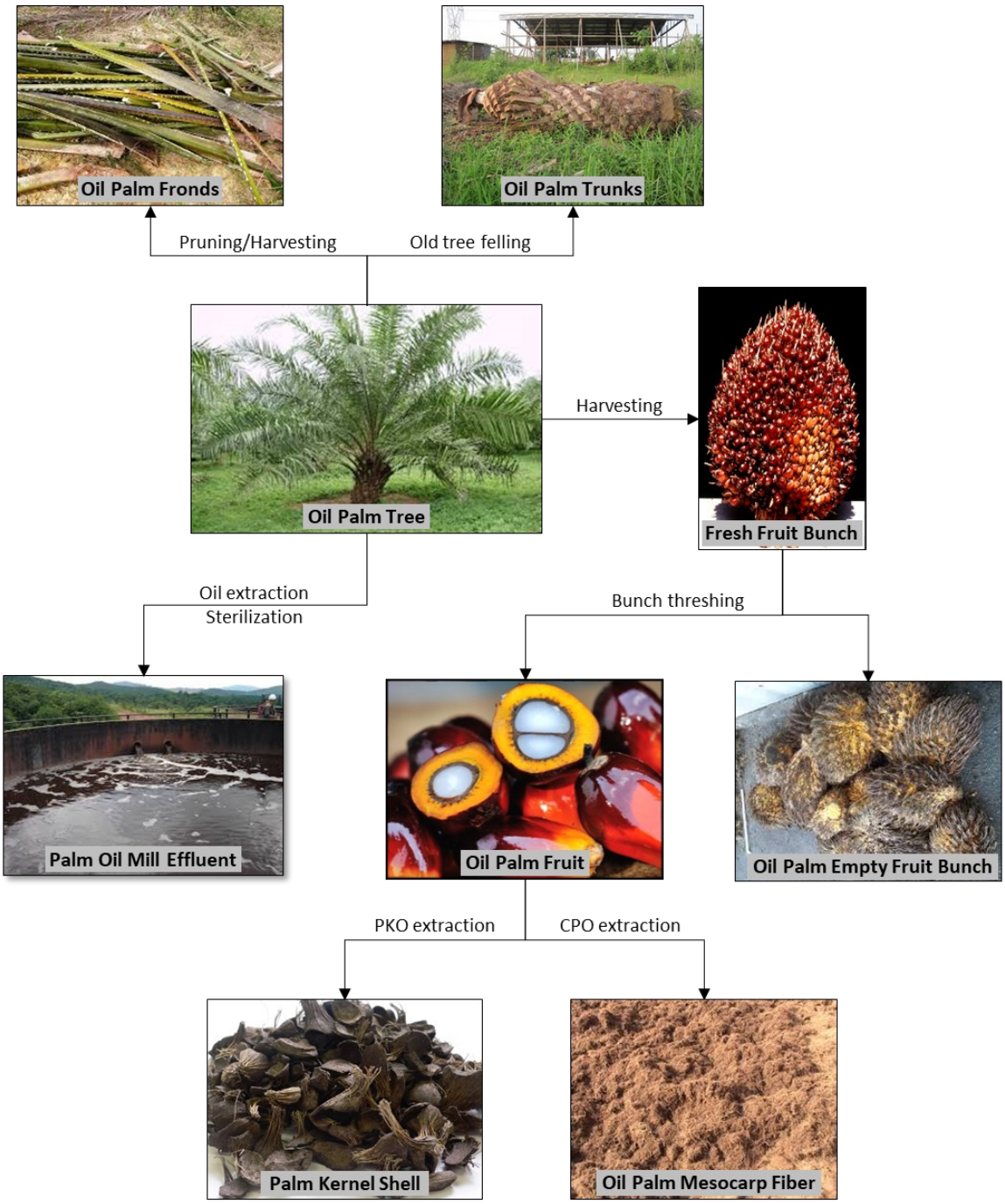

Figure 1.1: Biomass produced in the palm oil industry

Several reviews condensing all these research interests have been published, showing the extensive research being done in this field [4,5]. While myriads of studies and publications suggest a strong interest in the development of technologies for the palm oil industry, the rate of adoption and implementation was very low. Even through government incentives such as grants and enactment of laws to promote adoption, the industry still lags in implementation [6]. This problem can be attributed to high technological barrier, high capital expense due to specialized equipment and chemicals needed, and low revenue potential.

Composting of solid biomass produced in the mill or plantation such as is very popular due to its very simple method with the low technological requirement. Studies on quicker composting methods, the use of waste sludge from palm oil mills treatment ponds as a source of microbes, and new composter design were some of the new development reported in the field [7–9]. Some of these technologies are already being implemented in the industry. A palm oil mill in Malaysia has launched a biocompost plant in 2018 which produces compost from OPEFB and waste sludge from their mill. The composting process was developed with a local university and adopted methods from several published research [10]. This shows that the adoption of new technology is possible, given that the technology is simple, uses current technology with easy-to-understand process guidelines, and also produces value-added products that can help the industry recover their capital expenses and even gained more profit in the future. These are the important points that need to be covered in developing appropriate technology that will results in adoption by the palm oil industry.

This research focused on developing simple and appropriate technology for the palm oil industry that can be used to improve the industry sustainability, and also produce value-added products. The processes proposed in this research are relatively simple compared to other research in the literature, utilizing one or two-step processes. The processes also use equipment and resources already available in the palm oil mill such as fresh fruit bunch sterilizers and cheap and easy to source chemicals such as nitric acid and sodium hydroxide. The processes also produce value-added products and raw material for further processing which can be sold at a higher price compared to the original biomass, which can help recover capital expenses and provide extra revenue.

The first process proposed is a simple hydrothermal lignin removal process to remove lignin from not only oil palm biomass but also other biomass. The process produces biomass with relatively low lignin content, with high cellulose yield which is important for processes such as saccharification and fermentation where lignin recalcitrance is a big hurdle. The resulting treated biomass can also be further treated to produce higher-value products such as cellulose nanofiber. The second process proposed is a method of producing cellulose from biomass that can be dissolved in sodium hydroxide at room temperature using superheated steam (SHS) treatment. This process utilized treated biomass from the first process and uses only water as its reagent. The resulting biomass was able to dissolve in sodium hydroxide solution which can open numerous avenues for the use of cellulose. The third process focused on the functionalization of oil palm biomass and other carbon material via hydrothermal treatment using nitric acid. The resulting biochar performance improved significantly in removing dye and heavy metal from aqueous solution while maintaining its physical properties such as

surface area. This can help the industry provide a service to other industry, and also produce bioadsorbents that can be sold at higher prices.

1.2 Objectives

The objectives of this study include:

1. To develop a new, simpler, and appropriate method to remove up to 90% lignin from oil palm fronds using hydrothermal method and nitric acid, and determine the efficiency of the lignin removal process from biomass in terms of lignin removal percent, cellulose yield, purity, and crystallinity.
2. To determine the feasibility of the newly developed hydrothermal lignin removal process in removing lignin from other types of biomass such as oil palm empty fruit bunch and Matake bamboo.
3. To develop a new method of producing cellulose that can be easily dissolved in NaOH solution using combined superheated steam and hydrothermal treatment process and determine the feasibility of combined treatment in producing alkali-soluble cellulose on other types of biomass such as Matake bamboo.
4. To develop a new, simpler, and appropriate method of biochar surface functionalization to increase oxygen-containing surface functional groups using hydrothermal method and nitric acid as functionalizing agent, and determine the process efficiency in terms of increased surface functional groups and adsorption performance.
5. To determine the applicability of developed hydrothermal functionalization method on biochar from other biomass and commercially available activated carbon.

CHAPTER 2

LITERATURE REVIEW

2.1 Biomass

Biomass has many definitions depending on the context of the discussion at hand. Encyclopedia of Ecology refers to biomass as “mass of living organisms, including plants, animals, and microorganisms, or, from a biochemical perspective, cellulose, lignin, sugars, fats, and proteins.” and usually reported as dry mass per unit area (g/m^2 or Mg/ha)[11]. This quantity when measured over a length of time is also called the productivity of an organism [12]. While the term technically only refers to a living organism's dry weight, it has been widely used to represent organic material that comes from plants and animals. In sustainable related studies, the term biomass usually refers to renewable waste biomass produced by the industry, especially agriculture. This includes straws, fruit peel, pits and seeds, bagasse, fibers, shells leaves, and many more. Currently, waste biomass is mainly used as a fuel source, with about 10-14% of world waste biomass contribute to the world energy supply [13].

2.2 World production and usage

Billion-Ton Study published by the United States Department of Energy divides biomass resources into 3 categories; primary forestland resources, primary agricultural resources and secondary residues, and waste resources. Primary forestland resources include biomass produced in the forestland industry such as logging and wood milling. This comprises fuel wood, logging residues, thinning, and other removal residues. Primary agricultural resources encompass biomass produced as main and by-product of agricultural activities such as grain crops (paddy, wheat,

malt, etc.), oil crops (rapeseed, soybean, oil palm, rapeseed, corn, etc.), woody crops, energy crops, perennial grasses, and crop residues. The third category includes pulping liquors, mill residues, crop processing residues, waste oil and greases, animal manures, and urban wood wastes [14].

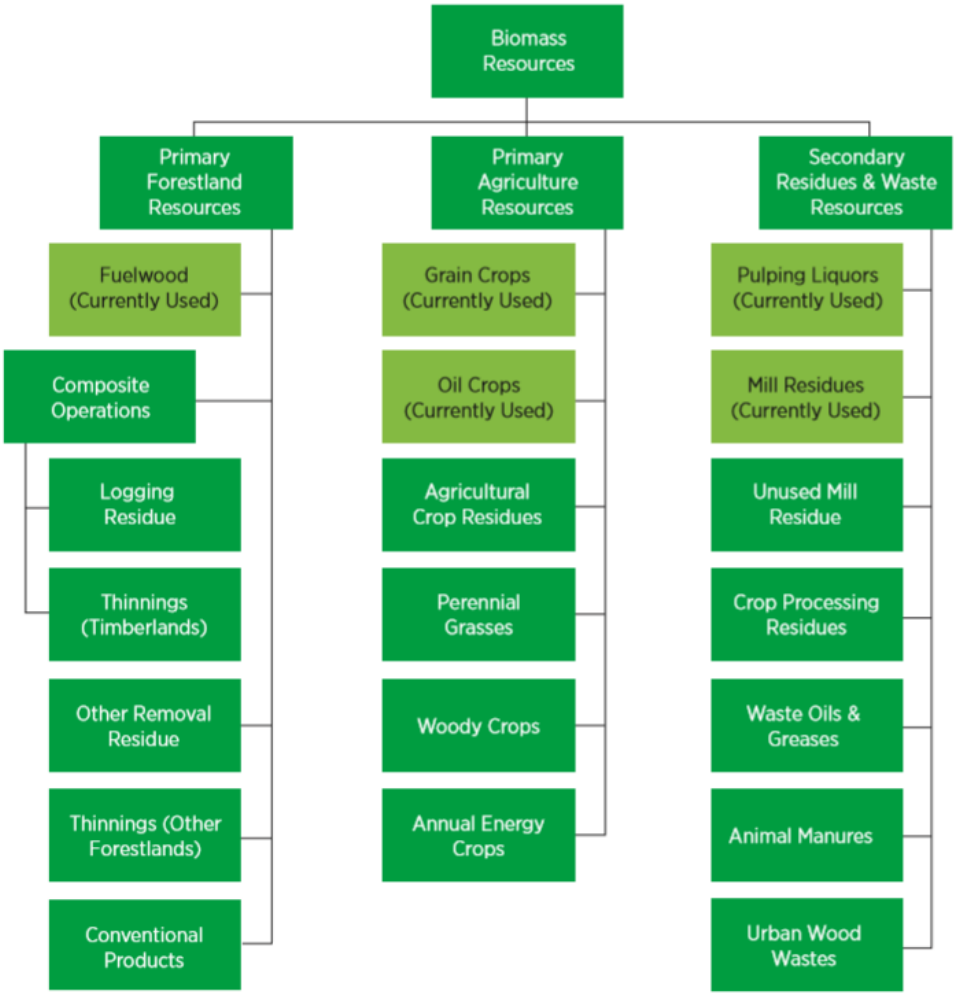

Figure 2.1: Biomass resources categorization (Adapted from Billion-Ton Study Report by United States Department of Energy, 2011 [15])

While biomass has been widely used throughout the world, the majority of waste biomass produced was discarded annually. Biomass is being used primarily as a source of fuel through direct combustion or conversion of biomass into a usable form of biofuels such as biogas or ethanol. Even though the amount of biomass produced in the world increases every year, the share of biomass used even as a source of energy has remained constant at about 17% since the start of the century [16]. Intensive usage of biomass as fuel via burning promotes deforestation, pollution, and rapid decrease of world biodiversity [17].

2.3 Oil palm industry and its biomass

Oil palm (*Elaeis guineensis*) or commonly known as African palm oil is a species of palm tree grown to produce palm oil. Other oil-producing palm species usually planted as crops are *Elaeis oleifera* and *Attalea maripa*. The species was originated from West Africa and imported over to the east between the 14^{th} and 17^{th} century [18]. The tree of the palm oil plant is single-stemmed, and at maturity can grow up to 20 m in length. It produces clustered flowers in a form of bunches, which later pollinated and form oil palm fruit, the main source of palm oil. It takes about 5-6 months for the oil palm fruit to fully mature [19]. The fruit comprises several layers; the outer skin called the exocarp, an oily pulp layer that contains the palm oil called mesocarp, a hard shell called endocarp or palm kernel shell, and lastly the palm kernel that contain palm kernel oil. The variety usually planted was the *tenera* variant, which is the hybrid of the variant *dura* and *pisifera* [20]. The *dura* variant fruit has a thick endocarp which corresponds to high palm kernel oil yield, while the *pisifera* variant fruit has a thick mesocarp which results in high crude palm oil yield [21] The *tenera* trait has the desirable trait of a palm oil fruit which is thick fleshy mesocarp, thin palm kernel shell and large kernel that can produce the maximum amount of oil [19].

Since oil palm is a tropical plant that can thrive in humid weather conditions. It especially flourishes in the area in between 10° north latitude and 10° south latitude, which covers most equatorial countries such as Malaysia and Indonesia, West African countries such as Cameroon, Côte d'Ivoire, Ghana, Liberia, Nigeria, Sierra Leone, Togo, and into the equatorial region of Angola and the Congo [22]. Since oil palm was first brought to Java in the early 20th century, it has outgrown its original purpose as ornamental plants to be the largest agricultural component of the Malaysian economy.

Malaysia is the second largest exporter of CPO in the world, with 19.14 million tonnes of CPO produced in 2020. The oil palm plantations cover 5.87 million hectares of land with fresh fruit bunch production of 16.73 tonnes per hectare as reported by the Malaysian Palm Oil Board (MPOB) [23]. Palm oil export has been steadily increasing worldwide, due to oil palm high oil yield per unit hectare of land planted compared to other oil crops such as corn, rapeseed, sunflower, and soybean. **Figure 2.2** shows the oil yield per hectare of major oil crops in the world.

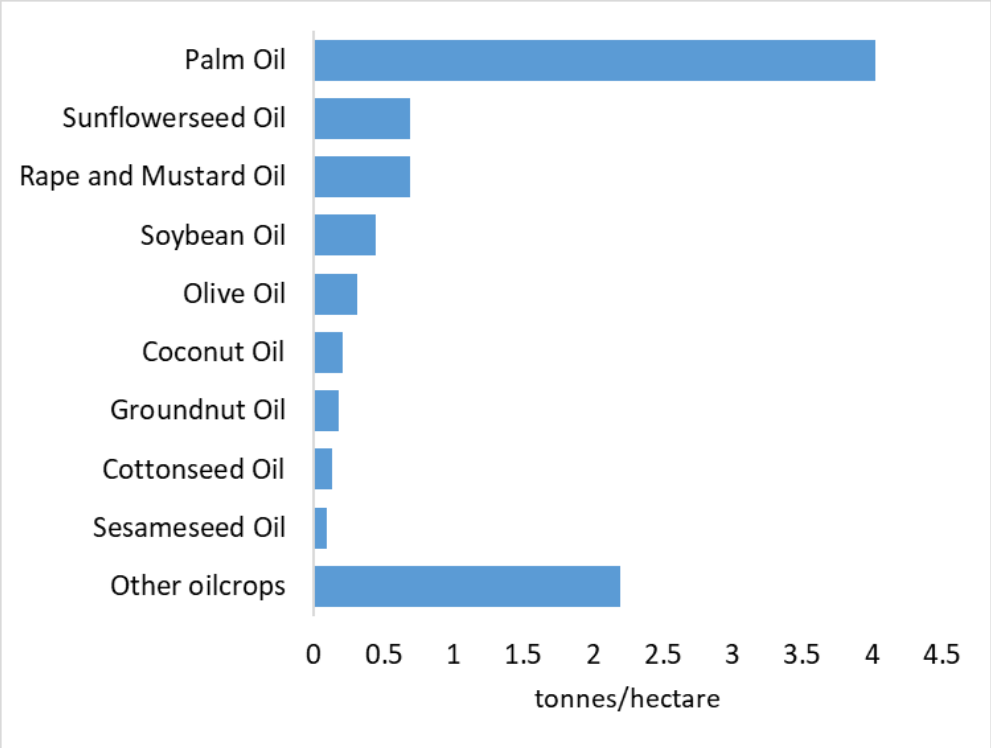

Figure 2.2: Oil crop yield per unit hectare [24]

The high production rate of palm oil trees and the development of better oil extraction technology has enticed the industry to further increase the opening of new plantations, **Figure 2.3** shows the growth of oil palm plantation in Malaysia and estimated plantation area in 2030 based on data reported by the National Biomass Strategy report. The estimated 2030 plantation area was calculated based on the historical increase of plantation area by 1% every year.

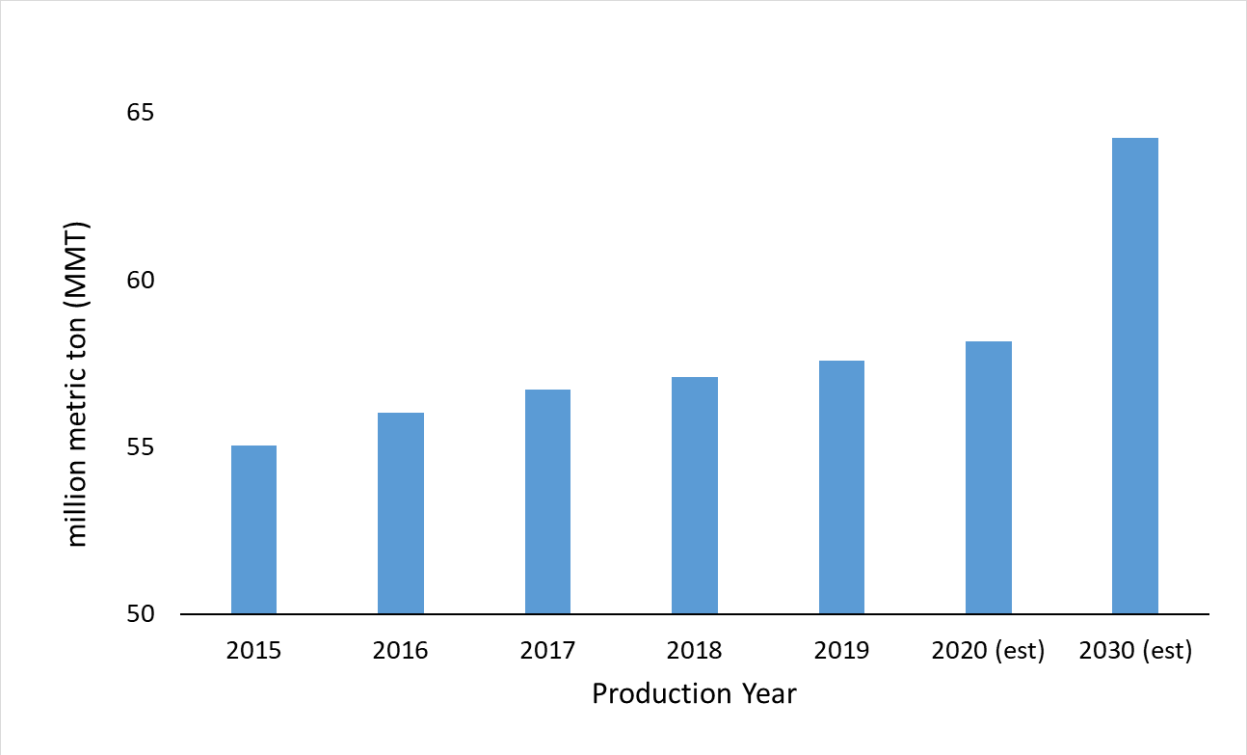

Figure 2.3: Oil palm plantation area growth per year [25]

The large area of plantation and large-scale production of crude palm oil results in an abundant amount of biomass being produced by the industry. The oil palm industry biomass can be divided into two types, solid and liquid biomass. Liquid biomass is produced during the normal oil extraction process from fresh fruit bunch. Palm oil mills utilized saturated steam during the sterilization process to denatured lipase activity and reduce free fatty acids (FFA) build-up, loosen up fruits to facilitate stripping, softening the pericarp for easier digestion, and preconditioning the palm nuts to reduce breakage during the pressing step [26,27]. The steam condensate after the sterilization process was collected together with separated water during the oil clarification step. This combined wastewater is called palm oil mill effluent (POME). This wastewater is treated through anaerobic ponds in the mill and later discharged into the river water as palm oil mill final discharge (POMFD) [28–30].

Solid biomass, on the other hand, is produced both in palm oil mills and plantations. This includes OPEFB, OPMF, OPF, OPT, palm kernel shell (PKS), and oil palm decanter cake (OPDC). OPEFB is produced in the fresh fruit bunch (FFB) threshing/stripping step when the oil palm fruit is separated from the bunch. OPMF is produced after pressed fiber and nut are separated for kernel extraction. PKS is produced after the separation of kernel and kernel shell from the palm nut and OPDC is produced as a byproduct of the oil clarification process. OPF and OPT were primarily produced in the plantations through normal pruning of palm trees and felling of old, non-productive trees (> 25 years old). The flow chart of the general palm oil mill and plantation waste biomass production route is shown in **Figure 2.4**.

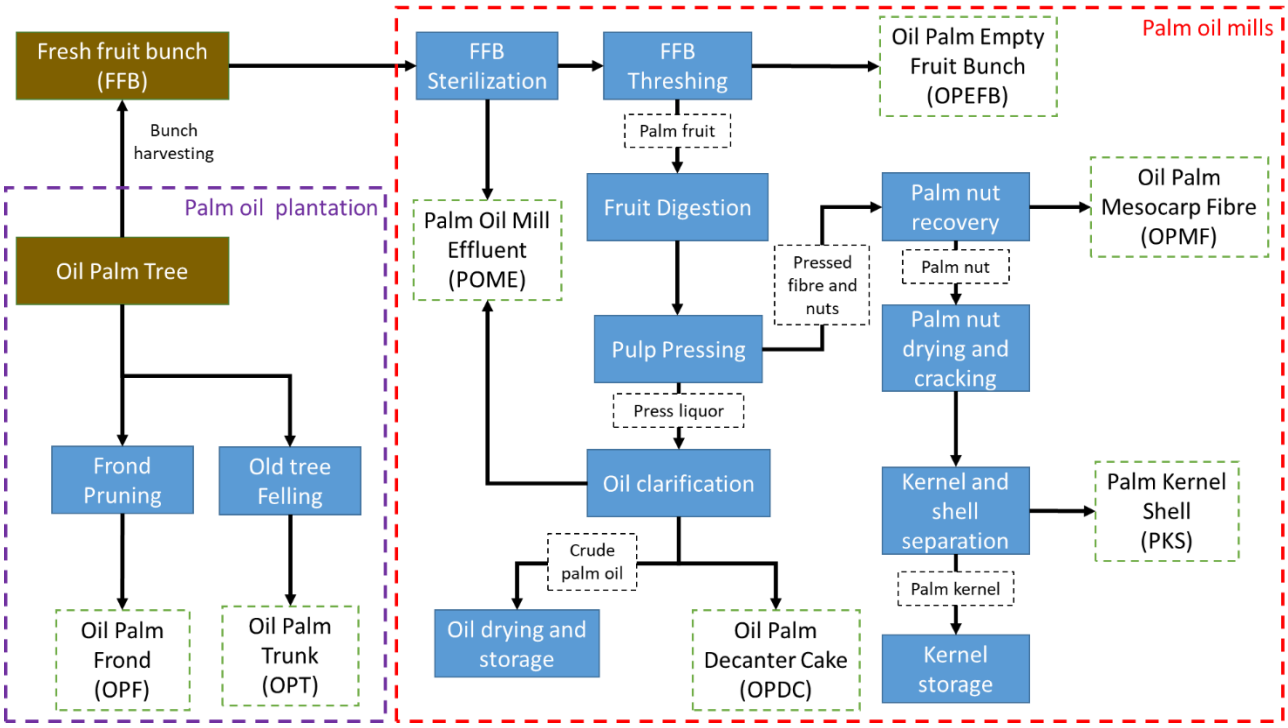

Figure 2.4: Oil palm industry biomass production flowchart

The main source of solid waste biomass in the palm oil industry comes from the plantation with about 75% of all solid biomass produced by weight in the form of OPF and OPT, with OPF as the largest by weight, at about 59% [31]. **Figure 2.5** shows the distribution of solid biomass produced by weight in 2012.

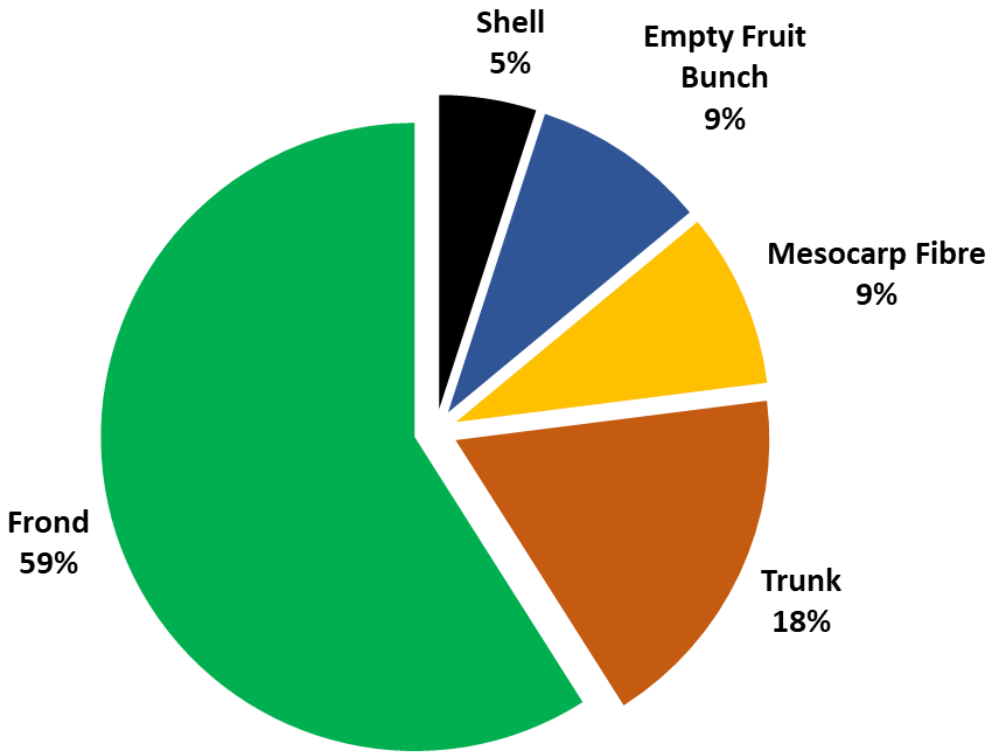

Figure 2.5: Palm oil industry solid biomass distribution by weight (2012)[31].

OPF is abundantly available throughout the year due to the pruning process and is directly related to the total area of the plantation. OPT is available when plots of palm trees are being felled due to old age, but the sheer volume of palm trees felled during this period contributes to the large annual production. OPEFB, OPMF, and PKS are produced daily through FFB processing, but OPMF and PKS are almost all being used as fuel for the boiler in the mills [32]. This is not possible for other waste biomass produced in the mills such as OPEFB, due to its high moisture content [33,34]. Traditionally, palm oil mills used to burn OPEFB as a means of disposal, and also to

produce ash that is recycled back to the plantations as a source of potassium due to OPEFB's high potassium content [35]. This practice however has been banned by the Malaysian government due to its emission problem [36]. The palm oil mills mulch the OPEFB instead, but due to slow degradation, most of the OPEFB produced daily by the mills is being dumped in landfills [37]. OPF is currently used as crude mulching for the oil palm tree and is usually left around the plantation after the pruning and harvesting process. This results in the accumulation of OPF in the plantations and OPEFB in the mills [38].

2.4 Oil palm biomass treatments and conversion technology

Research towards the use of oil palm biomass as a renewable source of raw material in Malaysia has grown steadily since the 1990s, with the main objective is to utilize abundantly available waste in the mills and plantations. Research interest in oil palm biomass utilization covers many methods and processes to either use oil palm biomass as raw material, or convert oil palm biomass into usable resources for next step processing, or producing value-added products. This section will explore some of the processes that have been extensively studied for the utilization and valorization of oil palm biomass.

2.4.1 Mechanical processing

Oil palm biomass is usually relatively large in particle sizes, especially waste biomass produced in the plantation. OPF and OPT are usually in the range of meters in size, due to the nature of the production process. Some of the biomass produced in the mills such as OPMF and PKS are already small in size which increases their usability. OPEFB are traditionally produced in bunches but more palm oil mills are shredding and pressing the OPEFB to extract additional oil absorbed by the fibers [39]. The biomass also contains high moisture content, which significantly reduces its calorific value [40]. **Table 2.1** lists down the calorific value of some of the oil palm biomass produced by the industry and its potential energy that can be generated in million tonnes of oil equivalent (mtoe) [41,42].

Table 2.1: Oil palm biomass energy potential [41,42].

Biomass type	Calorific value (MJ/kg)	Potential energy generated (mtoe)
OPEFB	18.8	7.65
OPMF	19.1	4.37
PKS	20.1	2.84
OPF and OPT	16.8	8.47

The easiest treatment that can be applied to oil palm biomass is through mechanical process. This includes size reduction (shredding, grinding, milling), densification (pelleting, briquetting), and drying (sun-drying, torrefaction). Some of the research includes the production of pellets from oil palm fibers (OPMF, OPEFB, OPF) [43], torrefaction of oil palm biomass to reduce moisture [44,45], and briquetting using fiber or a combination of biomass to improve its fuel properties [46]. The process proposed in these studies uses simple process to produce fuel products that can be used directly for other industries or the general public. The only disadvantage is that the process

usually needs additional equipment which requires training and maintenance which can increase capital and operating costs.

2.4.2 Biological treatment

Solid lignocellulosic biomass from oil palm contains cellulose and hemicellulose that can be digested to produce biofuels such as methane and hydrogen through saccharification and fermentation. Cellulose and hemicellulose can be digested into their constituent monomers which are glucose and xylose which can be utilized by microbes through fermentation [47]. Besides direct fermentation of solid biomass [48], direct fermentation of POME as a source of nutrient for hydrogen and methane production [49], co-fermentation of solid oil palm biomass with POME, and fermentation of pressed OPF juice [50] has also been reported. There are also researches to improve the fermentation process through physical and chemical pretreatment steps on the oil palm biomass. The processes mainly affect the lignin component through reduction of lignin content, and increasing cellulose and hemicellulose accessibility by microbes or enzymes [5,51].

Another popular biological treatment of oil palm biomass is composting. Almost all solid biomass produced by the palm oil industry has been composted and studied to some extent. The majority of the research focused on composting of OPEFB since it is the most abundant solid biomass in the palm oil mills [7]. Besides OPEFB, OPMF, OPF, OPF and OPT composting process has been reported which produce high-quality compost that can be used in-house as additional nutrition in the plantation, or sold as value-added products [8,52–54].

2.4.3 Heat treatment

Heat treatment has been used as a method to convert biomass into value-added products for centuries [55]. Charcoal is the usual product due to its simple and easy process. Heat treatment on oil palm biomass is shown in **Figure 2.6**

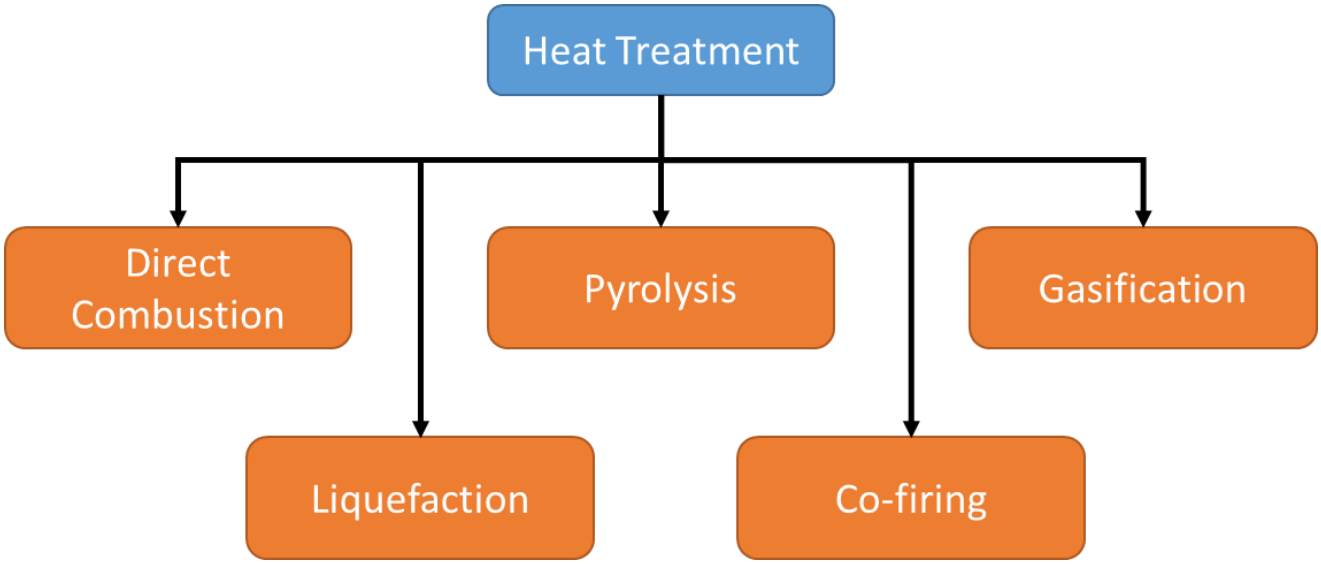

Figure 2.6: Oil palm biomass heat treatment technologies

Direct combustion of oil palm biomass has already been applied in palm oil mills for energy generation. Palm oil mills are mostly self-sufficient energy-wise, due to their location. Mills burn mainly OPMF and PKS in low-efficiency boilers to produce energy for their equipment and also steam for oil extraction [56]. OPEFB is not usually used as fuel in this manner due to its high moisture content as explained in **Section 2.4.1.** Some studies were done to improve the energy generation efficiency through the use of fuel cell furnaces, ovens, and spreader-stoker in two stages where the first step is mainly to dry the biomass, and the second stage to fully combust the biomass for energy production [57].

Pyrolysis and gasification of oil palm biomass produce 3 different products that can all be used as fuel: biochar, bio-oil, and fuel gases. Pyrolysis or carbonization is a thermal decomposition process under a low or no oxygen atmosphere to increase lignocellulosic biomass carbon content. Pyrolysis can be separated into 2 types, fast and slow pyrolysis. Fast pyrolysis usually produces bio-oils while slow pyrolysis produces solid char usually called biochar. All solid oil palm biomass has been reported to be successfully converted into fuel via pyrolysis methods. Juferi et al. reported successful OPEFB carbonization with biochar calorific value in the range of 23-25 MJ/kg. The process proposed by the study uses less energy, and produce low emission [58]. Kim et al. reported successful fast pyrolysis of palm kernel shell in producing bio-oil with a calorific value of 17.9 MJ/kg and yield of 47% [59].

Besides the production of fuel, pyrolysis can also produce carbon with a high surface area suitable for adsorption purposes. It is known that the carbonization of biomass results in biochar with an inherently porous structure [60]. The performance of the biochar can be further enhanced through the activation process where the porous structure of the biochar is developed through physical or chemical activation process. The processes related to activation of oil palm-based biomass or biochar have been extensively reported in the review by Rashidi et al. [61] While the process can successfully improve the performance of the biochar, it is usually energy intensive and use caustic chemicals that can produce toxic waste[62]. Another method that can be applied to biochar to improve its performance is through surface modification and functionalization. A review by Liu et al. has highlighted the many ways biochar surface can be modified and functionalized to add new surface functional groups that can be finely tuned depending on its specific target. The problem with the process currently reported in the literature is that the process uses very specialized chemicals and

equipment and can be very complicated, which can inhibit adoption by the industry [63]. Biochar surface modification and functionalization technology can be improved through the development of a simpler, easily implemented process that uses currently available equipment in the industry, especially in the palm oil mill industry.

2.4.4 Cellulose extraction

Oil palm biomass has been studied as a renewable source of cellulose due to its relatively high cellulose content. Usually, extraction of cellulose was done via the soda pulping method, where oil palm biomass is treated using sodium hydroxide as the pulping agent. The resulting pulp was then bleached with a bleaching agent such as sodium chlorite or hydrogen peroxide-based chemical mixtures [64]. This produces relatively high purity cellulose with high crystallinity. Another popular method of cellulose extraction is by using sodium chlorite ($NaClO_2$). Oil palm biomass was immersed in $NaClO_2$ solution acidified with acetic acid to remove lignin. Delignified biomass is then treated with potassium hydroxide (KOH) to remove hemicellulose. This process is usually used as a pretreatment step before the production of other specialized cellulose products such as microcrystalline cellulose (MCC), cellulose nanofiber (CNF), cellulose fibrils, and cellulose whiskers [65,66]. Besides the soda pulping and sodium chlorite method, other novel methods of cellulose extraction have been reported by other researchers. Abdullah et al. reported the use of ultrasonication and autoclave methods to extract cellulose from OPEFB. OPEFB fiber was sonicated in a sodium hydroxide (NaOH)/hydrogen peroxide (H_2O_2) bath and further bleached using a hydrogen peroxide-based chemical mixture [67,68]. Haafiz et al. reported the use of 2.5N hydrochloric acid (HCl) and 5% ammonium hydroxide (NH_4OH) solution to produce highly crystalline microcrystalline cellulose from OPEFB pulp bleached

using an oxygen-ozone-hydrogen peroxide process with Segal crystallinity index of 89% [69].

Previously reported processes in the literature have always focused on producing highly crystalline cellulose structure, usually in the form of MCC and CNF with crystallinity values were in the range of 60-80%, which is comparable to commercially available cellulose products in the market such as Avicel PH101 and Sigma-Aldrich MCC products. While highly crystalline cellulose is desirable in biocomposite manufacturing due to its high tensile strength properties, the lack of reporting on the yield can hide the important data that is required in implementing the technology in the industry. Process yield is important in calculating the cost of the process, which in turn can affect the revenue that can be collected. This will deter the industry, due to the uncertainty in cost and revenue. In addition to that, the process suggested in the literature almost always requires multiple steps of pretreatment, usually using specialize chemicals to first remove lignin from the biomass. As stated in the previous paragraph, the use of technology utilizing special chemicals such as ozone, or equipment such as ultrasonicator will incur additional capital expense in terms of chemical procurement, installation of new equipment, and safety measures. This will inevitably deter industrial players from adopting new technology since it will significantly increase expense and reduce revenue. Research into simpler, effective processes to treat and use oil palm biomass is needed to further improve adoption by the industry.

CHAPTER 3

HYDROTHERMAL LIGNIN REMOVAL FROM OIL PALM BIOMASS

3.1 Introduction

Biomass comprises 3 major components, lignin, cellulose, and hemicellulose. Cellulose especially, has been extracted and processed for centuries in the form of paper and textiles, and nowadays, advanced technologies are being developed to utilize cellulose as environmentally friendly feedstock for various productions such as biofuel through saccharification [70] and fermentation [71], filler in the production of biocomposites, biopolymers [72], bio-adsorbents [73], and pharmaceuticals [74]. Even though cellulose is versatile and abundant in the form of waste biomass, one main roadblock in the implementation and use of cellulose is lignin recalcitrance in its original lignocellulosic form. Plants use lignin to provide mechanical support, resistance to external pathogens, regulate responses to physical stressors, and play a role in water transport [75]. Lignin contributes to biomass resistance towards chemical and physical treatments due to its complex structural and compositional properties of macromolecules [76] which renders many treatment processes not viable. Because of this, lignin removal from biomass is an essential step before the utilization of cellulose.

Removal of lignin from oil palm biomass has been reported using chlorite and non-chlorite methods but it usually comprises multiple pretreatment steps with the use of many chemicals. Nazir et al., reported eco-friendly cellulose extraction from OPEFB using eco-friendly hydrogen peroxide and acetic acid, but require intensive pretreatment steps such as dewaxing with solvents and autoclave treatment with

NaOH and H_2O_2 to remove lignin before extraction [68]. Other processes reported use specialized equipment such as ultrasonicator which are expensive and inhibitive in the industry due to their steep capital expense [67] or use of complex organic reaction systems that require the use of an excessive amount of solvents that increase cost and produce more liquid waste. Another method suggested using a combination of acids to remove lignin produces modified cellulose that might limit its usage [77,78] or long time which will incur higher cost if constant mixing and heating is required [79]. To bolster the adoption of waste utilization and valorization by the oil palm industry, a simple and appropriate method to remove lignin from oil palm biomass comprises of simple process, use fewer chemicals, and utilize already available material and equipment in the palm oil mill or plantation needs to be developed.

In this study, the use of hydrothermal process to remove lignin from oil palm fronds was implemented using nitric acid. Oil palm frond was treated at 120°C for 30 min without any pretreatment steps. Treated OPF was rinsed with distilled water to remove excess nitric acid and lignin degradation byproduct. The proposed process is much simpler compared to the method stated in the previous paragraph, which only needs one single processing step to produce biomass with significantly lower lignin content, which in turn reduces the time needed, chemical cost, and waste by-product. The simpler process also reduces the technological barrier for adoption in the industry. The process can also utilize equipment and resources already available in the palm oil mill, such as pressure vessels in the form of fresh fruit bunch sterilizers, and steam from the palm oil mill's boiler which further reduce initial cost. The resulting treated OPF fiber was analyzed via scanning electron microscopy (SEM), Fourier Transform Infrared (FTIR) spectroscopy, X-ray powder diffraction (XRD), and thermogravimetric analysis (TGA) to determine its properties, and compared with commercially available

cellulose products. The same process was also applied to other types of biomass such as oil palm empty fruit bunch and bamboo to determine its applicability towards other types of biomass.

3.2 Materials and methods

3.2.1 Sample preparation

OPF was collected from Taman Pertanian Universiti, Universiti Putra Malaysia. Matake bamboo was provided by Sanwa Co. Ltd, Kitakyushu, Japan. All biomass was dried in an oven for 48 hr to reduce the initial moisture content before being ground and sieved to 0.25 to 1 mm particle size. Dried, ground biomass was kept in a sealed plastic bag at room temperature before autoclave treatments.

Concentrated nitric acid (68%), sodium hydroxide pellets, and glacial acetic acid are provided by FUJIFILM Wako Pure Chemical Corporation, Osaka, Japan. Sodium chlorite (80%) is sourced from Sigma-Aldrich, Massachusetts, USA. Stock solutions were prepared from pure chemicals and diluted to required concentrations using deionized water. Deionized water (18.25 MΩ.cm) was obtained from a Milli-Direct 16 Filtration system (MilliporeSigma, Massachusetts, USA).

3.2.2 Hydrothermal lignin removal

10 g raw OPF was added to a conical flask and mixed with 200 mL nitric acid solution (1:20 biomass mass to acid volume ratio) at different concentrations. The flask was covered with aluminum foil to avoid boil the mixture over during autoclave treatment. The biomass mixture was then autoclaved at a range of temperature and time. After autoclave, treated biomass was filtered and rinsed with distilled water to remove excess nitric acid until the pH of the rinse solution is 6-7 and colorless. Rinsed, treated biomass was dried in an oven at 80°C overnight and weighed for yield calculation.

3.2.3 Chemical composition analysis

Chemical composition of the original and treated biomass was analyzed using TAPPI (Technical Association of Pulp and Paper Industry) Standard Test Methods. Cellulose (T-203cm-99), holocellulose (Tappi useful Method 249-75), lignin (T-222om-88), and ethanol-toluene extractives (T-204cm-97) content of the samples were determined in replicates to obtain mean and standard deviation values.

Cellulose yield and lignin removal were calculated based on raw OPF lignocellulosic composition:

$$Cellulose\ yield\ (\%) = \frac{Treated\ OPF\ cellulose\ content\ (g)}{Raw\ OPF\ cellulose\ content\ (g)}$$

$$Lignin\ removal\ (\%) = \frac{Raw\ OPF\ lignin\ content\ (g) - Treated\ OPF\ lignin\ content(g)}{Raw\ OPF\ lignin\ content\ (g)}$$

3.3 Analysis

Surface structure and morphology were determined using SEM. Samples were viewed at 1000x magnification using JEOL-9000 SEM/EDX analyzer (JEOL, Japan). Thermal stability of samples was determined thermogravimetrically using EXSTAR TG/DTA7000 (Hitachi High-Tech, Japan). Samples were analyzed in the temperature range of 100-550°C at 10°C/min heating rate under nitrogen flow. The crystallinity of extracted cellulose was determined using a Rigaku X-ray diffractometer with Cu K-α radiation at 40 kV and 15 mA. Crystalline peak measurement was done at with 2θ range of 3-60° at a scan speed of 20°/min. Segal crystallinity index (CrI) was calculated using the Segal method [80] as follows:

$$CrI = \frac{I_{002} - I_{am}}{I_{002}} \times 100$$

Where I_{002} is the maximum intensity value at 22° (crystalline peak) and I_{am} is the minimum intensity value at 18° (amorphous scattering). Surface properties and functional groups of raw biomass and extracted cellulose were determined using FTIR spectroscopy analyzer. Samples were analyzed using attenuated total reflectance (ATR) method to compare differences in surface functional groups between raw biomass, treated biomass, and commercially available microcrystalline cellulose.

3.4 Results and discussions

3.4.1 Effect of treatment parameters towards lignin removal and cellulose content

Parameters such as treatment time, temperature, and nitric acid concentration affect the lignin removal and cellulose content of OPF fiber based on preliminary analysis. The relationship between the parameters and biomass composition was analyzed and discussed in this section. Several properties of treated OPF were analyzed through lignocellulosic compositional analysis and XRD to determine the efficiency of the process at a given parameter. Cellulose yield and lignin removal percent were calculated as the main indicator of how effective the hydrothermal process at removing lignin while maintaining cellulose content. CrI value was calculated from XRD analysis to determine the purity and structure of the cellulose post-treatment. High crystallinity will indicate that the crystalline structure of cellulose is not affected during treatment, which suggests a selective reaction with lignin. High crystallinity also indicates the removal of amorphous hemicellulose from the biomass.

3.4.2 Effect of nitric acid concentration

OPF was hydrothermally treated at different nitric acid concentrations (0.1 M – 2 M) while the temperature and time were constant at 30 min and 120°C. The treatment cellulose yield, lignin removal, and CrI values are shown in **Figure 3.1**.

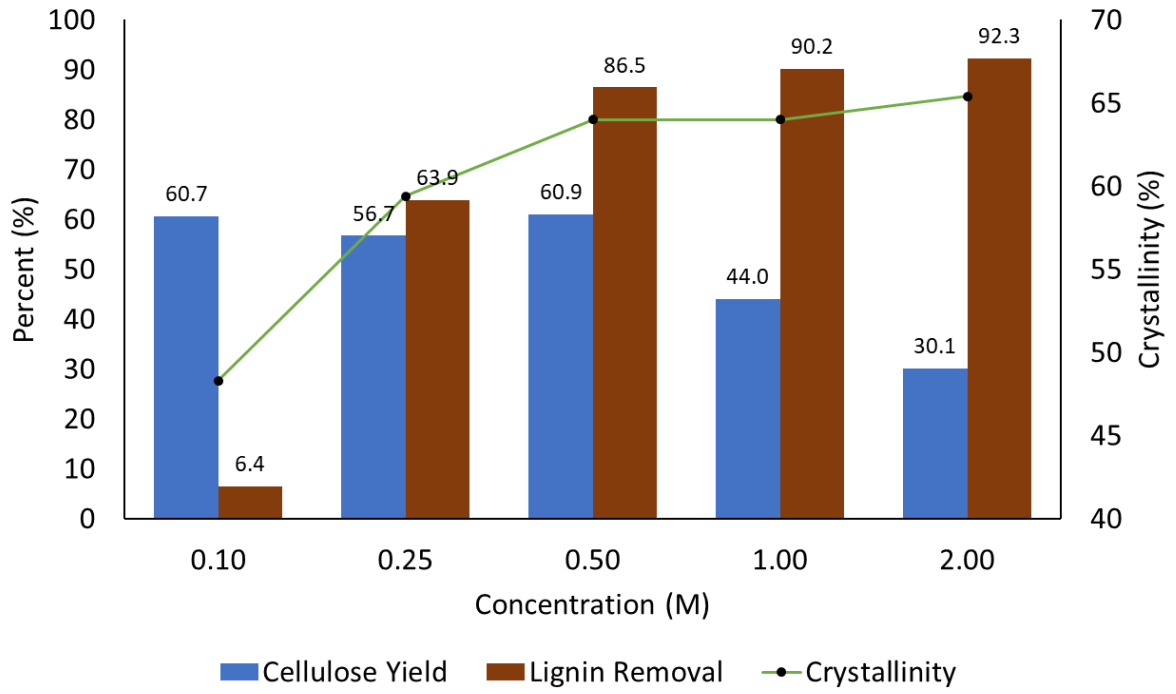

Figure 3.1: Effect of nitric acid concentration on cellulose yield, lignin removal and crystallinity of OPF

From **Figure 3.1**, we can see the trend of cellulose yield, lignin removal and crystallinity of the treated OPF fiber at different nitric acid concentrations. Cellulose yield stays relatively the same at 0.1 M until 0.5 M, before starting to drop significantly at higher concentrations. This might be due to the degradation of cellulose through acidic hydrolysis. The use of acid in concentrated and dilute acid hydrolysis process has been widely used as a method to produce fermentable sugars from biomass where acids such as sulfuric and acetic acid have been used in pretreatment process called saccharification to hydrolyze cellulose and hemicellulose into its monomers such as glucose and xylose. Treatment using sulfuric acid yielded glucose from cellulose in the range of 47-134 mg glucose per g of biomass [81–84]. Lignin removal efficiency shows an increasing trend as nitric acid concentration increases, with the highest lignin removal of 92.3% at 2 M. While this in itself is impressive, where lignin removal of more than 90% can be reached with a single step process, the amount of

cellulose degradation was too high, where 70% of the original cellulose content was lost during treatment. In addition to that, lignin removal at 0.5 M, 1 M, and 2 M shows a small improvement in lignin removal, with an increase of only about 4% from 0.5 M to 1 M, and 2% from 1 M to 2 M, suggest optimal nitric acid concentration for lignin removal has been reached at 0.5 M. In addition to that, the inverse relationship between lignin removal and cellulose yield infer that the process selectively reacts with lignin until the amount of lignin drops below a certain value, in which the process prefers cellulose hydrolysis reaction.

The crystallinity of cellulose in the treated OPF shows a small increase as the concentration increase, suggesting an increasing amount of crystalline cellulose in the treated OPF fiber. The crystallinity data also reflect the relationship between lignin removal and cellulose yield, where the increase in crystallinity can be attributed to the removal of lignin from the biomass. Degradation of amorphous cellulose and hemicellulose fraction during the hydrothermal treatment also increases crystallinity [85]. At lower concentrations, the increase in crystallinity was higher; 22.9% from 0.1 M to 0.25 M and 7.7% from 0.25 M to 0.5 M; and the increase levels out as concentration doubles after 0.5 M. This suggest that at higher concentration, the process starts to hydrolyze more crystalline cellulose from the biomass, resulting in constant cellulose crystallinity values but lower cellulose yield. From these data, it can be concluded that 0.5 M is the optimal concentration for the process and will be applied for subsequent parameter effect studies.

3.4.3 Effect of treatment time

Treatment time affect the process significantly, especially in term of cost-effectiveness. Since hydrothermal processes require a constant supply of heat to maintain reaction temperature and pressure, the shorter the process, the lower cost it will incur due to lower energy requirement. The process was repeated at 0.5 M nitric acid concentration at 120°C for different treatment period and resulting treated OPF properties is as shown in **Figure 3.2**

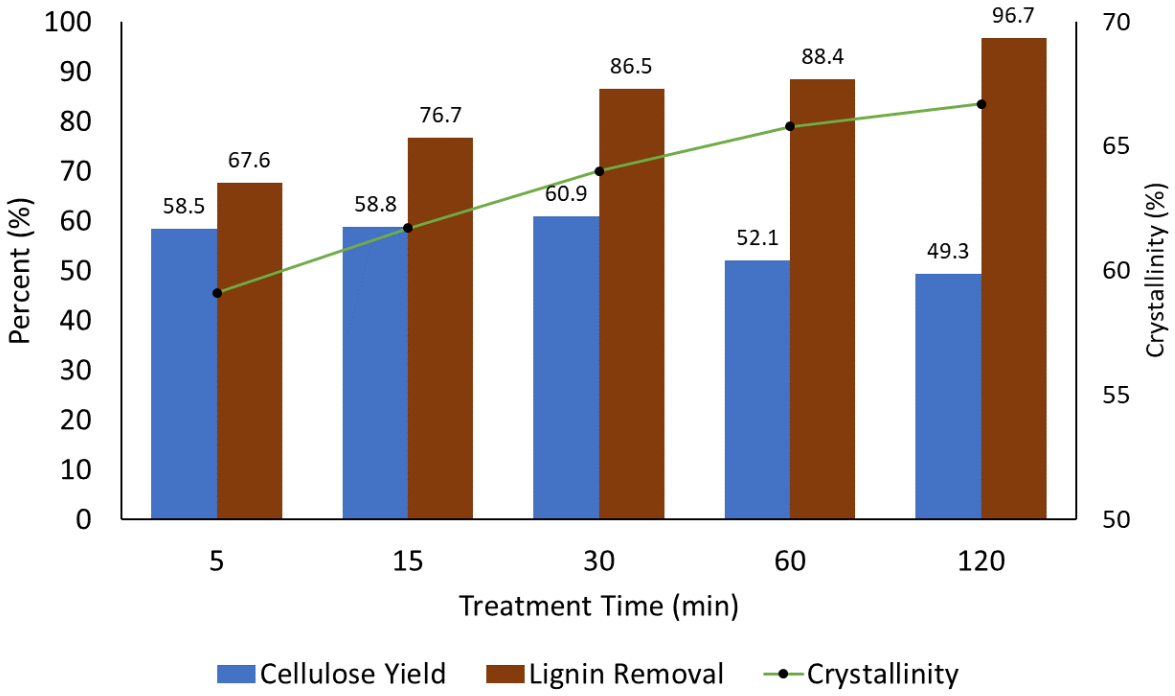

Figure 3.2: Effect of treatment time on cellulose yield, lignin removal and crystallinity of OPF

From **Figure 3.2**, it is apparent that as the treatment time increase, the amount of lignin removed also increases, with maximum lignin observed after 120 min of treatment. Cellulose yield, on the other hand, stays relatively similar at 5 min, 15 min, and 30 min, and starts to drop after 60 and 120 min of treatment. According to this trend, it can be inferred that at certain lignin content, the nitric acid started to hydrolyze

cellulose, as observed in the previous section. This might be explained by Le Chatelier's principle. Since the protective nature of lignin started to wear off as it is removed from the biomass structure, more surface area of cellulose is exposed to the acidic condition, which increases its possibility to react with nitric acid compared to lignin, therefore, increasing its reaction rate. At a lower treatment time, the process cannot proceed until the lignin content reached 10%, so the cellulose hydrolysis rate was lower, as shown in the cellulose yield data. Cellulose crystallinity increases gradually as the treatment time increase, but the increase is not significant at any temperature with about 1-2% change.

3.4.4 Effect of treatment temperature

Besides treatment time, treatment temperature also plays an important role in managing the energy requirement of a process. While the sterilizer in the palm oil mill can reach a temperature of 140°C, if the hydrothermal treatment operating process can be reduced, it can result in a large amount of energy being saved, due to the large specific heat of water. The hydrothermal treatment was applied using 0.5 M nitric acid for 30 min at different temperatures. The results are shown in **Figure 3.3**.

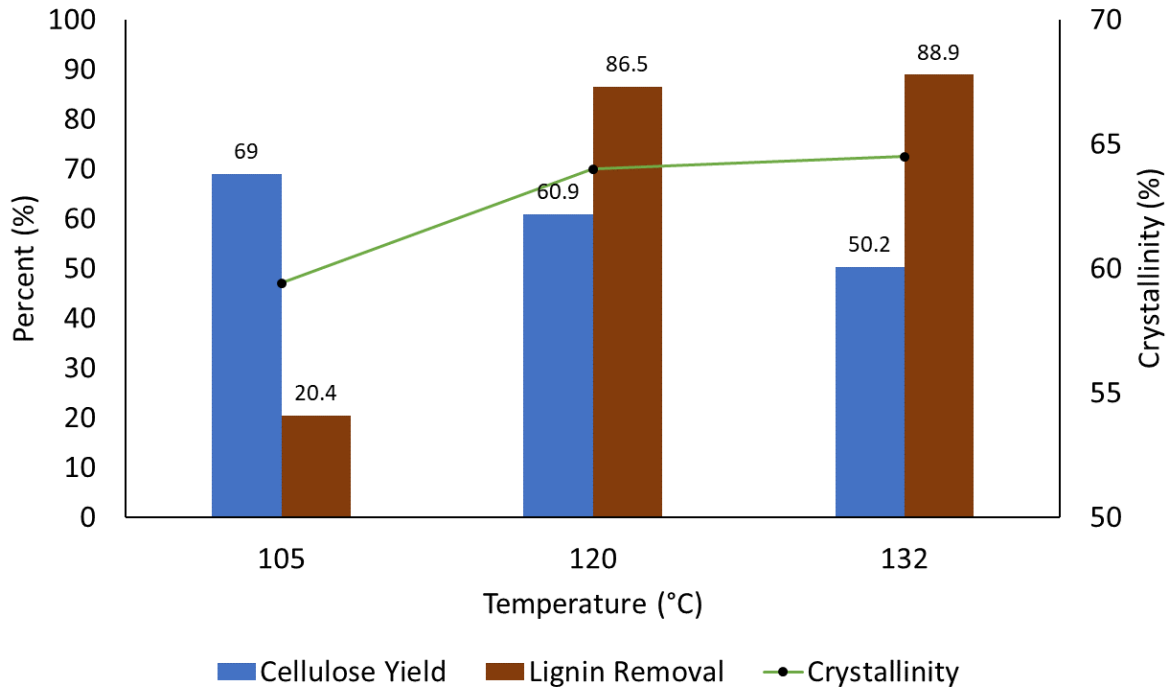

Figure 3.3: Effect of treatment temperature on cellulose yield, lignin removal and crystallinity of OPF

From **Figure 3.3**, the trend was similar to the first 2 parameters whereas the temperature increases, the lignin removal increases. For cellulose yield, it decreases as temperature increases. This might be due to the extra energy from higher temperatures increasing the reaction rate between nitric acid and lignin. As the lignin content reaches the 10% mark, the cellulose starts to hydrolyze faster which results in lower cellulose yield.

Based on these data, it can be concluded that the optimal parameters for the hydrothermal treatment of OPF using nitric acid are 0.5 M nitric acid concentration at 120°C for 30 min. Treatment at these parameters will result in the highest lignin removal while leaving as much cellulose unaffected as possible. Treated OPF at optimal parameters will be further analyzed and discussed in the next sections.

3.4.5 Lignocellulosic composition and yield

The lignocellulosic composition of raw and treated OPF is shown in **Table 3.1**. The cellulose yield after nitric acid hydrothermal treatment was 68.2% which is comparable with other previously reported methods. Abdullah et al. reported a 49% yield from ultrasonication treatment of oil palm empty fruit bunch [67] while Hafid et al. reported 65.5% cellulose yield from 2 steps sodium hydroxide and nitric acid/acetic acid/hydrogen peroxide mixture process from rice husk [86]. This shows that with a one-step process, lignin removal from oil palm frond can be achieved, producing fibers with relatively high cellulose content which can be further processed to produce other value-added products such as cellulose nanofiber or used as feedstock for saccharification or fermentation.

Table 3.1: Lignocellulosic composition of raw and treated OPF

	Composition (%)			
	Lignin	**Cellulose**	**Hemicellulose**	**Extractive**
Raw OPF	21.7 ± 1.0	32.6 ± 1.2	31.6 ± 1.2	14.1 ± 0.1
Treated OPF	9.3 ± 0.2	70.4 ± 0.8	20.3 ± 0.8	ND

While lignin is not totally removed, with lignin removal of 86.5%, this can be an advantage especially in the production of biocomposites. Several studies have reported that lignin-containing biomass-based fillers such as lignin-coated cellulose nanocrystals [87] and lignin-containing cellulose nanofibrils [88] show excellent compatibility with poly(lactic acid) with increased strength and flexibility due to increased crystallinity of PLA and improved adhesion between lignin-containing fillers and PLA matrix.

3.4.6 SEM micrograph

Both raw OPF and hydrothermally treated OPF were analyzed using a scanning electron microscope to determine the change in the bulk and surface structure of the OPF after treatment. The SEM micrographs are shown in **Figure 3.4**.

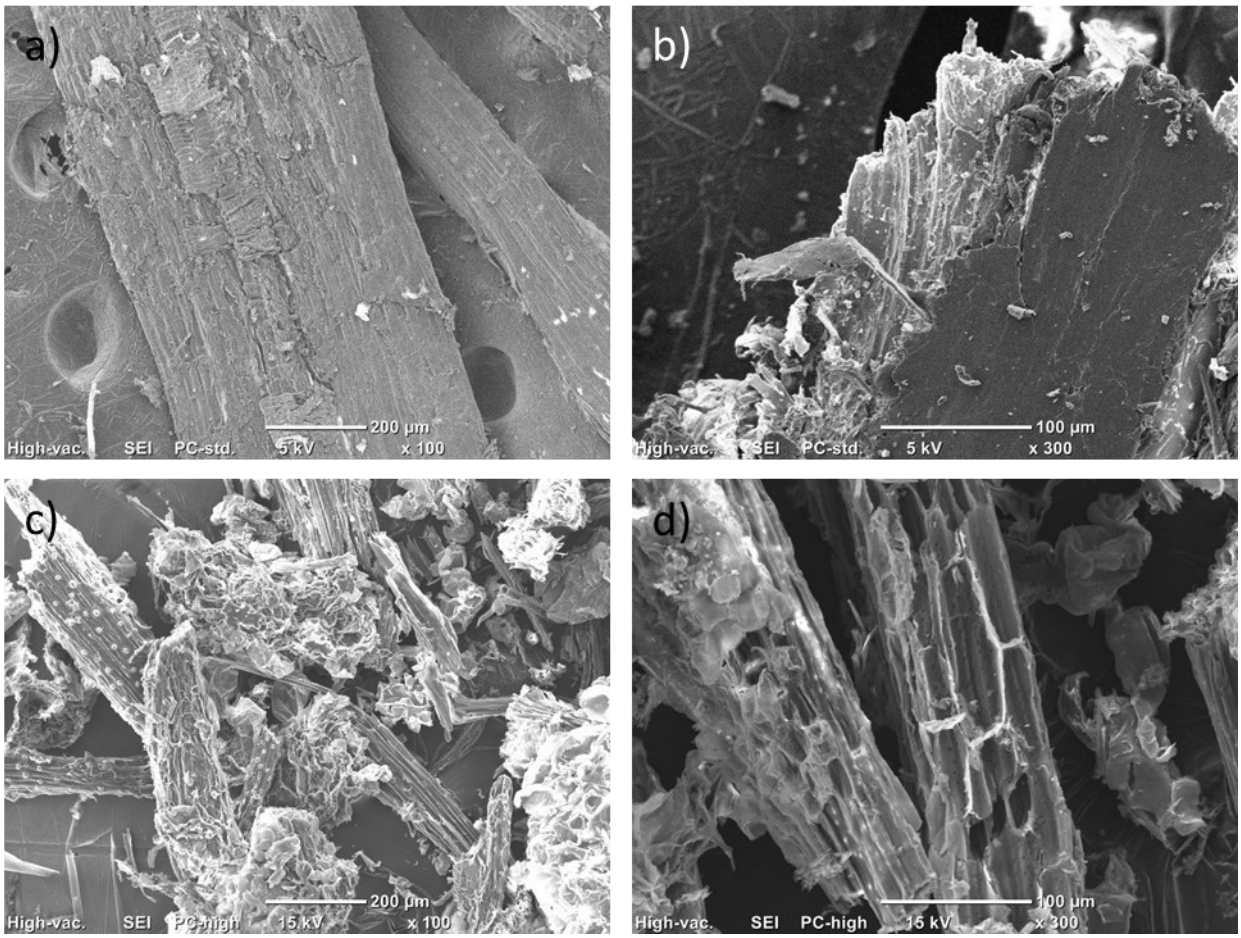

Figure 3.4: SEM micrographs of a,b) Raw OPF and c,d) treated OPF

SEM micrographs at 100x magnification show differences in particle size between raw and treated OPF. Treated OPF has a smaller particle size compared to raw OPF as expected. This is due to the treatment process breaking down the lignin that holds the structure of the OPF particle together, producing smaller particles. From the 300x magnification micrograph, it is apparent that raw OPF has bundled structure, with lignocellulosic structure bound together. After hydrothermal treatment, the structure was separated, where internal structure inside the OPF particle can be seen. Treated

OPF shows porous structure, suggesting that some of the cellulose and hemicellulose were degraded during treatment. This supports the lignocellulosic composition result where the calculated cellulose yield is reduced by about 40% from the original cellulose content.

3.4.7 Thermogravimetric analysis

Raw and treated OPF fibers were subjected to thermogravimetric analysis to determine their thermal stability and infer their crystallinity through their degradation temperature. The thermogravimetric/differential TG (TG/DTG) curve of both raw OPF and treated OPF is as shown in **Figure 3.5** below.

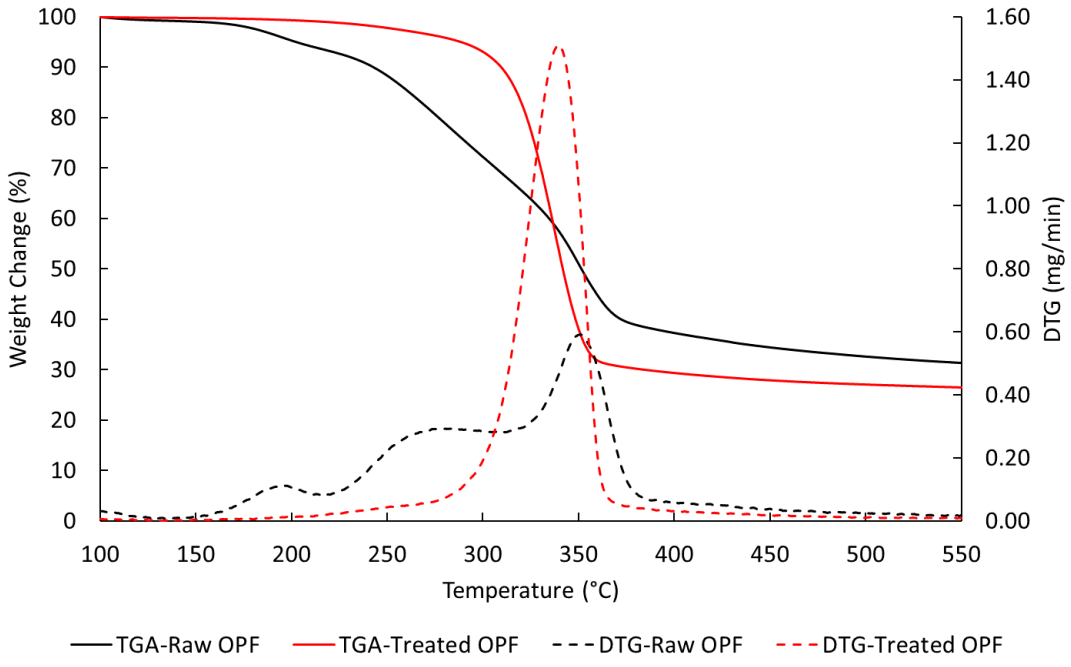

Figure 3.5: TG/DTG curve of raw and treated OPF

Raw OPF shows 3 degradation stages with DTG peaks at about 195°C, 275°C, and 350°C. The first degradation peak can be attributed to the degradation of wax and other soluble extractives in the OPF fibers [89]. This is supported by the high extractive content from the previous section. The TG curve reported by Megashah et al. does not have this peak due to their sample being pressed and washed before analysis and treatment [64]. The 2nd and 3rd peaks correspond to the degradation of the hemicellulosic and cellulosic components of the biomass. Similar degradation profiles were also reported by Nordin et al. with thermal analysis of oil palm mesocarp fiber with similar hemicellulose and cellulose content [90]. The TG/DTG curve changed significantly after hydrothermal treatment, with only one DTG peak at about 340°C. Small degradation started at around 200°C can be attributed to the degradation of remaining low molecular weights lignin and hemicellulose. From the TG/DTG curves, it can be concluded that treated OPF fiber contains cellulose with relatively high purity and low lignin content.

3.4.8 Fourier transform Infrared (FTIR) spectroscopy analysis

Raw and treated OPF were subjected to FTIR analysis to determine its surface chemical properties. A comparison was also made with commercially available MCC by Sigma-Aldrich. The FTIR spectra are shown in **Figure 3.6.**

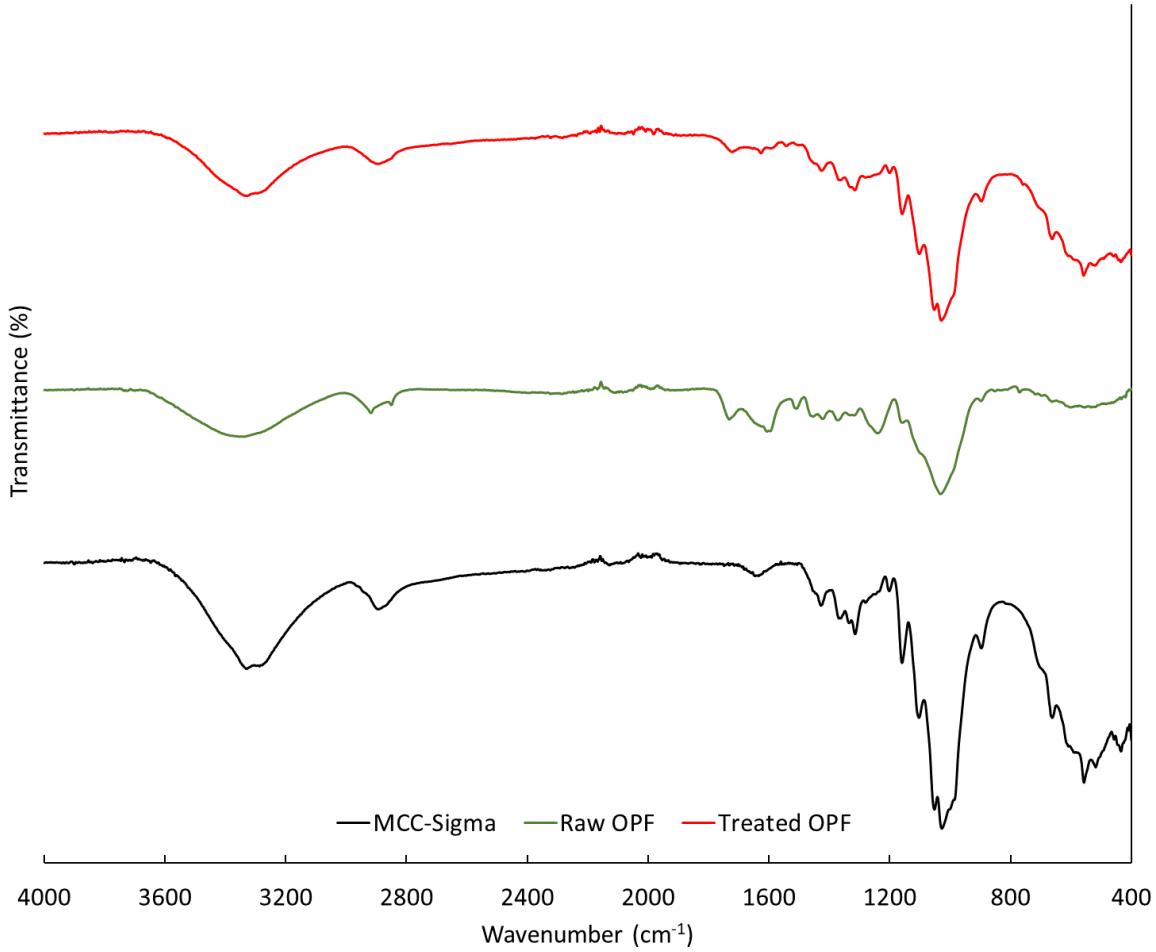

Figure 3.6: FTIR spectra of Raw OPF, treated OPF and commercial MCC as a reference.

FTIR spectra of all samples show similar peaks, especially transmittance peaks corresponding to cellulose. Those peaks are O-H stretching (3320 cm^{-1}), C-H stretching (2880 cm^{-1}), and O-H bending peak (1630 cm^{-1}). The strength of those peaks significantly increased after treatment, suggesting an increase in cellulose content [91]. A similar increase in absorption strength and shape for peaks in the fingerprint region (800-1100 cm^{-1}) associated with cellulose were also observed such as peaks at 1157, 1101, 1036, 1025, and 895 cm^{-1} which corresponds to cellulose C-O stretching, C-O-C asymmetric bridge stretching in cellulose and hemicellulose, aromatic skeletal and C-O stretching in cellulose, C-O stretching in cellulose and hemicellulose, and C-O-C stretching of β-(1-4) glycosidic linkage of cellulose, respectively. Furthermore, peaks attributed to lignin such as aromatic C=C stretching (1505 cm^{-1}), aryl C-O stretching (1235 cm^{-1}), and carbonyl C=O stretching (1730 cm^{-1}) [90] were also present in the raw OPF but significantly reduced in treated OPF, suggesting a reduction in lignin content of OPF after hydrothermal treatment. Comparing treated OPF spectrum with commercial MCC, both spectra show similar peaks, with the only difference with the lignin absorption peaks explained earlier. This suggests that while the fiber in its current state is not as pure as commercially available cellulose products, polishing treatment such as bleaching to remove the remaining lignin and hemicellulose can be applied to purify the fiber if needed.

3.4.9 X-ray diffraction (XRD) analysis

XRD analysis of raw OPF, treated OPF and commercial MCC was done to determine the crystallinity of the cellulose present in the fiber before and after treatment. XRD patterns for all sample is shown in **Figure 3.7** and CrI values are shown in **Table 3.2**.

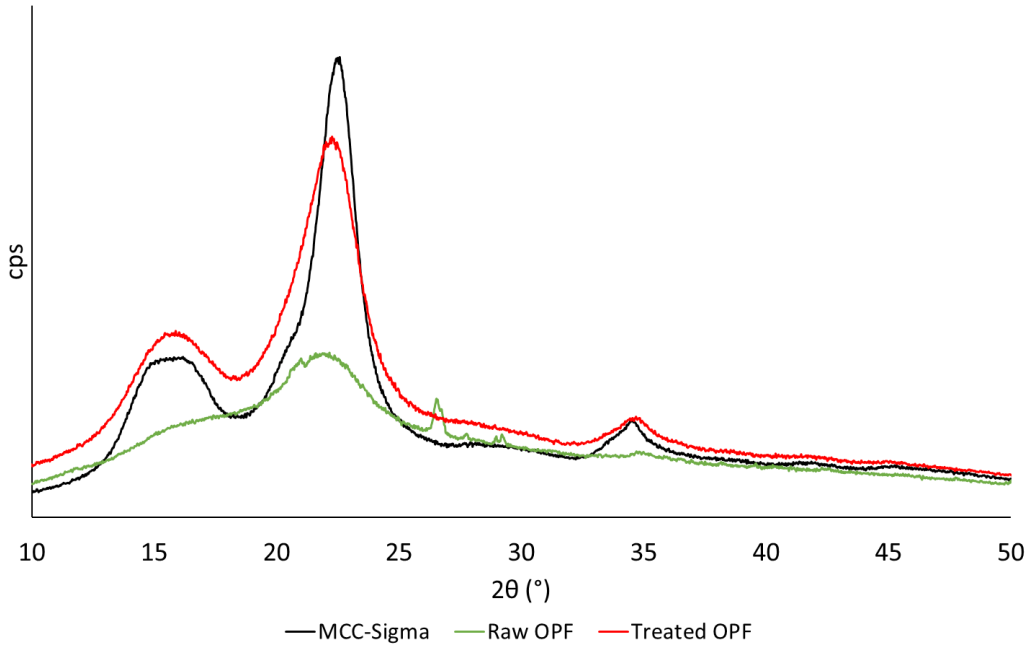

Figure 3.7: XRD diffraction patterns of raw OPF, treated OPF and MCC as a reference

Table 3.2: Segal crystallinity values of raw OPF, treated OPF, and commercial MCC

Sample	Raw OPF	Treated OPF	MCC Sigma
CrI (%)	38.2	63.1	77.7

From the XRD pattern, it is apparent that cellulose crystallinity of OPF increased significantly after hydrothermal treatment compared to raw OPF. The calculated Segal crystallinity index also shows an increase of 65.1%. This shows that the hydrothermal selectively removes lignin and leaves behind a crystalline cellulose structure. The amorphous peak at 2θ value of 18° was still relatively higher compared to MCC, due to the remaining hemicellulose in the fiber but it is much lower relative to raw OPF. This could be attributed to the removal of some of the amorphous hemicellulose and cellulose during treatment. CrI value of treated OPF is comparable to other more complex methods reported in the literature. Wang et al. reported bamboo-based cellulose with a crystallinity index of 74.1% while Galiwango et al. reported date palm waste-based cellulose with a crystallinity index of 52.7% [79,92].

3.5 Application of hydrothermal treatment to different types of biomass

Hydrothermal treatment was applied to other biomass (OPEFB and Matake bamboo; *Phyllostachys bambusoides*) to determine the feasibility of this process in treating other types of biomass. This is important for future studies where the feasibility of this method in removing lignin from other types of biomass proves that the process is not specific towards one type of biomass. Similarities in the cellulose content, crystallinity and the yield of the process using other biomass would show that this process is not severely limited by the biological difference of the biomass and the process performance can be improved through process parameters optimizations. In the point of view of the palm oil industry, this can be a new way to generate revenue through the processing of biomass from other industries. OPEFB was selected due to its abundance in the palm oil mills as the major byproduct of oil extraction from palm oil fruit while Matake bamboo was selected as one of the main bamboo species in Japan. Biomass samples were treated according to the method explained in **Section 3.2.1** without any modification. Sample lignocellulosic composition, thermal degradation profile, and surface functional groups were analyzed to determine the effectiveness of the method in removing lignin from the biomass and its effect on cellulose purity. The results for all of the analysis are as shown in **Figure 3.8 - Figure 3.12** and **Table 3.3**

Table 3.3: Lignocellulosic composition of raw and treated OPEFB and Matake

Sample	OPEFB		Matake	
	Raw	Treated	Raw	Treated
Lignin (%)	29.7 ± 0.6	10.4 ± 0.0	31.3 ± 0.5	14.0 ± 0.3
Cellulose (%)	37.7 ± 0.8	65.5 ± 0.7	45.3 ± 0.3	59.0 ± 0.9
Hemicellulose (%)	32.6± 0.8	24.1 ± 0.7	23.6 ± 0.3	27.0 ± 0.9

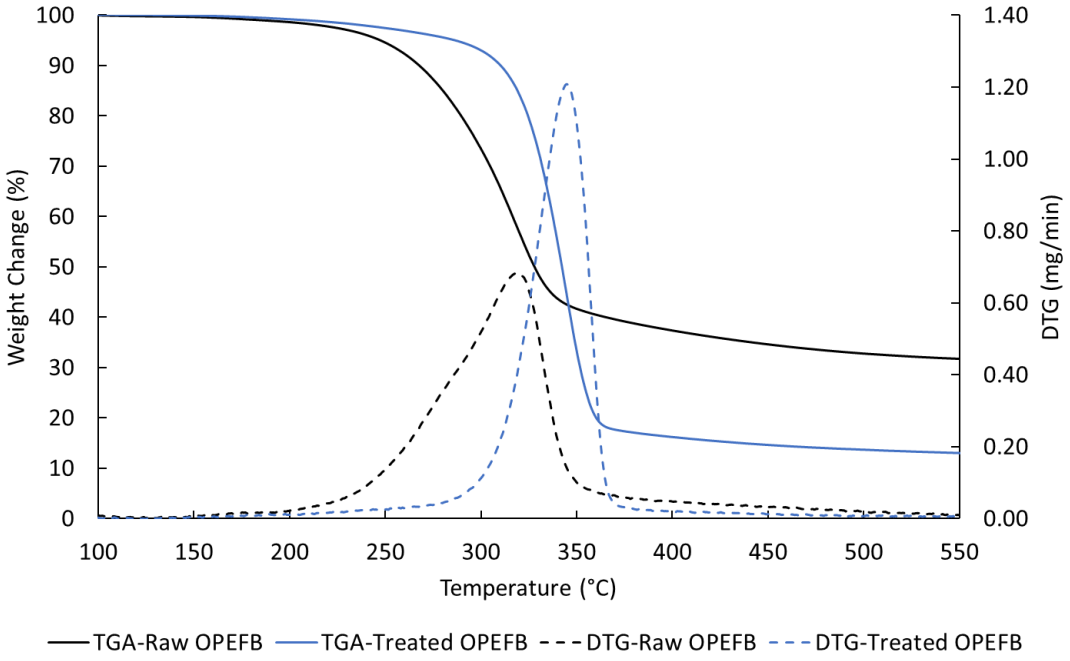

Figure 3.8: TG/DTG curve of raw and treated OPEFB fiber

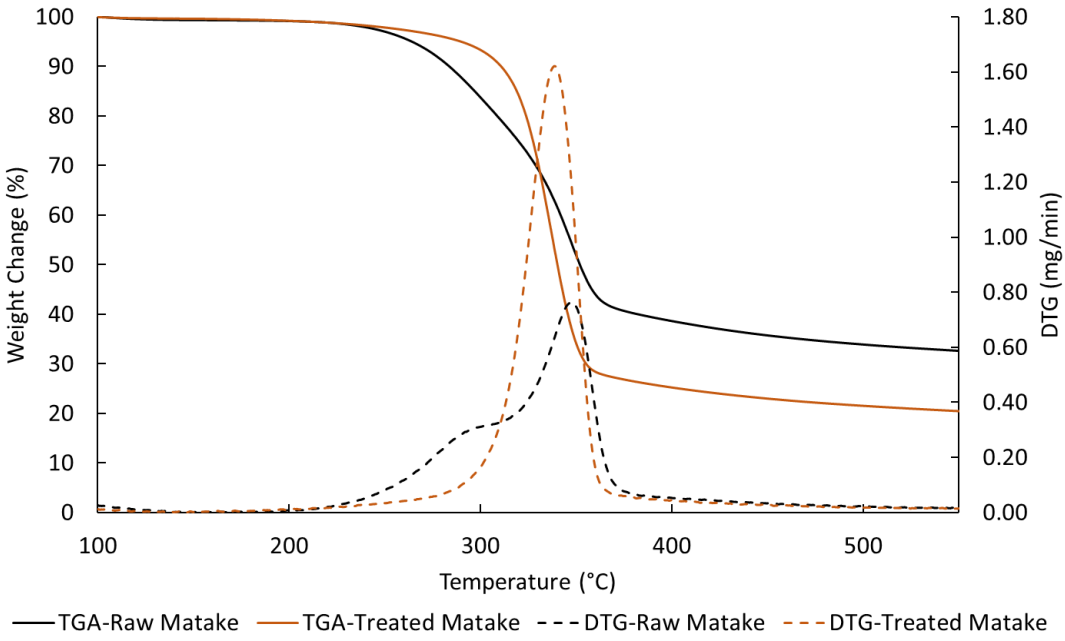

Figure 3.9: TG/DTG curve of raw and treated Matake bamboo

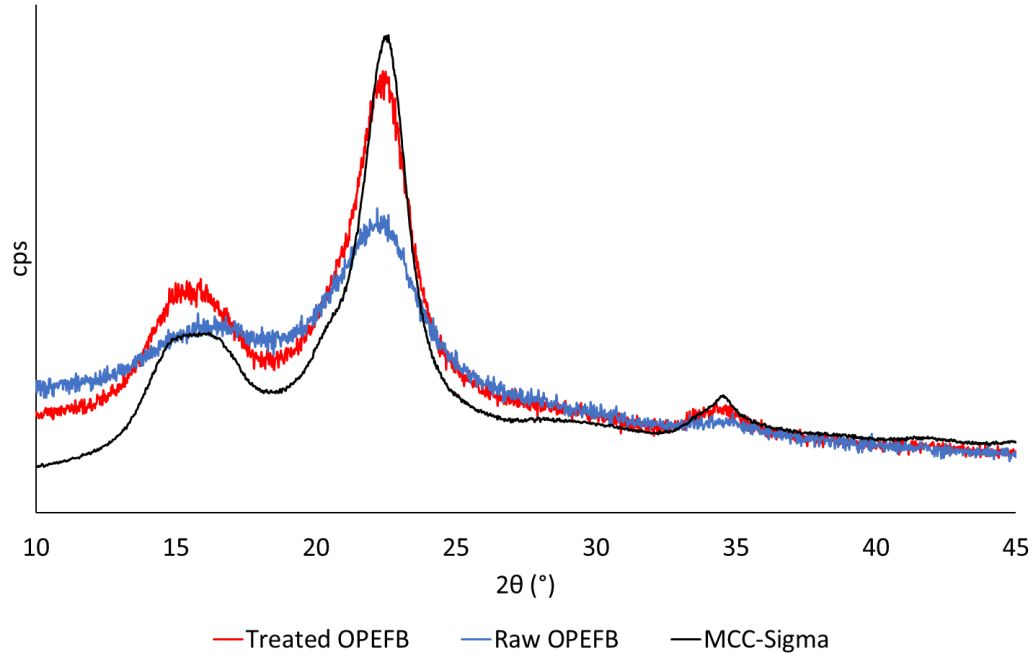

Figure 3.10: XRD pattern of raw OPEFB, treated OPEFB and commercial MCC

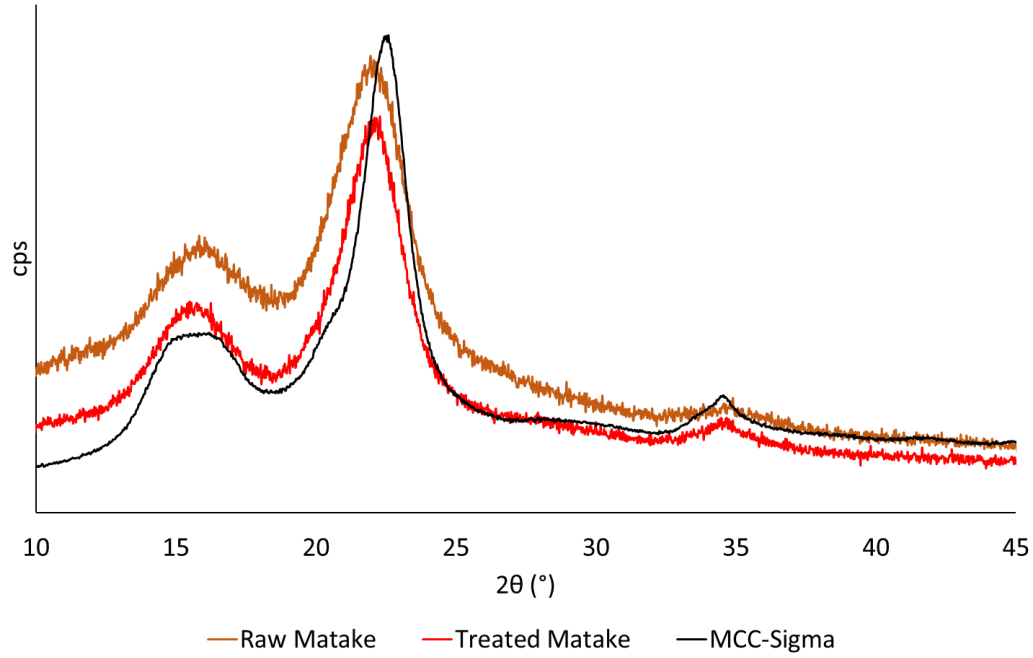

Figure 3.11: XRD pattern of raw Matake bamboo, treated Matake and commercial MCC

Table 3.4: Segal crystallinity of raw and treated biomass

Sample	Raw OPEFB	Treated OPEFB	Raw Matake	Treated Matake	MCC Sigma
CrI (%)	41.6	65.2	50.3	64.4	77.7

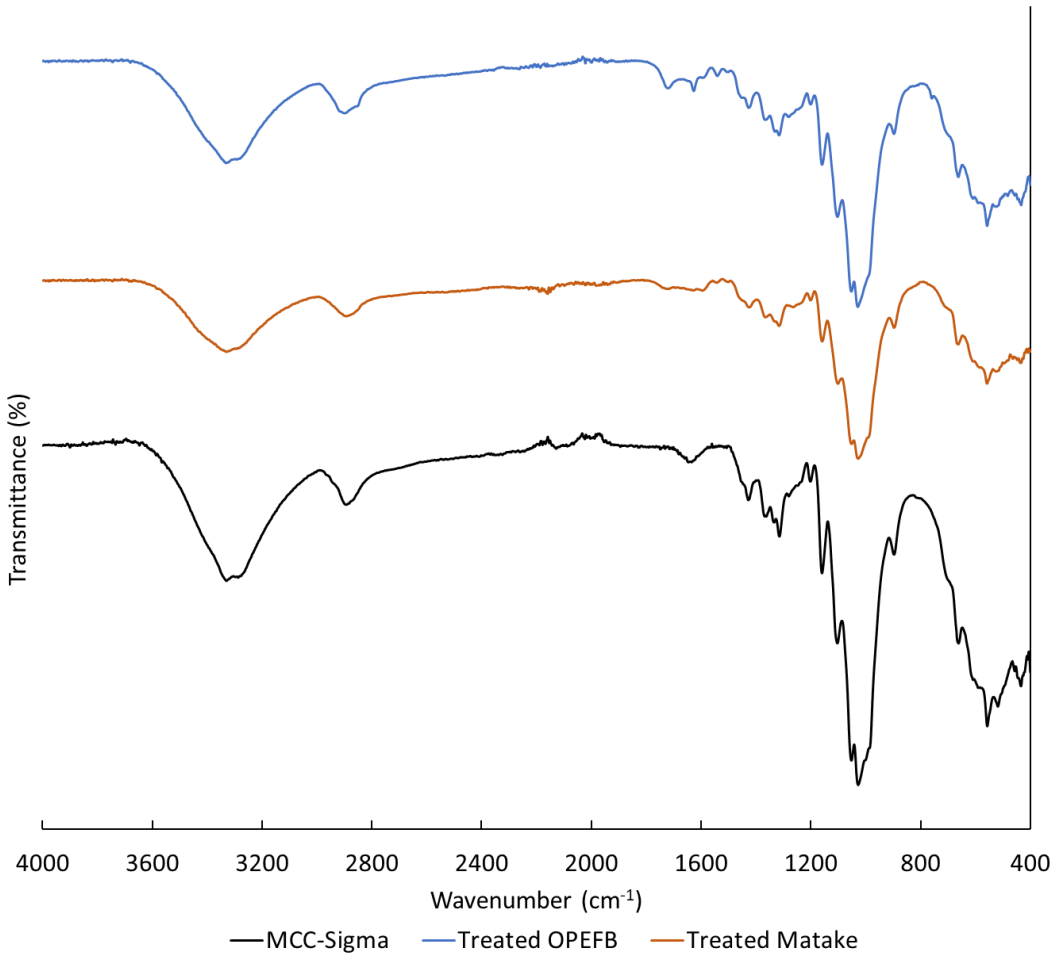

Figure 3.12: FTIR spectra of treated OPEFB, treated Matake and commercial MCC

From compositional analysis, it is apparent that hydrothermal treatment was able to remove a significant amount of lignin from OPEFB and Matake bamboo. OPEFB shows lignin removal of 86.0% while Matake bamboo 77.6%, with cellulose yield based on original cellulose content, was calculated to be 69.7 and 64.9%, respectively. Lignin removal and cellulose yield for OPEFB was similar to OPF, and this might be due to similarity in the cellular structure of the same plant. Abdul Khalil et al. reported that cell wall thickness, lumen diameter, and fiber length, and diameter between OPF and OPEFB are similar compared to other structures in the oil palm tree such as OPT [93] Lower lignin removal for Matake bamboo can be attributed to the harder woody structure of the biomass which might affect the treatment efficiency compared to OPF and OPEFB. Differences in the plant cell wall structure and composition between different species would result in different lignocellulosic compositions, and also the character of each biomass under physical or chemical treatment [94]. TG/DTG curve of both OPEFB and Matake shows an appreciable difference in terms of thermal stability and degradation profile before and after treatment. For both biomass, untreated biomass TG/DTG curve shows early degradation onset, with OPEFB showing degradation at around 200°C and Matake at around 250°C, with peak degradation temperature of around 310 and 350°C, respectively. After hydrothermal treatment, the degradation profile shows increased thermal stability, with a single degradation peak at around 350°C for both biomass. This suggests higher cellulose purity and crystallinity which improves its thermal stability. XRD analysis shows a significant increase in Segal crystallinity values for both OPEFB and Matake bamboo after hydrothermal treatment. Reduction of the amorphous peak at 2θ value of 18° is more significant in Matake bamboo compared to both OPEFB and OPF, which can be attributed to the difference in the lignocellulosic structure of the different types of

biomass as stated earlier. FTIR spectrum of both biomass after hydrothermal treatment was compared to commercial MCC as a reference. Both treated biomass shows similar spectra, with small lignin absorption peaks still present. This result supports the compositional analysis result, which shows a small amount of lignin still remains on the biomass after treatment.

3.6 Conclusion

From the result presented in the previous sections, it can be concluded that the hydrothermal treatment using nitric acid can be used as a simple, easy, and appropriate technology in the palm oil mill to remove lignin from biomass. The effect of nitric acid concentration, treatment temperature, and treatment time shows that the optimal parameters for the hydrothermal treatment of OPF were 0.5 M nitric acid, 120°C, and 30 min. The result from one factor at a time experiments also shows that there is a possibility to control the lignocellulosic composition of biomass by controlling the treatment parameters. Properties of treated OPF biomass show low lignin content, with relatively high cellulose content and crystallinity. Optimal hydrothermal treatment conditions were also applied to other types of biomass from the oil palm industry (OPEFB) and bamboo. The treatment successfully removes lignin from both types of biomass, suggesting that the process can be applied to other types of biomass with some parameter optimization. This also shows the versatility of the process in treating biomass without the need for additional chemicals or equipment. This process with a simpler method, no additional pretreatment steps with the use of relatively low concentration of chemical compared to other reported processes in the literature can be a good addition to the arsenal of biotreatments and bioprocesses to utilize waste biomass in the palm oil industry, and in the agricultural industry in general.

CHAPTER 4

COMBINED HYDROTHERMAL AND SUPERHEATED STEAM (SHS) TREATMENT ON BIOMASS

4.1 Introduction

Hydrothermal treatment from the previous chapter has shown the possibility of removing lignin from biomass. While delignified biomass can be used for many purposes such as saccharification and fermentation for the production of biofuel, the remaining hemicellulose content can cause problems especially in the production of biocomposite and nanofibrils from biomass-based cellulose. A study on hemicellulose influence in biocomposite production from wood pulp shows that hemicellulose content of the wood pulp can affect the cellulose aggregation during molding, and in turn affect its strength [95]. Another study by Norrahim et al. also shows that hemicellulose content plays a significant role in the electrospinability of dissolved biomass in ionic liquid [96]. A method to remove or control the hemicellulose content in biomass is needed to better utilize biomass as a cellulose source. SHS treatment is a good candidate due to its use of water as the only chemical, and it can be done in normal atmospheric pressure, which avoids the use of pressure vessels compared to hydrothermal treatment. Many studies on SHS treatment on oil palm biomass have shown that SHS treatment was able to remove hemicellulose from the bulk biomass structure and improves its workability in terms of mechanical pretreatment before usage [97] and usage as raw material in biocomposite and nanofibril production [98]. Due to these reasons, it is hypothesized that combined treatment using SHS to remove hemicellulose, and hydrothermal treatment to remove lignin can produce high purity cellulose from oil palm biomass

Initially, SHS was applied to biomass to remove hemicellulose first and then followed by hydrothermal treatment for lignin removal (SHS→NAAC). This follows the reported method by Nordin et al., where SHS treatment was applied without any pretreatment [90]. Lignocellulosic composition, TGA and FTIR analysis of combined treated SHS/NAAC OPF (OPF-SN) shows that cellulose produced from this process was lower in purity and quality compared to single hydrothermal treatment. To mitigate this problem, the order of treatment was changed, where OPF is hydrothermally treated first before being treated with SHS.

Surprisingly, under the second treatment order, the SHS treatment inadvertently produces biomass that has a novel property of dissolving in NaOH solution at room temperature. The dissolution process was relatively quick at low biomass loading. This chapter will also explore the properties of this combined treated biomass in terms of its solubility and regeneration capability.

4.2 Materials and methods

4.2.1 Sample preparation

For SHS/NAAC combined treatment, the same raw biomass sample from the previous chapter is used without any pretreatment. Collected OPF and Matake bamboo was dried and ground before any SHS or hydrothermal (NAAC) treatments. For NAAC/SHS combined treatment, treated OPF and bamboo samples from previous experiment is used as it is without any pretreatment. Raw biomass was weighed and mixed with 0.5M nitric acid solution at 1:20 biomass weight to acid solution volume ratio. The mixture was autoclaved for 30 min at 120°C, and then cooled and rinsed with deionized water. The treated biomass was then dried before treated with SHS.

Chemicals used for bleaching, dissolution and regeneration experiment such as NaOH, glacial acetic acid, and acetone was supplied by FUJIFILM Wako Pure Chemical Corporation, Osaka, Japan. Sodium chlorite (80%) is sourced from Sigma-Aldrich, Massachusetts, USA. Stock solution was prepared from pure chemical and diluted to required concentrations using deionized water. Deionized water (18.25 MΩ.cm) was obtained from a Milli-Direct 16 Filtration system (MilliporeSigma, Massachusetts, USA).

4.2.2 Superheated steam treatment

Raw and hydrothermally treated biomass (Biomass-NAAC) are weighed before treatment for yield calculation. Weighed raw biomass and Biomass-NAAC were spread thinly on an aluminum foil sheet (~2-3 mm) before SHS treatment. SHS treatment was applied using DC Quto QF-5200C superheated steam oven (Naomoto Corp, Japan) at 265°C superheated steam temperature and 230°C oven temperature for 5 min. SHS temperature was selected based on TGA analysis of raw OPF, with hemicellulose degradation peak was detected at 265°C. The oven temperature was lowered from 265°C to 230°C to avoid excessive thermal degradation based on preliminary experimentations. After SHS treatment, the SHS treated Biomass-NAAC (Biomass-NS) was quickly removed from the SHS oven to avoid runaway thermal degradation and left to cool at room temperature. Biomass-NS was weighed and kept in airtight plastic containers for further analysis and experiments.

SHS treated raw biomass (Biomass-SHS) is cooled and kept in airtight plastic containers before hydrothermal treatment to produce hydrothermal treated Biomass-SHS (Biomass-SN).

4.2.3 Bleaching

Biomass-NS was bleached using sodium chlorite to remove excess lignin and color. The bleaching method was modified from TAPPI Standard method T-222om-88. 4 g of Biomass-NS was weighed and added to a 500 mL beaker. 240 mL of hot water, 3.2 g of sodium chlorite, and 320 µL of glacial acetic acid were added to the beaker. The mixture was agitated continuously at 75°C for 1 hr. After 1 hr, 2.4 g of sodium chlorite and 480 µL of glacial acetic acid were added and mixed at 75°C for another 1 hr. Bleached Biomass-NS (Biomass-NSblc) was rinsed with distilled water and acetone before being dried at 80°C for 24 hr. Dried Biomass-NSblc was collected and weighed for yield calculation.

4.2.4 Fiber dissolution

Biomass-NSblc was added to 5-15wt% NaOH solution at a 1% ratio (fiber:NaOH solution). The mixture was agitated for 40 min at room temperature until all the fiber dissolves completely. Other fiber concentrations (2%-6%) and base solutions were prepared for comparison. Dissolved fiber solution was kept at room temperature for the regeneration experiment.

4.2.5 Cellulose regeneration

10wt% of acetic acid was added to 5 mL dissolved fiber solution under constant mixing until the solution pH reached pH 7. Precipitated regenerated cellulose was then centrifuged for 15 min at 4500 rpm. The supernatant was removed and the regenerated cellulose pellet was rinsed 3 times with 50 mL distilled water to removed excess salts from the neutralization of sodium hydroxide. After rinsing, the regenerated cellulose was freeze-dried for 24 hr and kept in an airtight container at room temperature for further analysis.

4.3 Analysis

Surface structure and morphology were determined using scanning electron microscopy (SEM). Samples were viewed at 1000x magnification using JEOL-9000 SEM/EDX analyzer (JEOL, Japan). Wet sample morphology and extent of dissolution from dissolution experiment was analyzed using 3D laser scanning confocal microscope (LSCM) model VK-X 100 (KEYENCE Corporation, Osaka, Japan). A red semiconductor laser was used as a focusing and imaging light source with a wavelength of 658 nm, power of 0.95 mW, and pulse width of 1 ns. Thermal stability of samples was determined thermogravimetrically using EXSTAR TG/DTA7000 (Hitachi High-Tech, Japan). Samples were analyzed in the temperature range of 100-550°C at 10°C/min heating rate under nitrogen flow. The crystallinity of extracted cellulose was determined using Rigaku X-ray diffractometer with Cu K-α radiation at 40 kV and 15 mA with 2θ range of 3-60° at a scan speed of 20°/min. ^{13}C solid-state cross-polarization, magic angle spinning (CPMAS) NMR spectra of OPF sample after hydrothermal treatment and after SHS treatment was analyzed using JEOL JNM-ECZ-500R spectrometer to determine the change in hydrogen bonding in the OPF. Dry biomass samples were added to zirconia tubes and spun at a 6 kHz spin rate where the NMR spectra were obtained at 75.3 MHz. Surface properties and functional groups of samples at each step of treatment were determined using Fourier transform infrared spectroscopy (FTIR) analyzer. Samples were analyzed via attenuated total reflectance (ATR) method to compare differences in surface functional groups after each treatment step. Sample FTIR spectra were also compared with commercial MCC and its regenerated cellulose.

4.4 Results and discussions

Results and discussions for combined treatment will be presented in two sections. The first section will discuss SHS/NAAC treatment order, and followed by NAAC/SHS treatment order.

4.4.1 SHS/NAAC treatment order

4.4.1.1 Lignocellulosic composition and yield

Table 4.1: Lignocellulosic composition of OPF-SHS and OPF-SN

	Composition (%)			
	Lignin	**Cellulose**	**Hemicellulose**	**Extractive**
Raw OPF	21.7 ± 1.0	32.6 ± 1.2	31.6 ± 1.2	14.1 ± 0.1
OPF-SHS	44.0 ± 0.8	24.2 ± 4.0	31.8 ± 4.0	ND
OPF-SN	10.0 ± 0.2	45.7 ± 0.7	44.3 ± 0.7	ND

Lignocellulosic composition of OPF after treatment with SHS and combination of SHS and hydrothermal method is shown in **Table 4.1**. It is hypothesized that the treatment using SHS will reduce the hemicellulose content of the biomass, which will, in turn, produce higher purity cellulose after hydrothermal treatment. The compositional analysis result shows that it is not the case, with hemicellulose content of SHS treated OPF is at a similar value with raw OPF. Cellulose degradation on the other hand was significant, with cellulose content decreased from 32.6% to 24.2%, a reduction of about 25%. This is contrary to other reported research where SHS treatment of OPMF successfully reduces hemicellulose content. This can be attributed to the difference in the temperature used and the treatment time. Nordin et. al. reported successful hemicellulose reduction from OPMF using SHS treatment at 210°C for 1 hr, which is significantly longer than what is applied in the study [90].

In addition to the significant degradation of the cellulose component, the lignin content of the biomass after SHS also shows a significant increase compared to raw OPF. This can be attributed to the development of pseudo-lignin in the bulk structure and the surface of the biomass during SHS treatment. Degradation of the cellulose polymer and dehydration of glucose monomers produced 5-hydroxymethylfurfural (5-HMF) and other subsequent formaldehyde, which in turn re-polymerize into an insoluble polymer. This polymer can increase the apparent lignin content of biomass after thermal and thermochemical treatment, especially in acidic conditions [81]. Direct production of pseudo-lignin from glucose, fructose, and 5-HMF [99] and pseudo-lignin development on birch wood after steam explosion has been reported [100] which suggests that other steam-based treatments such as SHS can cause pseudo-lignin to be developed in the biomass post-treatment.

For combined treated OPF-SN, it can be seen that the increased apparent lignin content of the biomass does not affect the lignin degradation efficiency of the hydrothermal process. On the other hand, the hemicellulose and cellulose fractions show a similar amount per unit mass, suggesting that both components do not degrade during hydrothermal treatment. In addition to that, cellulose yield for OPF-SN shows a similar value with OPF-NAAC, but hemicellulose content for OPF-SN is significantly higher. An increase of apparent lignin content affects the hydrothermal treatment, where the increased lignin content reduces the degradation of hemicellulose fraction compared to OPF-NAAC.

Based on the lignocellulosic composition analysis, it can be concluded that SHS treatment negatively impacted the subsequent hydrothermal treatment through an increase in apparent lignin content and reduced efficiency of the hydrothermal process in removing hemicellulose component from biomass.

4.4.1.2 SEM micrograph

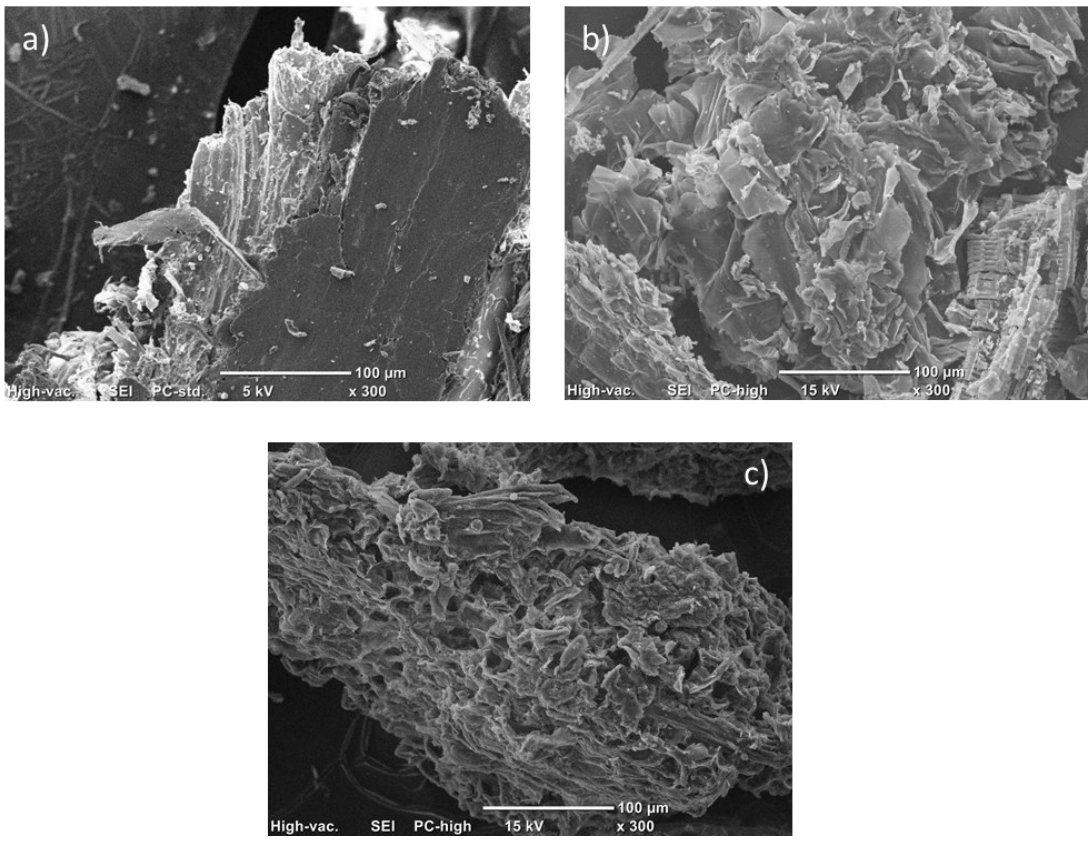

Figure 4.1: SEM micrograph of a) raw OPF, b) OPF-SHS and c) OPF-SN

SEM micrograph of raw OPF, OPF-SHS, and OPF-SN is shown in **Figure 4.1**. It can be seen that consecutive treatments of SHS followed by hydrothermal treatment affect the surface and bulk structure of the OPF biomass significantly. After SHS treatment, the surface of the OPF biomass was cracked and damaged. This can be attributed to the drying of the surface, followed by the internal biomass structure. The high thermal energy of SHS has been used extensively as a method of drying [101], with very high drying efficiency. Differences in moisture content between the surface and the inside of the biomass can introduce stresses that can damage the biomass structure. The subsequent hydrothermal treatment further increases the damage that can be seen from the OPF-SN SEM micrograph, through the removal of the lignin component as shown in the previous section.

4.4.1.3 FTIR analysis

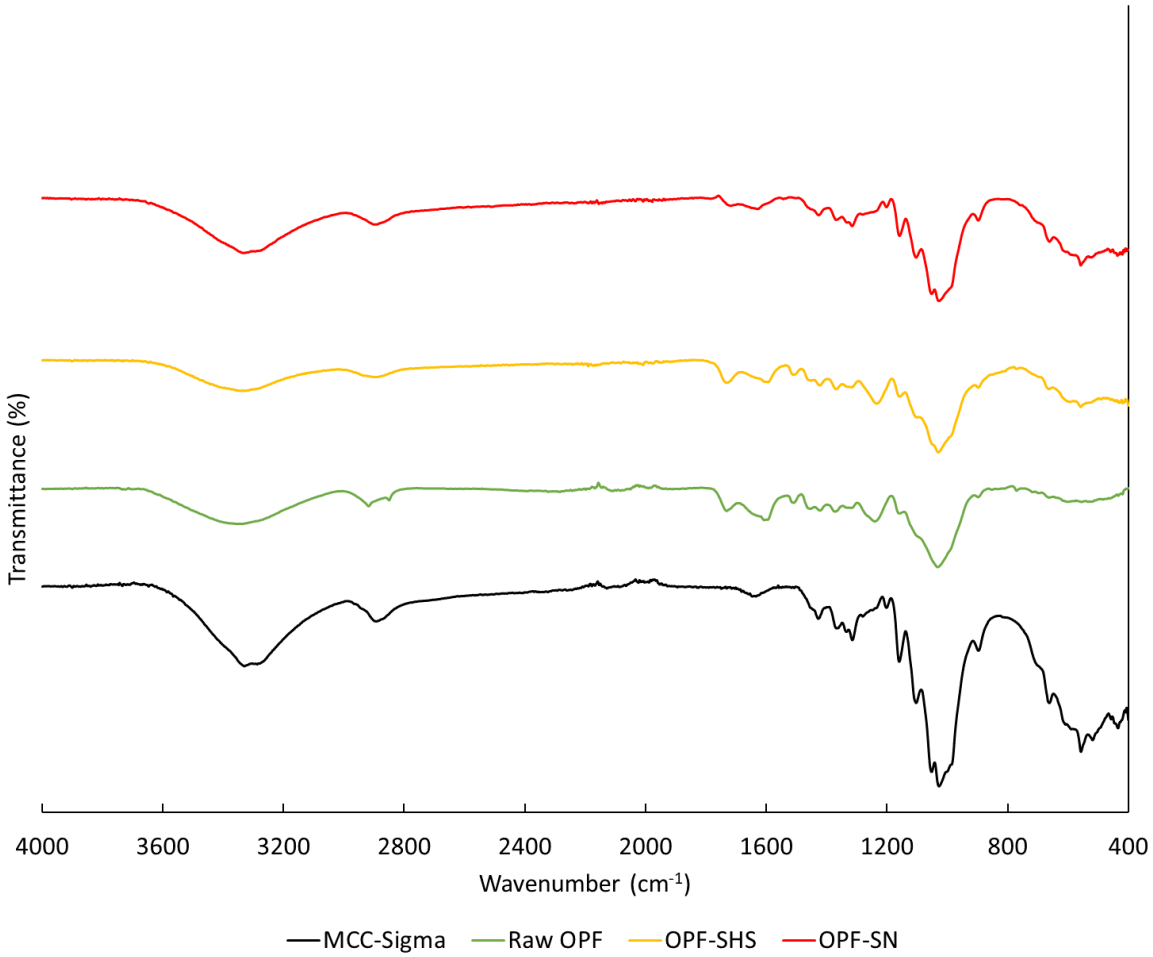

Figure 4.2: FTIR spectra of MCC, Raw OPF, OPF-SHS and OPF-SN

FTIR analysis of sample after single hydrothermal and combined hydrothermal and SHS treatment is shown in **Figure 4.2**. From the spectra, it can be seen that the SHS treatment does not significantly change OPF-SHS surface chemical properties compared to raw untreated OPF. This suggests that the SHS treatment does not change the surface properties of the biomass significantly, while the heat energy from the SHS degrades the components of the biomass, as shown by the reduction of cellulose content from the lignocellulosic compositional analysis. Peaks attributed to lignin such as aromatic C=C stretching (1505 cm^{-1}), aryl C-O stretching (1235 cm^{-1}), and carbonyl C=O stretching (1730 cm^{-1}) does not show any changes related to the

development of pseudo-lignin, but this might be due to overlapping peaks of glucose-derived pseudo-lignin peaks such as peaks at 1625 and 1710 cm^{-1} as previously reported [99]. OPF-SN on the other hand, shows a significant difference compared to OPF-SHS, with lignin-related peaks decrease and characteristic cellulose peaks increases. Carbonyl peaks at 1600-1700 cm^{-1} range show a significant decrease, but not as significant as single hydrothermal treated OPF. This suggests that the presence of pseudo-lignin might reduce the efficiency of the process, as shown through compositional analysis. An increase in treatment time or concentration of nitric acid might be able to remove more lignin but might result in more cellulose and hemicellulose degradation.

4.4.1.4 TGA analysis

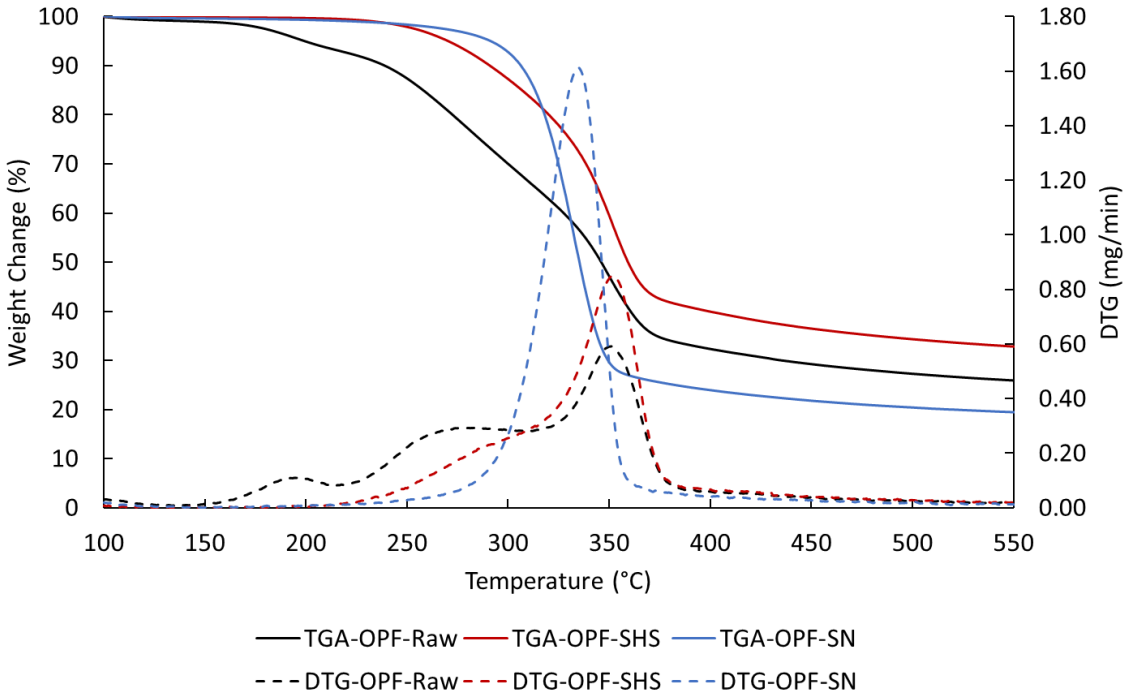

Figure 4.3: TG/DTG curve of raw OPF, OPF-SHS and OPF-SHS

TG/DTG curve of raw OPF, OPF-SHS, and OPF-SN is shown in

Figure 4.3. From the DTG curve of OPF-SHS, it is apparent that there are some hemicellulose degradations after SHS treatment, where degradation peak at around 265°C has decreased after SHS treatment compared to raw OPF. Cellulose degradation peak also increased compared to raw OPF which suggests higher thermal stability of the cellulose fraction after SHS treatment. This might be due to the degradation of the amorphous cellulose fraction that contributes to pseudo-lignin production. After subsequent hydrothermal treatment, the hemicellulose peak was removed from the DTG curve, with an increased degradation rate of cellulose component, suggesting higher cellulose content. The peak degradation temperature also shifted to a lower temperature compared to OPF-SHS, from 350°C to 330°C. This can be due to smaller OPF-SHS particle size after SHS treatment as shown in the SEM micrograph in **Section 4.4.1.2**.

Based on the SEM, TGA, FTIR, and lignocellulosic composition analysis, it can be concluded that the SHS/NAAC treatment order is not ideal in producing high purity cellulose from biomass. The degradation of cellulose and hemicellulose components of the biomass during SHS even at relatively lower temperature and treatment time introduces pseudo-lignin which negatively affects the subsequent removal of lignin and cellulose yield during subsequent hydrothermal treatment. The resulting biomass also still contains a relatively high percentage of hemicellulose compared to single hydrothermal treatment, which might affect its usability in the next processing steps, especially in the production of biocomposites [102] and cellulose fibers through electrospinning [98]. Due to these results, the treatment order was changed where hydrothermal treatment was applied first, before SHS treatment. Results regarding the process order will be presented in the next sections.

4.4.2 NAAC/SHS treatment order

Due to the negative impact SHS treatment has on hydrothermal treatment of biomass, the treatment order was changed where biomass is hydrothermally treated first, before being treated with SHS. A similar process method was applied without any major changes from the previous section. Surprisingly, combined treated biomass with NAAC/SHS order (Biomass-NS) has the novel property of dissolving in NaOH at room temperature. The process was applied to both OPF and Matake biomass to determine the process applicability towards other types of biomass. The physical properties of both OPF-NS and Matake-NS and their dissolving and regeneration properties were explored and presented in the next sections of this chapter.

4.4.2.1 SEM micrograph

Biomass-NAAC, Biomass-NS, and Biomass-NSblc surface morphology were analyzed via SEM to determine any changes in the bulk structure of the biomass at each step of treatment. **Figure 4.4** shows the SEM micrograph of OPF and Matake bamboo at each treatment step.

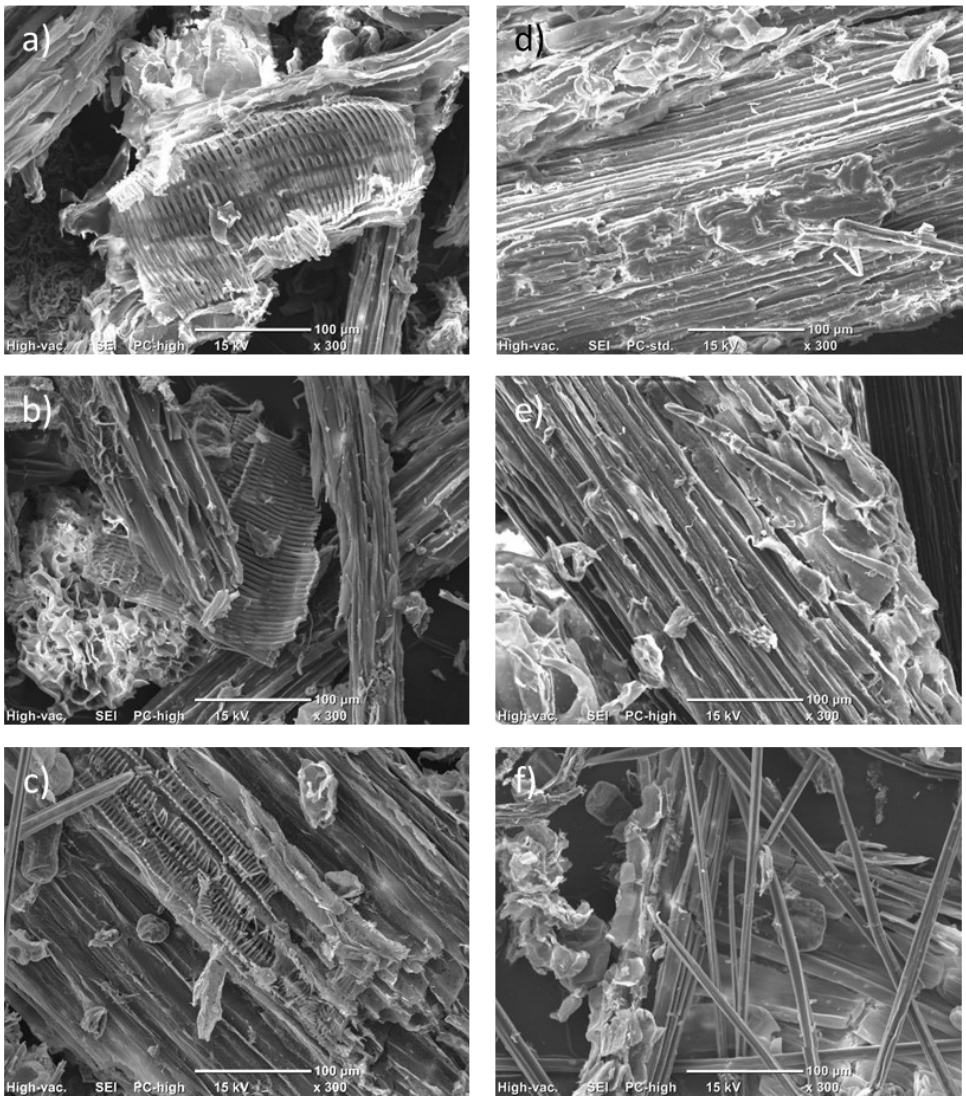

Figure 4.4: SEM micrographs of a) OPF-NAAC b) OPF-NS, c) OPF-NSblc d) Matake-NAAC e) Matake-NS and f) Matake-NSblc

From the SEM micrograph, it can be seen that each treatment affects the bulk structure differently. For OPF, OPF-NAAC shows fibrillation of the biomass has started to occur. This can be attributed to the degradation of the lignin backbone that holds the macrostructure of the OPF biomass together. Particle size was also much smaller compared to the original raw OPF, as shown in the previous chapter. This provides additional surfaces for the SHS treatment to act upon which improves the process efficiency. After SHS treatment, OPF-NS shows a similar structure to OPF-NAAC, which suggests the treatment does not change the bulk structure significantly. This is expected since the treatment was at a temperature lower than the degradation temperature of cellulose, and at a relatively short time of 5 min. After the bleaching step, more fibrillation can be observed due to additional degradation of the biomass. This can be due to degradation by sodium chlorite as it can also degrade cellulose and hemicellulose components [103]. But based on the yield calculated in **Section 4.4.1.1**, the degradation is not significant. Besides degradation by sodium chlorite, size reduction can also be attributed to the mechanical action of mixing during the bleaching step. This can mechanically separate and cut the fibers, which results in the reduction of the fiber size as seen in the SEM micrograph. Comparing OPF and Matake samples, a similar conclusion can be drawn, with differences in the bleached Matake samples where fibrillation is more pronounced, with single fibers present. These differences can be attributed to the different cellular structures of OPF and Matake bamboo even though both of them are monocotyledon-type plants. Bamboo cells are constructed into distinct fibrovascular bundles which results in long strands of fiber shown in the SEM micrograph [104], while OPF and other oil palm fibers closely resemble wood cells with various sized vascular bundles covered in thin-walled parenchymal ground cells [93]. The lack of significant change on the bulk structure of

the OPF and Matake fiber after SHS shows that the process improves fiber solubility in NaOH solution through changes in surface functional groups or mild degradation of lignocellulosic components such as hemicellulose and cellulose that helps improves solubility.

4.4.2.2 TGA Analysis

TGA analysis of Biomass-NAAC, Biomass-NS, and Biomass-NSblc was done to determine its thermal degradation properties. Through this analysis, the purity of the biomass at each treatment step can be deduced and compared with the combination of other analysis data. The degradation data can also give some information regarding the thermal stability of the biomass, which can be used to infer its purity in terms of lignocellulosic composition, and also its particle size. **Figure 4.5** shows the TG/DTG curve of OPF samples while **Figure 4.6** shows TG/DTG curves for Matake bamboo samples.

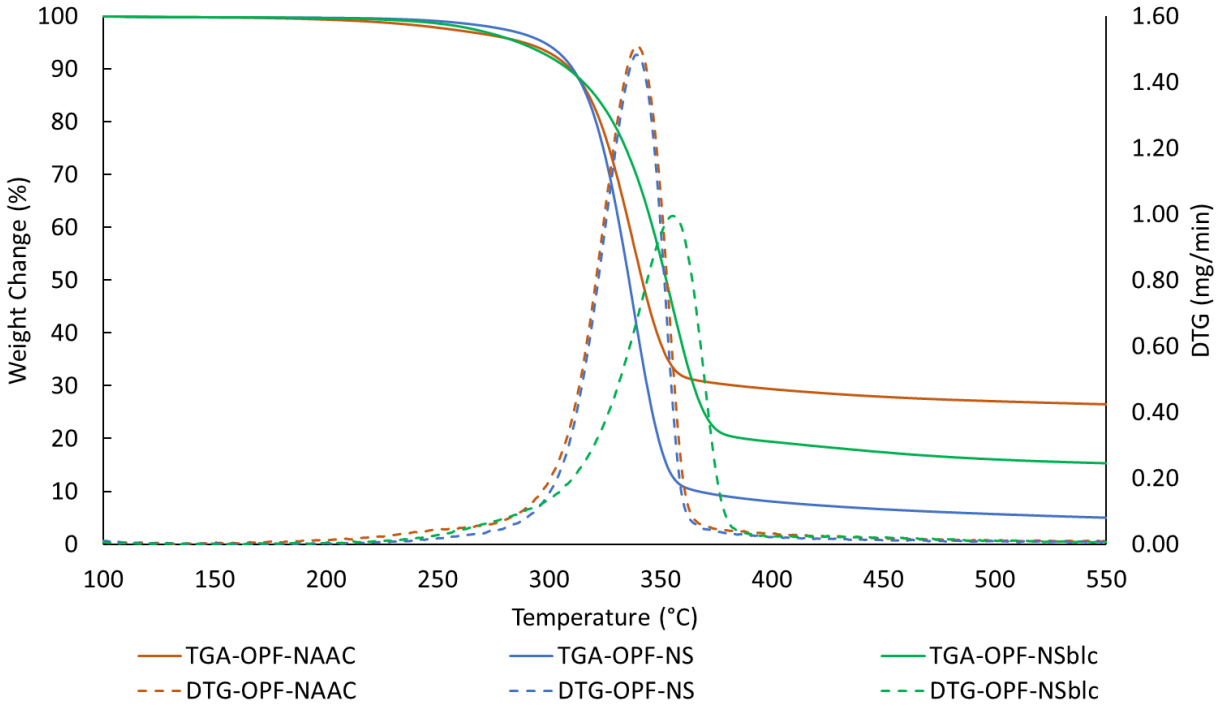

Figure 4.5: TG/DTG curve of OPF-NAAC, OPF-NS and OPF-NSblc

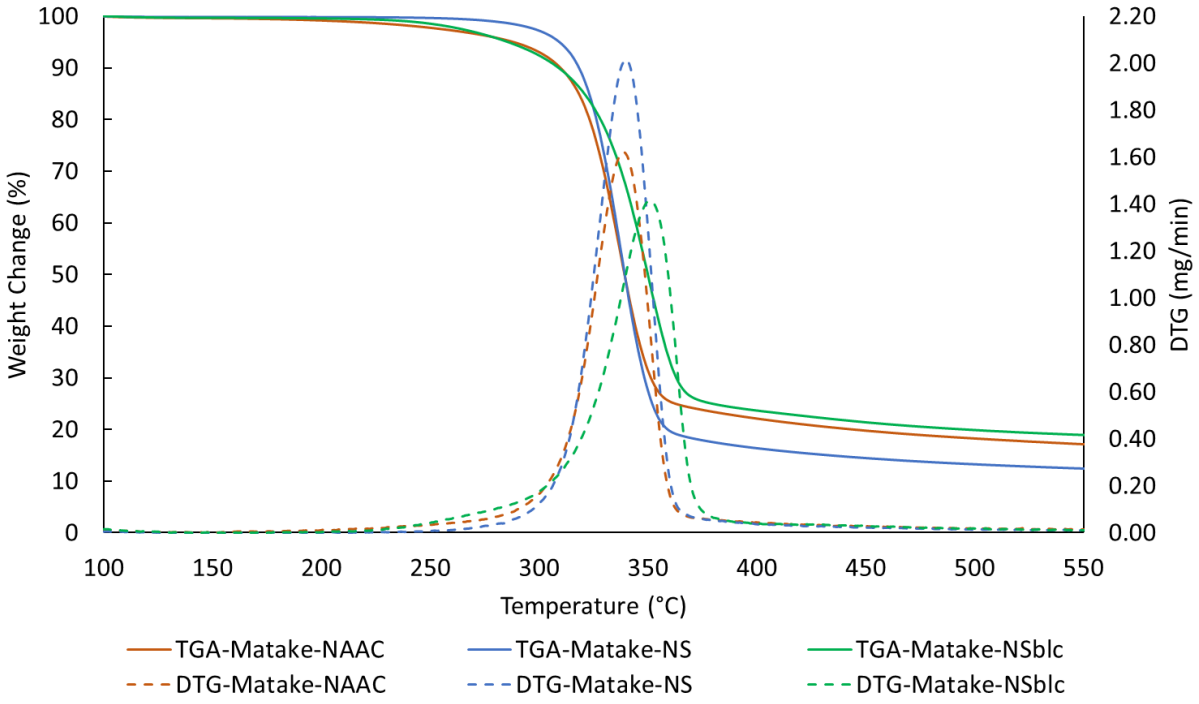

Figure 4.6: TG/DTG curve of Matake-NAAC, Matake-NS, and Matake-NSblc

Based on the TG/DTG curve of both biomass types, it can be concluded that the SHS treatment does not change the composition of the biomass, where the peak degradation temperature after SHS treatment and after bleaching step is around 345-350°C. However, both OPF and Matake bamboo samples show increase thermal stability after bleaching steps, which suggests the removal of SHS pyrolyzed byproduct which was low molecular weight compounds from previous treatment steps improves the purity of the cellulose fraction, hence its thermal stability [105]. After SHS treatment, both OPF and Matake bamboo show no significant difference in peak thermal degradation temperature and degradation rate. Even though hemicellulose degradation might occur at the temperature of SHS treatment as reported previously [90,97], the short treatment time, low steam power, and lower oven temperature compared to the previously reported methods might inhibit volatilization of the hemicellulose degradation by-products which leads to similar thermal degradation behavior.

4.4.2.3 FTIR analysis

FTIR analysis of Biomass-NAAC, Biomass-NS, and Biomass-NSblc was conducted to determine if there is any significant change in the surface functional groups of the biomass after each treatment step. The spectra of all samples are shown in **Figure 4.7** and

Figure 4.8.

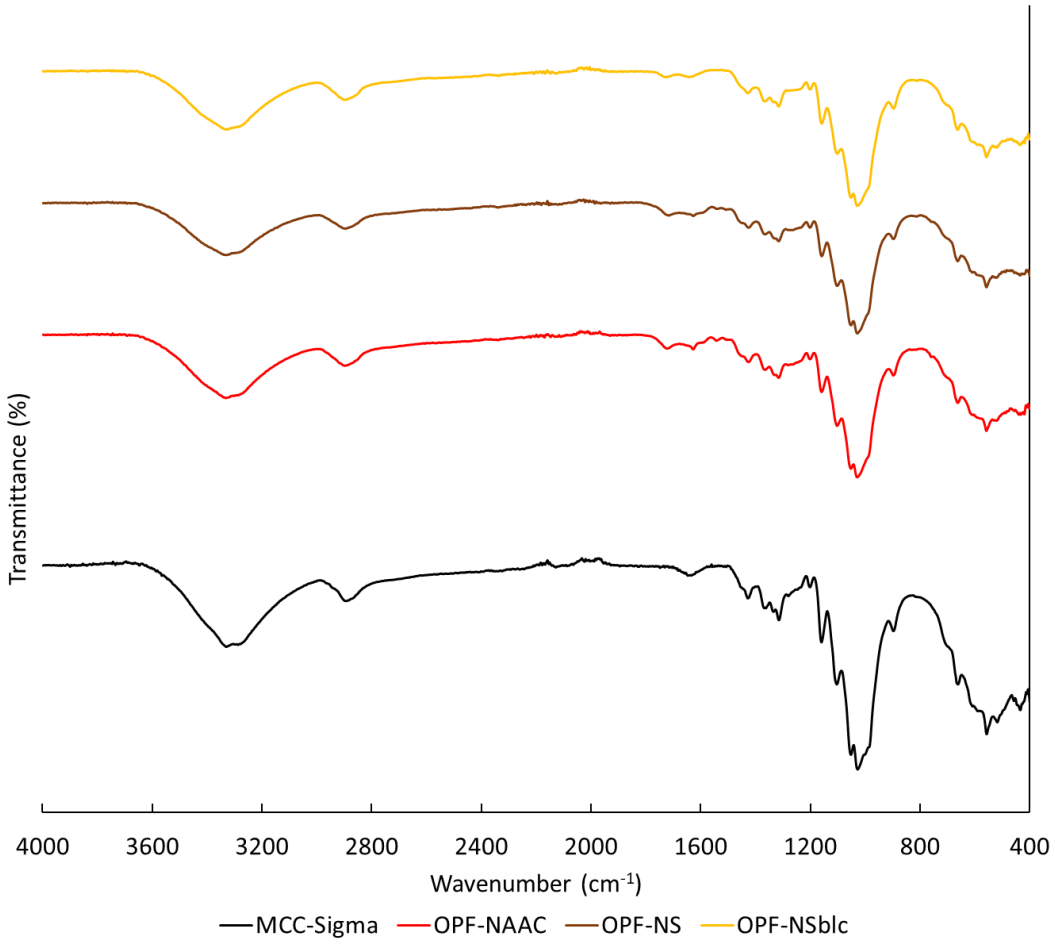

Figure 4.7: FTIR spectra of OPF-NAAC, OPF-NS, OPF-NSblc, and commercial MCC

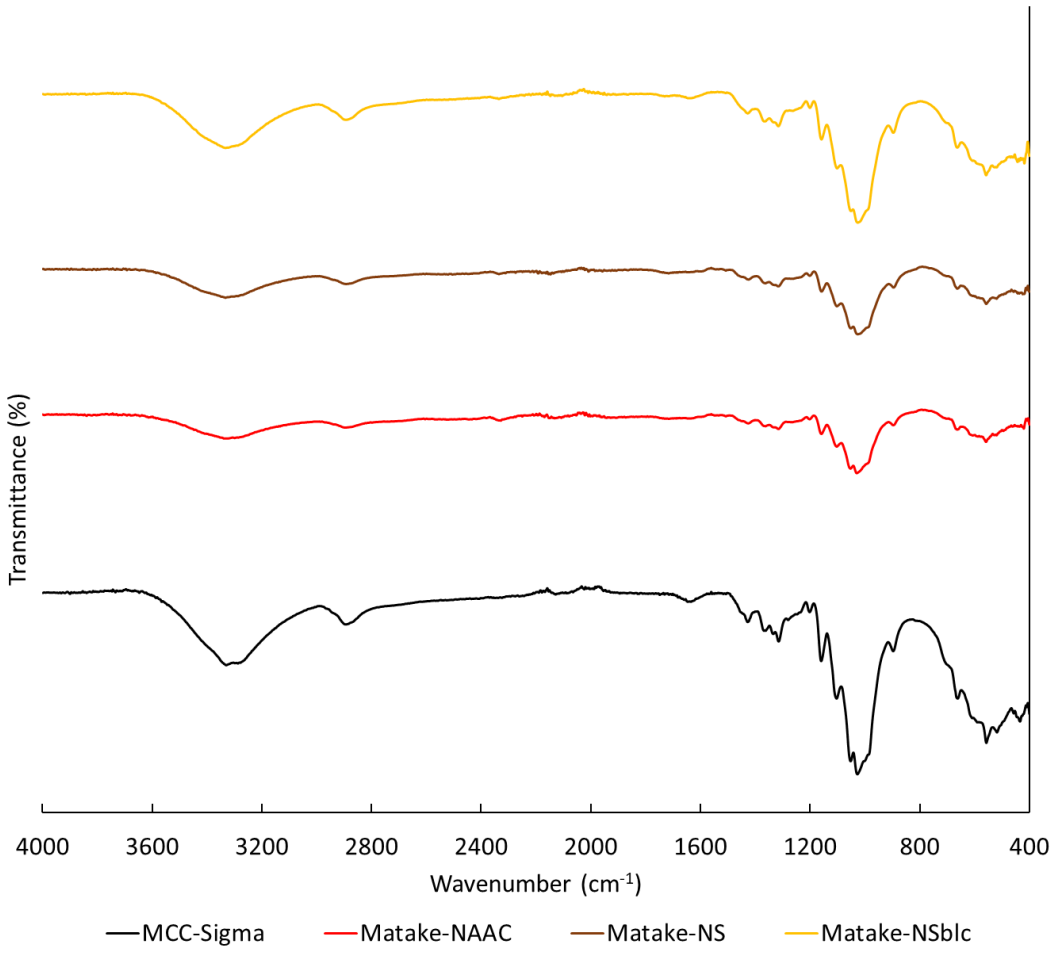

Figure 4.8: FTIR spectra of Matake-NAAC, Matake-NS, Matake-NSblc, and commercial MCC

Based on the FTIR spectra of both OPF and Matake, there are no significant changes on the surface of the biomass after SHS and bleaching treatment. Compared to initial NAAC samples, the SHS treated samples spectra are relatively the same. The peaks seen in the NAAC samples as explained in the previous chapter are present after SHS treatment. Peaks related to lignin such as peaks at aromatic C=C stretching (1505 cm^{-1}), aryl C-O stretching (1235 cm^{-1}) and carbonyl C=O stretching (1730 cm^{-1}) [90] is still present after SHS treatment and reduced after bleaching treatment with sodium chlorite. Peaks related to cellulose such especially in the fingerprint region shows increase absorption after bleaching especially for Matake bamboo samples.

4.4.2.4 XRD analysis

XRD analyses were done on both OPF and Matake bamboo samples to see whether the SHS treatment change the crystal structure of the cellulose and to determine the crystallinity of the cellulose fiber. **Figure 4.9** and **Figure 4.10** show the XRD patterns of the biomass samples and comparison with commercial MCC. **Table 4.2** shows the Segal crystallinity index (CrI) values calculated from the XRD data.

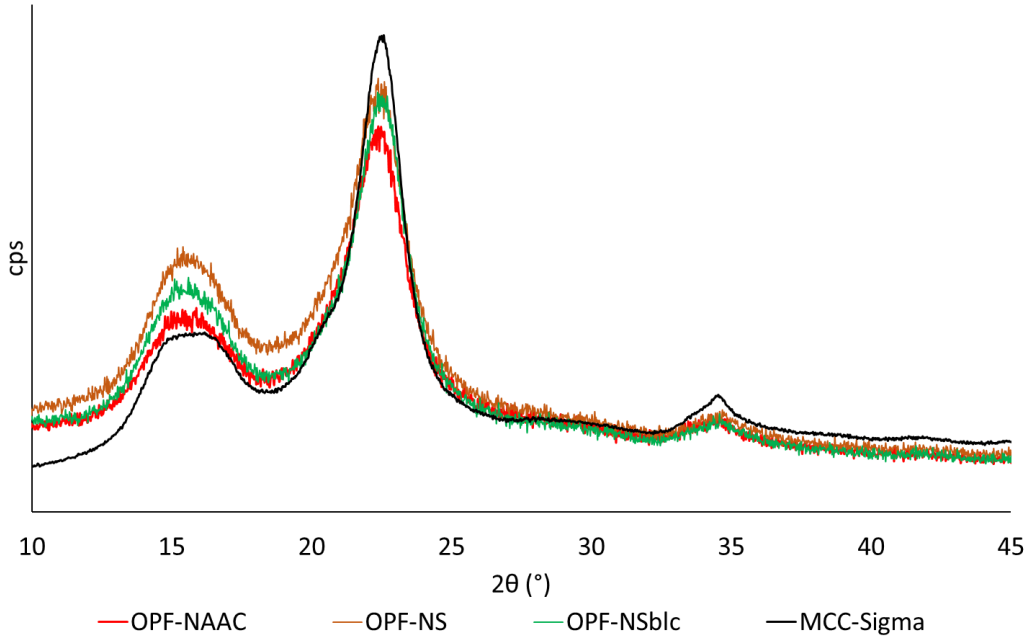

Figure 4.9: XRD pattern of OPF-NAAC, OPF-NS, OPF NSblc, and commercial MCC

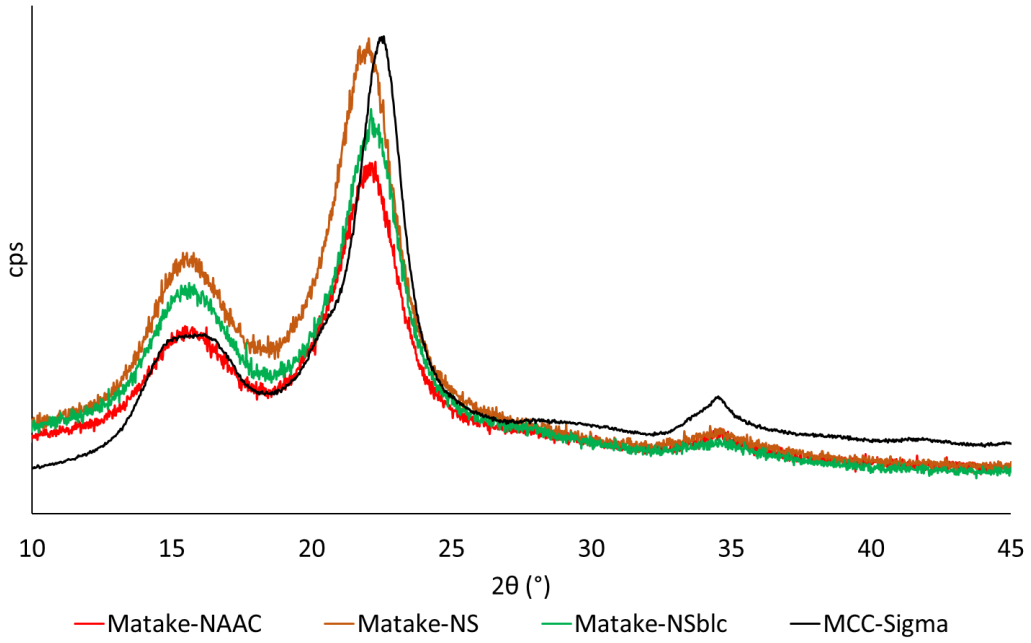

Figure 4.10: XRD pattern of Matake-NAAC, Matake-NS, Matake-NSblc, and commercial MCC

Table 4.2: Segal crystallinity index of OPF and Matake samples

Sample	OPF				Matake		
	MCC-Sigma	**NAAC**	**NS**	**NSblc**	**NAAC**	**NS**	**NSblc**
CrI (%)	77.7	65.2	61.7	65.7	64.4	65.4	65.5

Based on the XRD pattern, it can be seen that the SHS treatment slightly increases the amorphous peak height at 2θ=18°. This might be due to the SHS treatment degrading some of the hemicellulose and cellulose crystal structure, reducing its crystallinity. This is much apparent in the OPF where the CrI value decreases by 4% after SHS treatment. Reduction of the cellulose degree of polymerization (DP) might also contribute to the increase of amorphous structure in the biomass after SHS treatment. This behavior has been reported by Megashah et al., where SHS treatment on OPEFB derived cellulose affect its DP at different treatment time [102]. However, the increase in the amorphous peak was not accompanied by a decrease in crystalline peak at 2θ=22°, which suggests that the SHS treatment affects the hemicellulose component more compared to cellulose. This is supported by the XRD pattern of bleached samples, where the amorphous peak decrease, indicating that the bleaching treatment removes some of the degraded hemicellulose components of the biomass.

4.4.2.5 Nuclear magnetic resonance (NMR) spectroscopic analysis

^{13}C NMR spectra can shine some light on the strength of hydrogen bonding of the cellulose, through the change in chemical shift values of the carbons in the cellulose. The assignment of chemical shift values of each peak in cellulose can be referred to

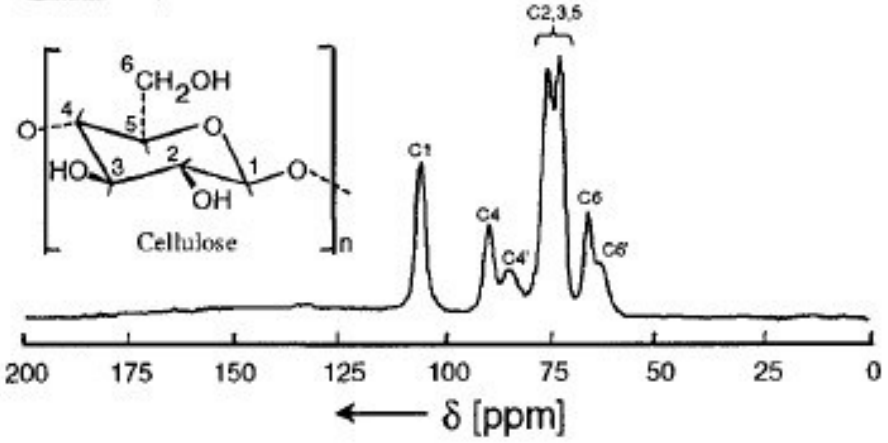

Figure 4.11.

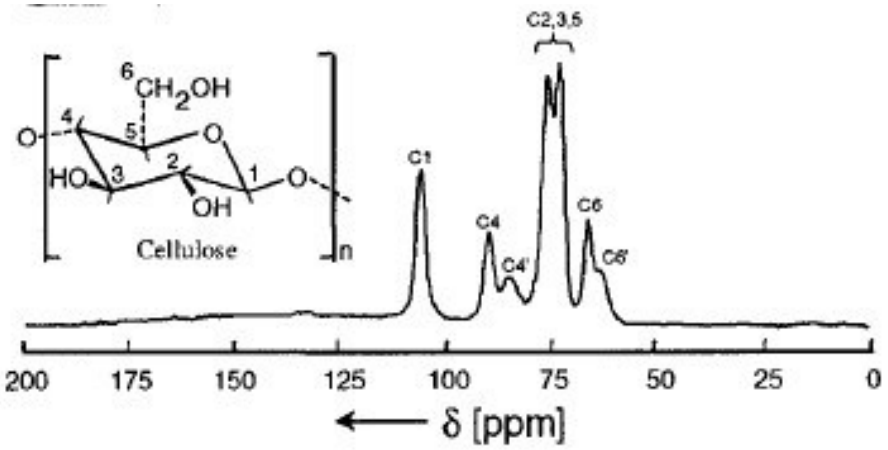

Figure 4.11: Chemical shift assignment for cellulose [106]

It is widely accepted that the hydrogen bonding interaction of cellulose macrostructure can be divided into 3 different interactions [107]. First, intra-chain hydrogen bonding, between oxygen and hydrogen atoms bonded to C2, C3, C5, and C6 and highlighted in blue in **Figure 4.12**. Reduction of these hydrogen bonds strength will rearrange and increase electron cloud density around C2 and C3 carbons, resulting in an upfield shift (decreasing value) of its chemical shift value. Second, inter-chain hydrogen bonding, involving C3 and C6 carbon is highlighted in red. The reduced strength of these

hydrogen bonds will result in a downfield shift (increasing value) of its chemical shift values [108,109]. Finally, inter-sheet hydrogen bonding, which can be deduced through the chemical shift values of C1 and C4 carbons. This hydrogen bonding interaction might be affected by the strength of hydrogen bond between hydrogen atoms on C4 carbon and oxygen atoms on C2 carbon [110], and the orientation of the cellulose polymer with respect to the β(1→4) glycosidic bond, specifically the torsional angle ϕ which correlates well with the C1 chemical shift values. Changes towards C1 chemical shift values would suggest the rotational shifting of cellulose monomers with respect to the glycosidic bonds, which in turn affect the inter-sheet distance and hydrogen bonding strength. With the decrease in hydrogen bonding strength, we should see an upfield shift (decreasing value) of C1 and C4 peaks [111,112].

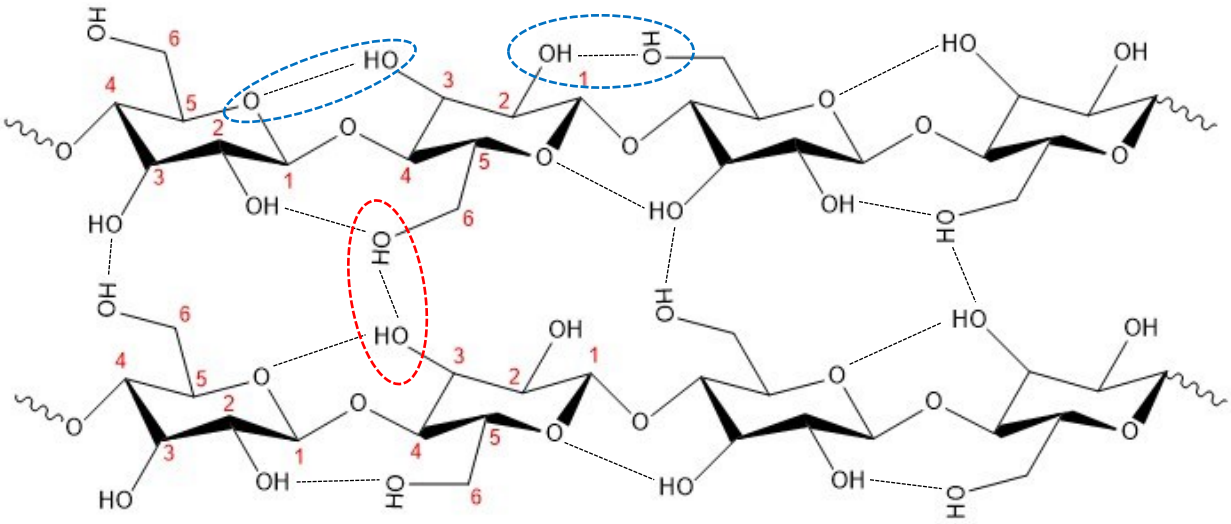

Figure 4.12: Molecular representation of cellulose polymer chain. Dashed line represents hydrogen bonding between oxygen and hydrogen atoms in the cellulose polymer.

From the NMR spectra of OPF-NAAC and OPF-NS, it can be seen that there is some decrease in hydrogen bonding strength of the cellulose after SHS treatment, especially in intra-chain and inter-sheet interaction. Chemical shift values of OPF-NAAC and

OPF-NS can be referred to in **Table 4.3**. This can be seen from the chemical shift values of the OPF sample before and after SHS treatment. Inter-sheet hydrogen bonding strength reduction is the highest, with a C1 chemical shift decrease from 105.71 to 105.47. This suggests that the SHS were able to enter the fibers of the biomass and reduce the hydrogen bonding between large sheets of cellulose polymers in the biomass. This correlates well with the result of the dissolution of the cellulose fiber in NaOH at different cellulose loading (**Section 4.4.2.8**), where at higher cellulose loading, more fiber can be seen in the microscope image. The fiber seen in the microscope images was translucent, suggesting very thin layers or sheets of cellulose were separated, but not completely dissolves. Decrease in C2, 3, 5, and C4 chemical shifts suggest a reduction of intra-chain hydrogen bonding strength and redistribution of electron cloud density between C4 and C5 respectively, which contributes to the decrease in inter-sheet hydrogen bonding strength. C6 chemical shift does not change after SHS treatment, which suggests that inter-chain hydrogen bonding was not disrupted, which also explained the observation in **Section 4.4.2.8.**

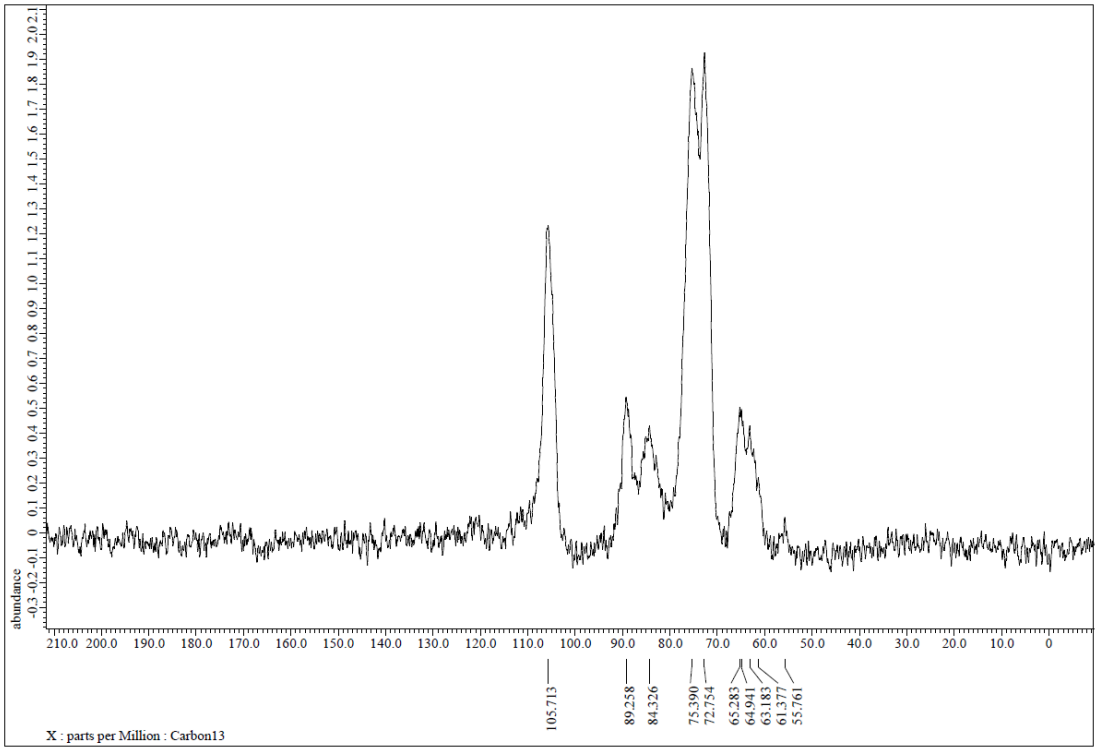

Figure 4.13: ^{13}C NMR spectra of OPF-NAAC

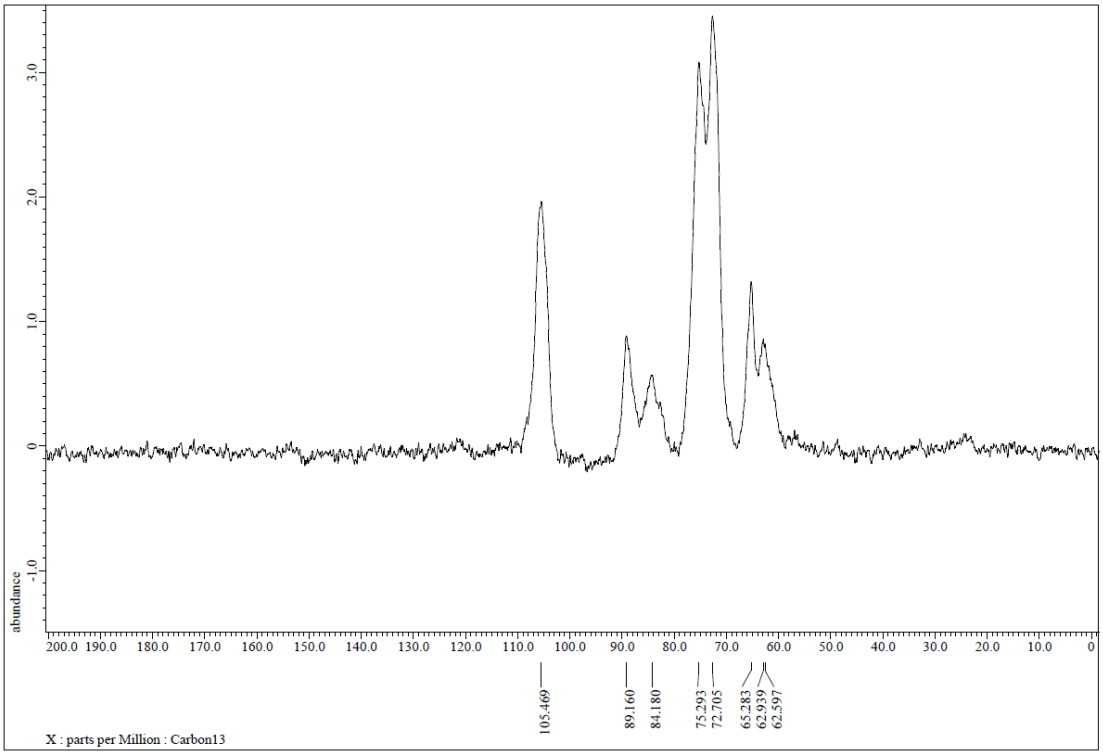

Figure 4.14: ^{13}C NMR spectra of OPF-NS

Table 4.3: Chemical shift values of OPF-NAAC and OPF-NS

Sample	Chemical shift,δ (ppm)			
	C1	**C2,3,5**	**C4**	**C6**
OPF-NAAC	105.71	75.39, 72.75	89.26	65.28
OPF-NS	105.47	75.29, 72.70	89.16	65.28

4.4.2.6 Solubility of biomass after SHS treatment

Solubility of hydrothermally treated biomass after treatment with SHS was studied to determine the reasoning behind the change in properties. Alpha-cellulose is not soluble in sodium hydroxide solution, and this property was used in TAPPI analysis where beta-cellulose (hemicellulose) that will dissolve in NaOH is removed to gravimetrically determine the cellulose content of biomass. Hydrothermally treated biomass was found to be able to dissolve in NaOH solution after SHS treatment to produce a stable solution.

Figure 4.15 and **Figure 4.16** shows comparison pictures and microscope images of OPF at different treatment steps and its solubility in 10% NaOH solution. Several experiments were conducted to determine the solubility of biomass using different parameters to try to tease out the reason behind this novel property.

Figure 4.15: OPF biomass in 10wt% NaOH solution. From left: Raw OPF, OPF-NAAC, OPF-NS, OPF-NSblc

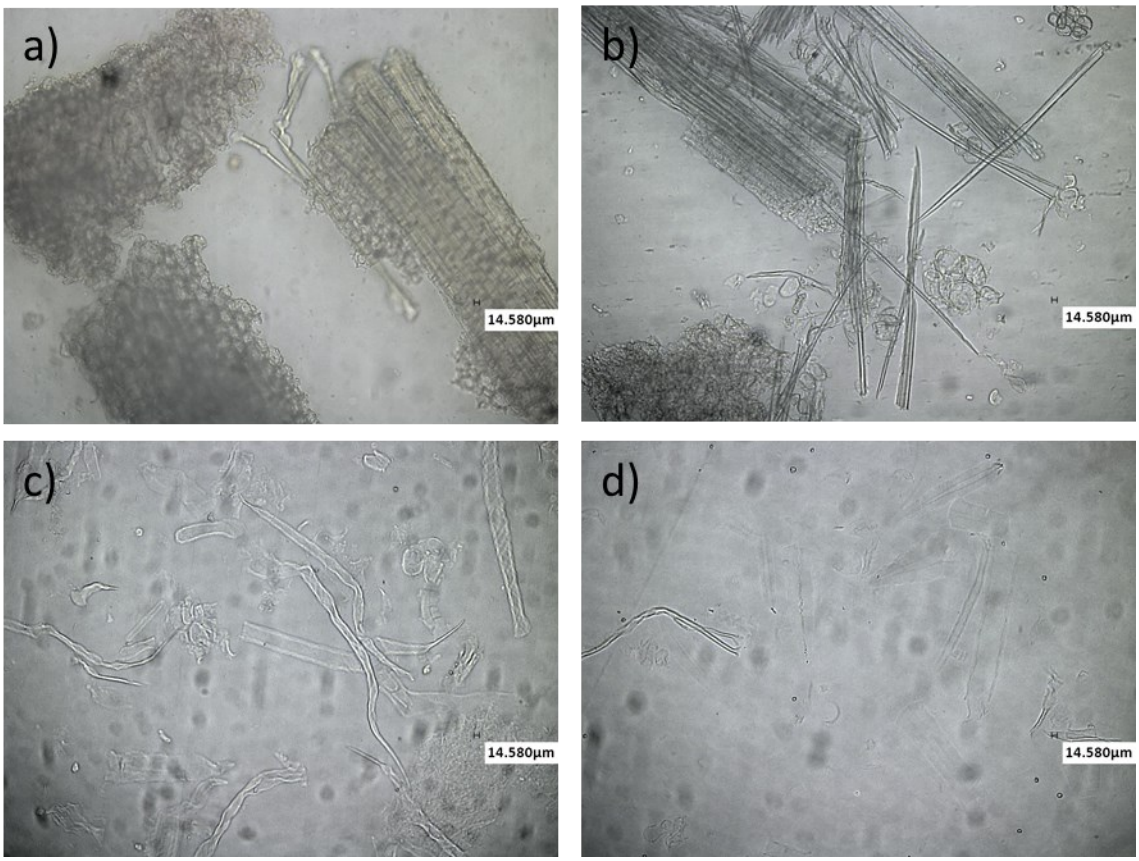

Figure 4.16: Microscope images of a) Raw OPF, b) OPF-NAAC c) OPF-NS and d) OPF-NSblc in 10wt% NaOH solution at 1% fiber loading

4.4.2.7 Effect of NaOH concentration

OPF-NSblc was added to different concentrations of NaOH solution to determine whether the dissolution process was affected by the amount of NaOH in the solution or the process was affected by pH. The resulting solution pictures and microscope images are as shown in

Figure 4.17 and **Figure 4.18** below.

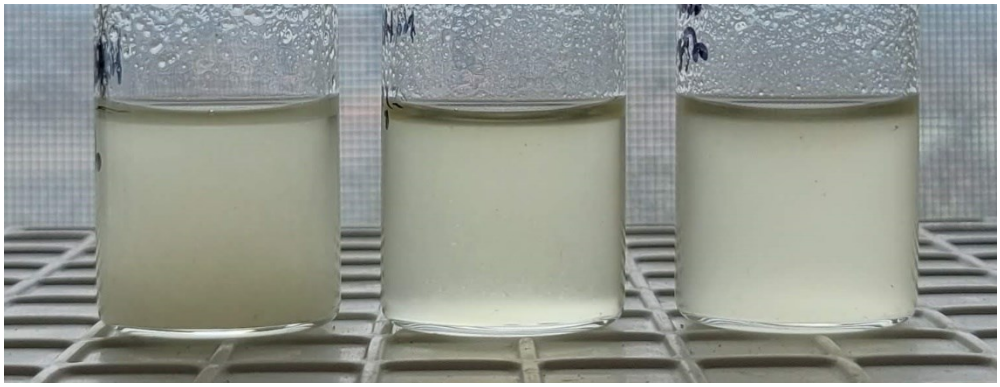

Figure 4.17: Solubility of OPF-NSblc in different NaOH concentration solutions. From left: 5wt%, 10wt% and 15wt%

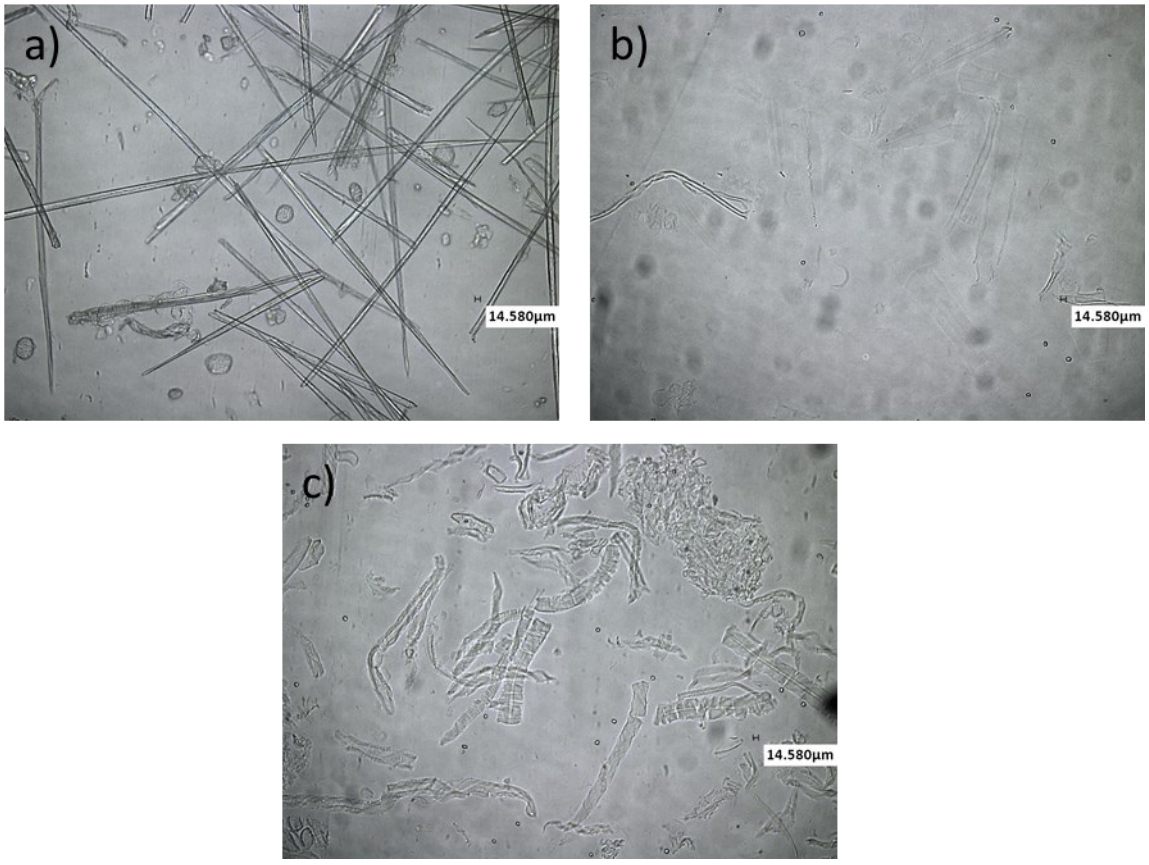

Figure 4.18: Microscope images of OPF-NSblc in a) 5wt% NaOH b) 10% NaOH and c) 15wt% NaOH solution

From visual observation, OPF-NSblc was able to dissolve to a degree in 10wt% and 15wt% NaOH solution but failed to dissolve in 5wt% NaOH solution. This suggests that the process requires a minimum amount of dissolved NaOH in the solution to properly dissociate the cellulose fiber into the solution. There is also a slight difference in solubility between 10% and 15% NaOH solution where OPF-NSblc dissolves in 15wt% NaOH solution is cloudier compared to the 10wt% NaOH solution. Microscope images of 10wt% and 15wt% NaOH solution also show more undissolved particles in the 15wt% solution compared to the 10wt% solution. Similar results were reflected in the cold alkali process reported by Yamashiki et al. where the dissolution of specially prepared cellulose with NaOH at below 4°C happens at about 2.5 mol/L of NaOH concentration, which corresponds to about 10wt%. The major difference between the reported processes was the cellulose needs to be specially prepared to break down intramolecular hydrogen bonds in the cellulose crystal using mechanical processing. The process also requires low temperatures to achieve dissolution and the use of strong mixing for a long time (8 hr)[113]. Combined hydrothermal and superheated steam treatment was able to produce cellulose that can dissolve in NaOH solution at room temperature relatively quickly (1 hr).

4.4.2.8 Effect of fiber loading

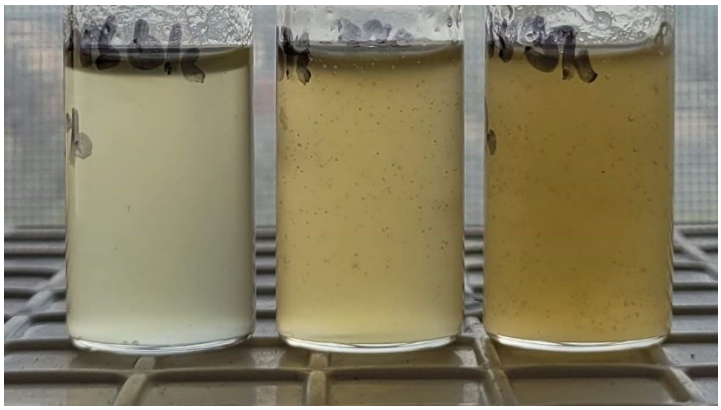

Figure 4.19: Solubility of OPF-NSblc at different fiber loading. From left: 2%, 4%, and 6% (w/v)

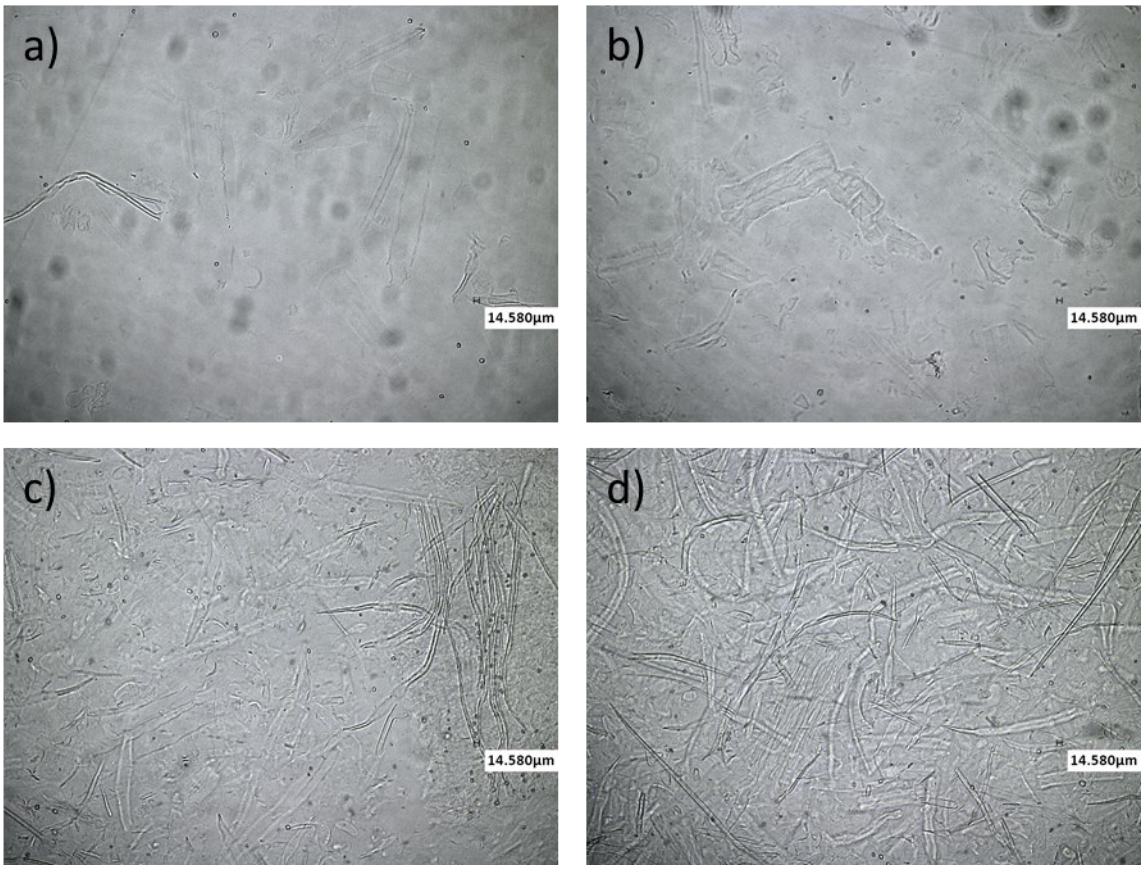

Figure 4.20: Microscope images (x10) of OPF-NSblc in 10wt% at different fiber loading: a) 1% b) 2% c) 4% and d) 6% (w/v)

OPF-NSblc solubility in NaOH solution decreased as the concentration of fiber in the solution increased. This can be seen clearly from Figure **Figure 4.19**, where the solution becomes cloudier as more fiber is dissolved in the solution. Laser microscope images from **Figure 4.20** also shows more undissolved fiber as the fiber concentration increase. This phenomenon is due to the lack of NaOH hydrates to cover the surface of the cellulose polymer, which inhibits hydrophobic interaction between the cellulose polymer molecules. As the concentration of cellulose increases, the amount of NaOH hydrates available decreases, decreasing the solubility of the additional cellulose [114]. The optimal cellulose concentration for 10wt% NaOH solution is between 2-4% (w/v) of cellulose.

4.4.2.9 Effect of different bases

The OPF-NSblc was also subjected to dissolution in different kinds of bases to determine whether the dissolution process is similar to the cold alkali attack reported previously in the literature[115,116], or only requires a basic solvent. Several hydroxides (lithium hydroxide and potassium hydroxide), amines (ethylamine, benzylamine, tetrabutylamine), and other popular bases such as urea, ammonia, and tetrabutylammonium chloride were tested. All dissolution was done at 1% fiber loading using 10wt% aqueous base solution and mixed continuously for 1h at room temperature. The resulting solution picture is shown in **Figure 4.21 - Figure 4.26**

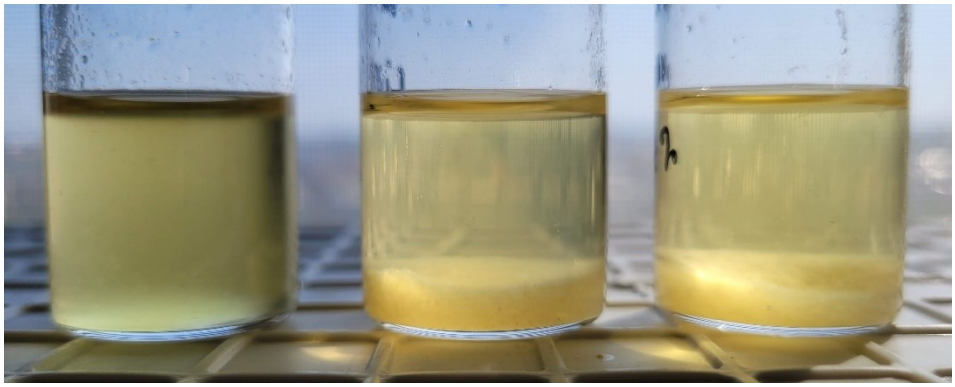

Figure 4.21: Solubility of OPF-NSblc in different hydroxide bases. From left: 10% NaOH, 10% lithium hydroxide (LiOH), 10% potassium hydroxide (KOH)

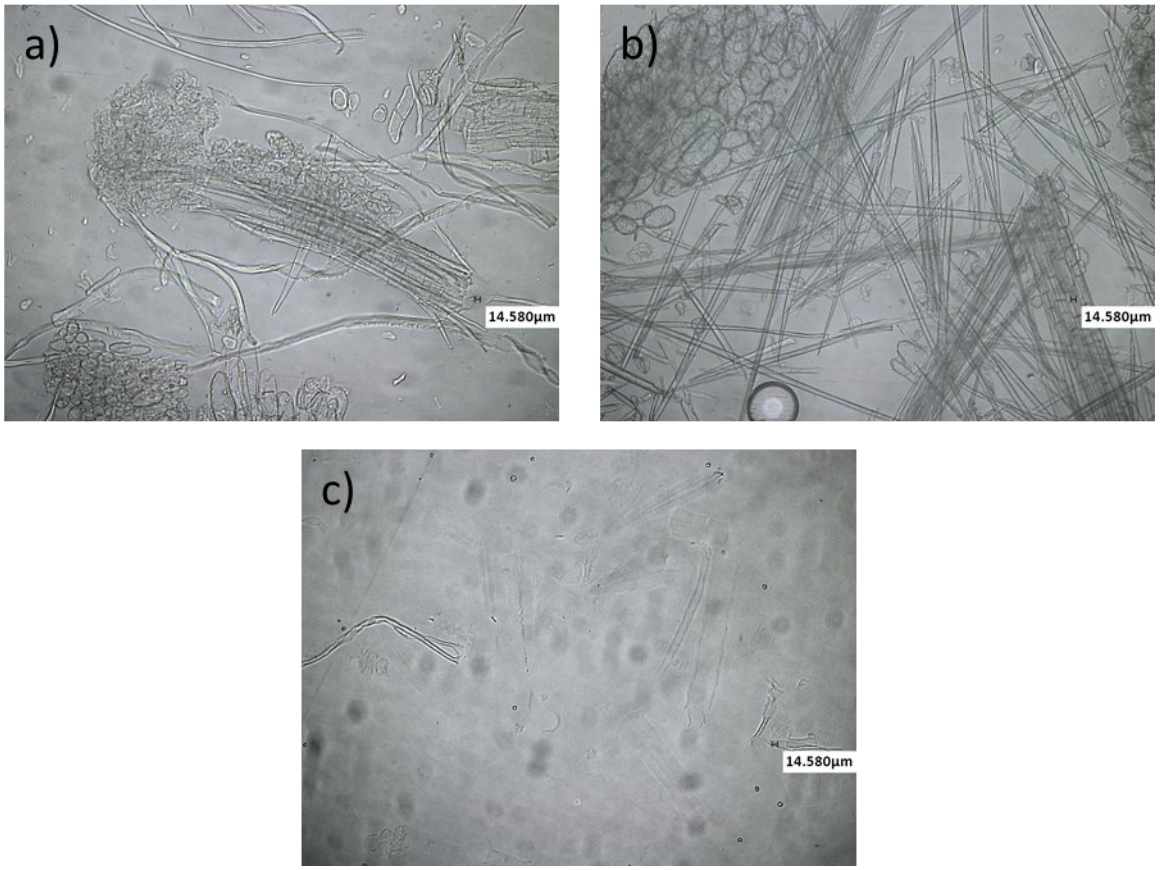

Figure 4.22: Microscope images (x10) of OPF-NSblc in a) 10wt% LiOH b) 10wt% KOH and c) 10wt% NaOH

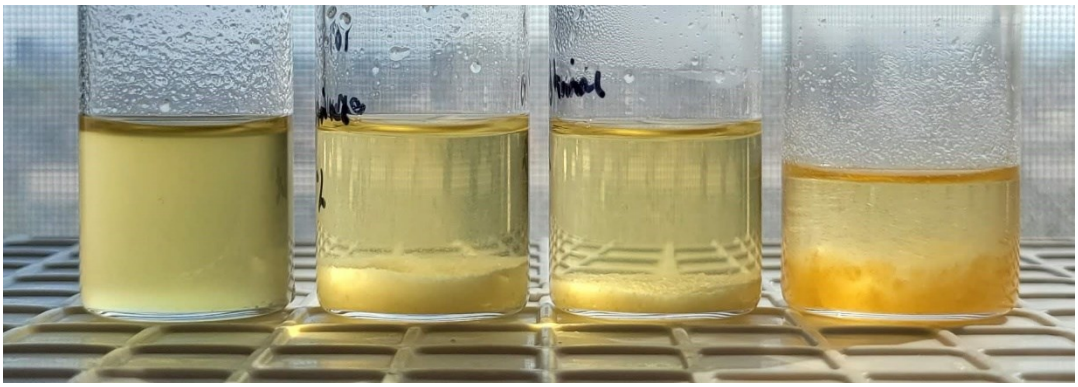

Figure 4.23: Solubility of OPF-NSblc in different organic amines. From left: 10% sodium hydroxide (NaOH), 10% ethylamine, 10% benzylamine, and tetrabutylamine.

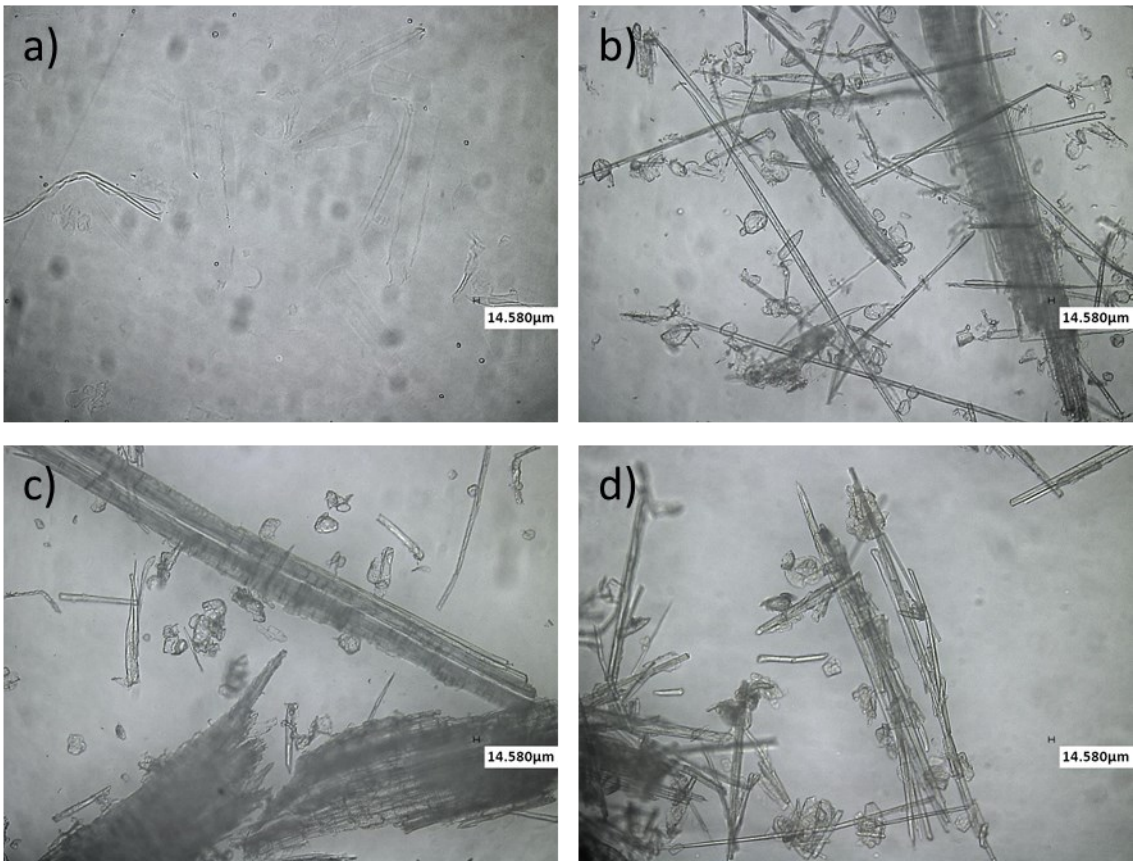

Figure 4.24: Microscope images (x10) of OPF-NSblc in a) 10wt% NaOH b) 10wt% ethylamine c) 10wt% benzylamine and d) pure tetrabutylamine

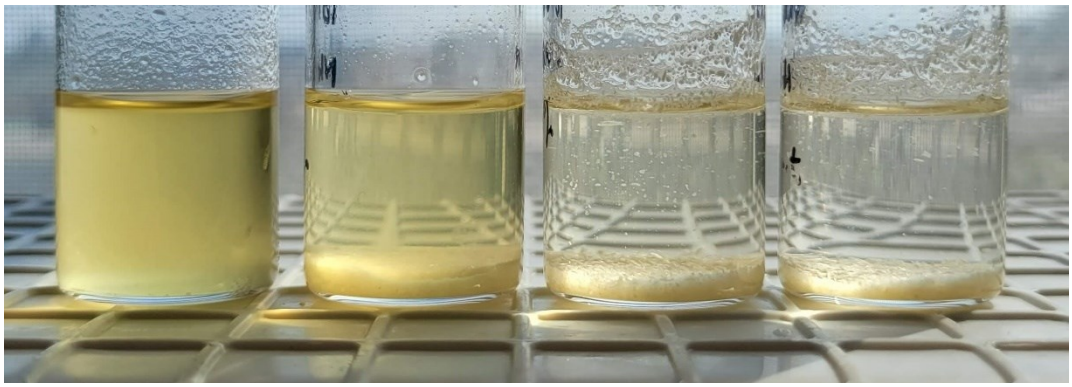

Figure 4.25: Solubility of OPF-NSblc in different bases. From left: 10% NaOH, 10% aqueous ammonia (NH_3), 10% urea, 1% tetrabutylammonium chloride.

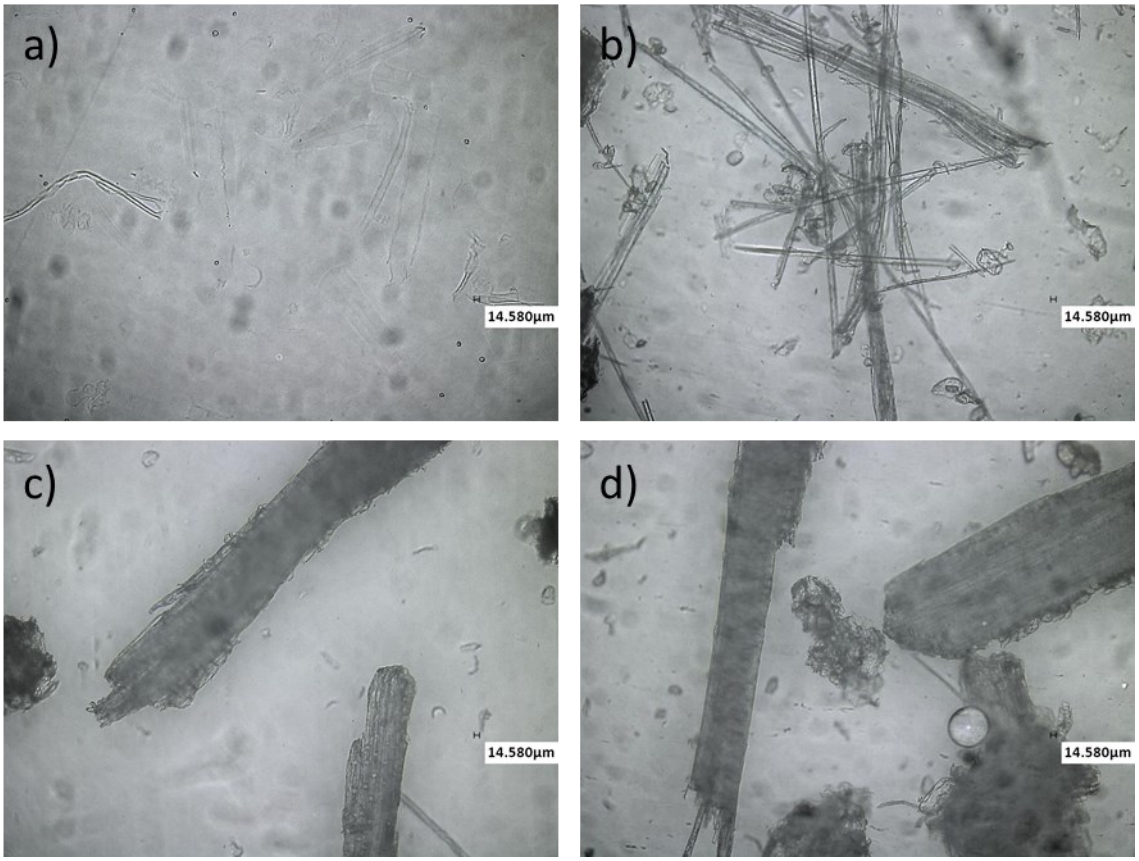

Figure 4.26: Microscope images (x10) of OPF-NSblc in different bases. From left: 10% NaOH, 10% aqueous ammonia (NH3), 10% urea, 1% tetrabutylammonium chloride.

From **Figure 4.21**, it can be seen that other hydroxides were not able to dissolve OPF-NSblc as well as NaOH solution. While OPF-NSblc in LiOH solution shows some swelling, the fiber was not dissolved completely and large fiber can still be seen. This is contrary to other reported literature where NaOH and LiOH were able to dissolve cellulose albeit using urea as an additive to stabilize the separated cellulose polymers [117]. OPF-NSblc also shows a similar reaction in KOH solution with lower swelling. Microscope image of LiOH and KOH solution shows fibril structure of the original biomass still visible in the solution, which is almost not detected in the NaOH solution. This provides a better alternative in producing dissolved cellulose solution due to NaOH being easily available and cheap compared to lithium hydroxide.

Figure 4.23 and **Figure 4.25** show the solubility of OPF-NSblc in organic amines and other bases. The bases were not able to dissolve the biomass as well as the NaOH solution had. OPF-NSblc in ethylamine and benzylamine solution shows slight swelling, while tetrabutylamine shows no swelling. This might be due to the low solubility of tetrabutylamine in water, reducing its interaction with hydrophilic cellulose structure. For ammonia and ammonium-related bases, ammonia shows the most swelling, while urea and tetrabutylammonium chloride shows no swelling. Microscope images (**Figure 4.24** and **Figure 4.26**) of the solutions also reflected the result discussed above. Large cellulose particles and fibrils of the treated biomass can be seen clearly which suggests a very low amount of dissolution if present. This result indicates that the dissolution process is closely related to the mechanism of cold alkali dissolution previously reported using NaOH or LiOH with urea, thiourea, or zinc oxide as additive [115,118–120].

4.4.2.10 Suggested mechanism of dissolution in NaOH solution

Based on the experiment conducted in previous sections, several hypotheses can be drawn to explain the dissolution of biomass after combined hydrothermal and SHS treatment. Firstly, the SHS treatment affects cellulose by reducing its hydrogen bonding strength. NMR results show that intra-chain and inter-sheet hydrogen bonding strength decrease after SHS treatment, which can be a contributing factor to the dissolution of the biomass in NaOH. As explained in length in **Section 4.4.2.5**, SHS treatment disrupted the hydrogen bonding in the cellulose structure, specifically intra-chain and inter-sheet interaction. Disruption of these hydrogen bonds, improves penetration of the metal cation and hydroxide anion into the cellulose structure, improving its solubility.

In addition to that, other factors might positively affect the solubility of the cellulose-based on previous literature. SHS treatment has been shown to reduce the DP of cellulose through depolymerization [102]. High-temperature treatment below the degradation temperature of cellulose could depolymerize the cellulose and produce cellulose with a smaller DP value that is easier to dissolve in alkali solutions. This is supported by earlier research on cellulose dissolution where complete dissolution can be achieved easier using cellulose with a smaller DP value [121].

Second, the dissolution of other components of lignocellulosic biomass especially hemicellulose in NaOH acts as an additive, similar to how urea and thiourea were used in the literature. There are many mechanisms of these additives that have been suggested in the literature that helps the dissolution process. Some authors suggest that the additives interact with NaOH hydrogen-bonded cellulose to form an inclusion complex (IC), which would lead to full dissolution[122]. Besides that, other studies suggest that the additive was preferentially interacting with cellulose, inhibiting the

hydrophobic interaction of cellulose polymers that can lead to reagglomeration [117]. Hemicellulose and its oligomers such as xylans, mannans, and glucomannan has been reported to have surfactant-like properties, which could improve the dispersion and stability of the dissolved cellulose polymers [123].

Based on the analysis results and reported data in the literature, it can be concluded that the main reason for the increased solubility of cellulose in NaOH solution is the reduction of hydrogen bonding in the cellulose structure. Other factors such as the decrease in DP of cellulose and hemicellulose by-products acting as additives similar to urea/thiourea can be speculated to improve cellulose dissolution but are not proven.

4.4.2.11 Regeneration of cellulose after biomass dissolution

The dissolved biomass was regenerated using acetic acid to produce regenerated cellulose. The regenerated cellulose was analyzed using TGA, FTIR, and XRD to determine its properties. **Figure 4.27** shows the process flow and biomass condition of OPF and Matake bamboo after each treatment step and final regeneration steps. The hydrothermal treatment removes the bulk of the lignin content, and the SHS treatment modifies the biomass to be able to dissolve in NaOH. Regenerated cellulose is mostly cellulose, based on the FTIR and XRD results that will be discussed in the next sections. Matake bamboo shows better dissolution properties compared to OPF, which can be attributed to differences in biomass internal structure and composition.

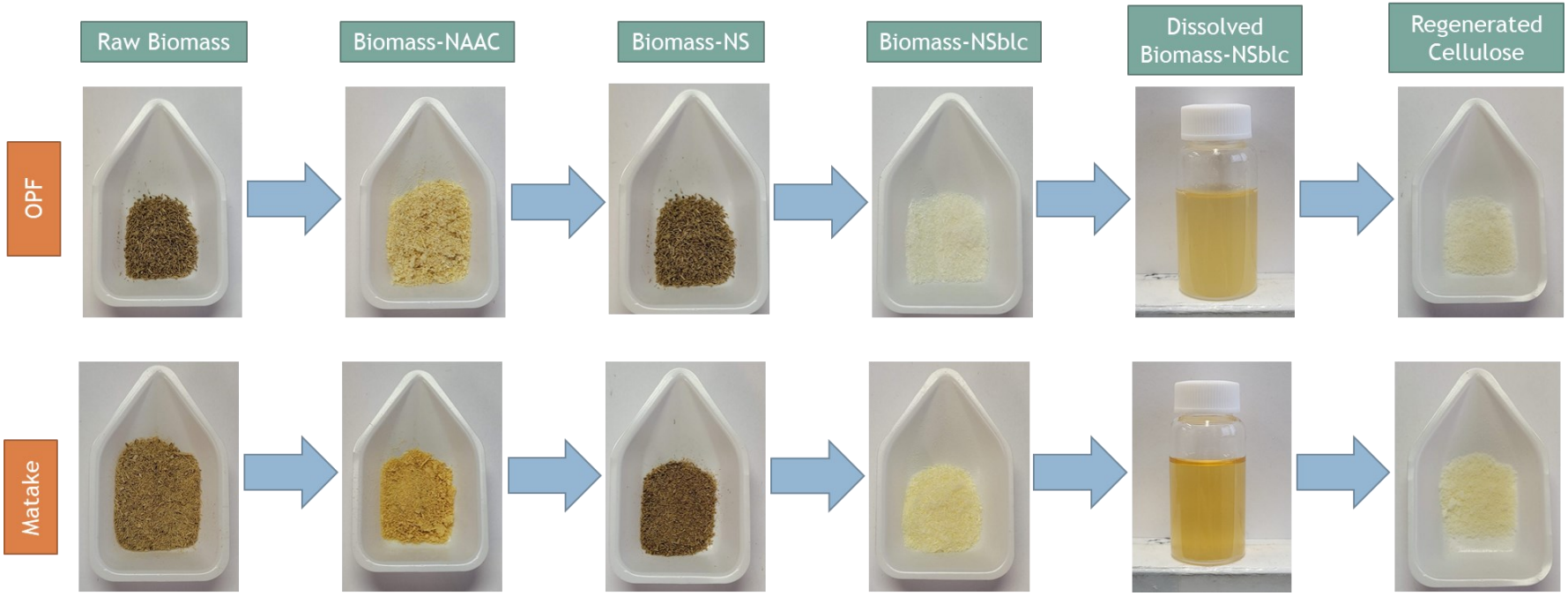

Figure 4.27: Progress flow of treatment and regeneration of OPF and Matake bamboo

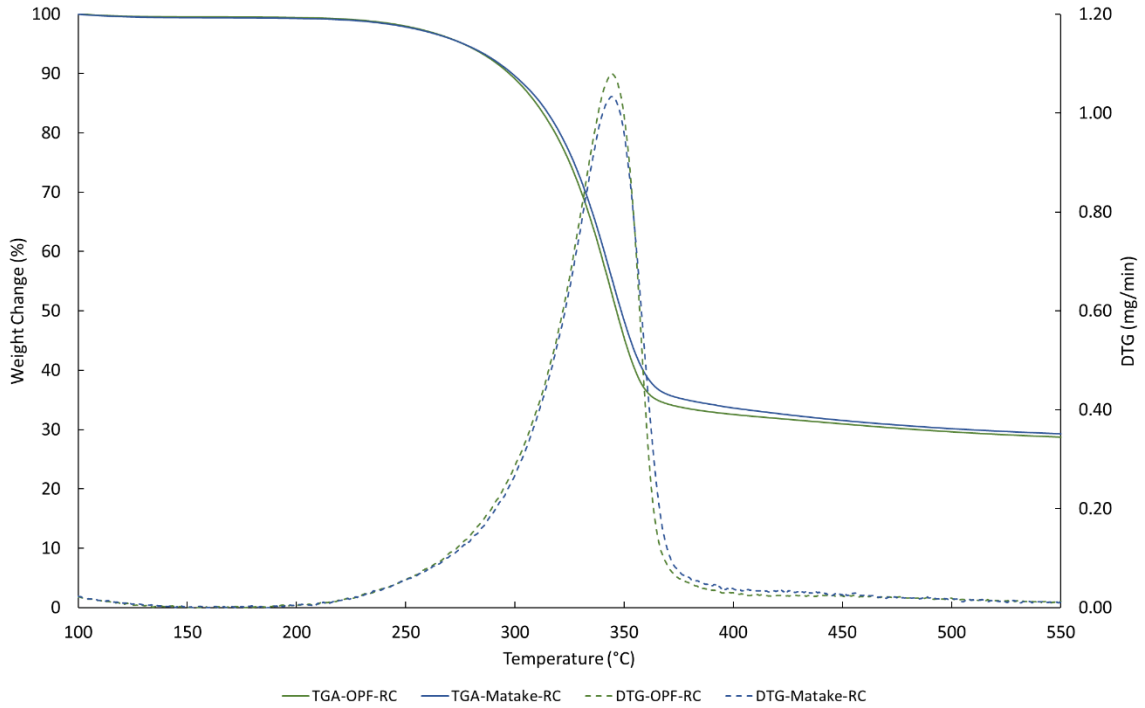

Figure 4.28: TG/DTG curve of OPF-RC and Matake-RC

TG/DTG curve of both OPF (OPF-RC) and Matake (Matake-RC) regenerated cellulose is shown in **Figure 4.28**. Both samples show similar degradation behavior, with peak degradation temperatures of about 350°C, which corroborate with pure cellulose degradation temperature[124]. Degradation of the regenerated cellulose started at about 200°C, which can be attributed to the small particle size of the regenerated cellulose.

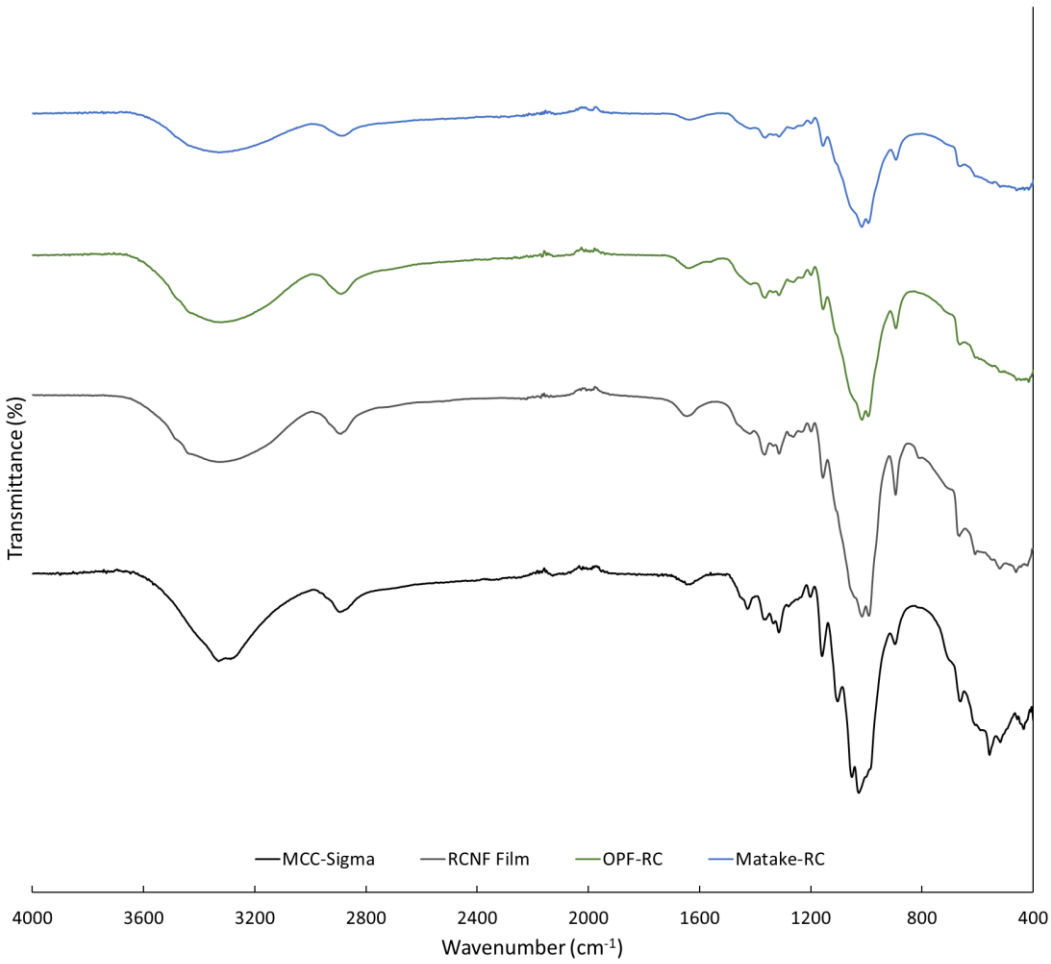

Figure 4.29: FTIR spectra of OPF-RC, Matake-RC, commercial MCC, and regenerated cellulose film

FTIR spectra of both OPF-RC and Matake-RC were compared with commercial MCC and regenerated cellulose film (RCNF) produced from cellulose nanofiber. Both OPF-RC and Matake-RC spectra closely resemble the RCNF spectrum, with the characteristics asymmetric stretching peak at 1100 cm^{-1} of cellulose I missing in all regenerated cellulose, suggesting cellulose II crystal structure. Another set of peaks characteristic of cellulose II are 2 peaks at around 3400-3480 cm^{-1} but it is not so pronounced in OPF-RC and Matake-RC samples compared to RCNF film [125]. This result suggests that the regenerated cellulose samples from OPF and Matake bamboo have a cellulose II crystal structure.

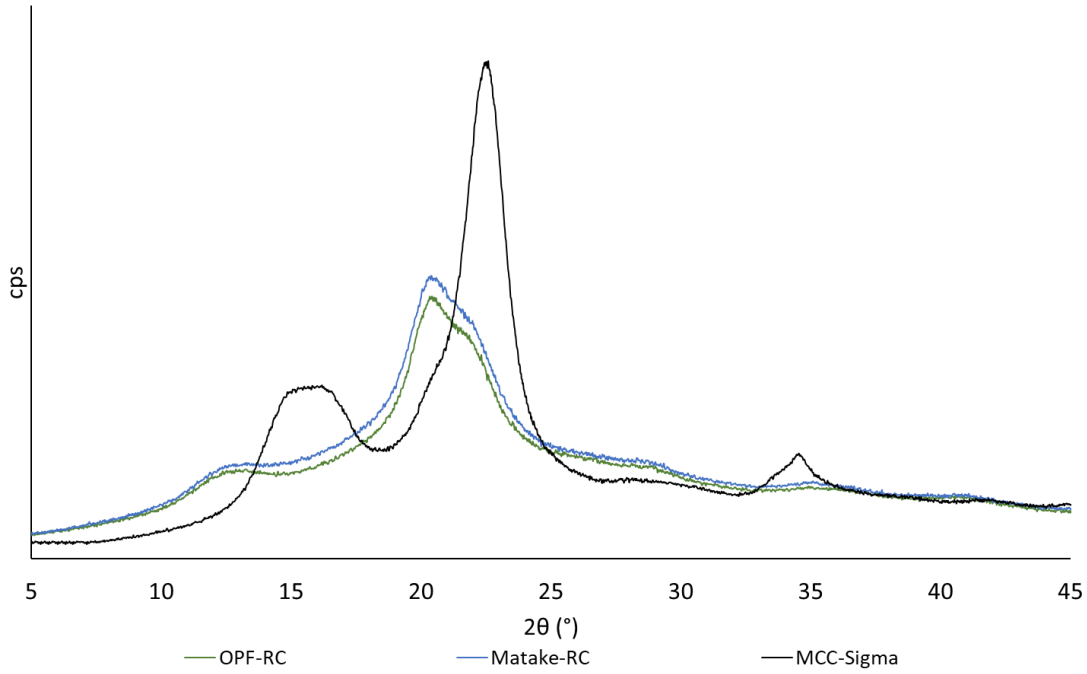

Figure 4.30: XRD pattern of OPF-RC, Matake-RC, and commercial MCC

To confirm FTIR results, XRD analyses were also subjected to all samples to determine their crystal structure. The XRD pattern shows that all regenerated samples have cellulose II structure, with peaks at 2θ values of 12, 20, and 22°. Compared to commercial MCC which is cellulose I with major peaks at 16 and 22°.This result suggests that the biomass was successfully dissolved and regenerated producing cellulose with a significantly different crystal structure compared to its initial state.

4.4.2.12 Process yield

The dry weight basis yield of each step of the process was calculated to determine losses through normal processing and chemical treatments. The flow chart of the process steps is as shown in **Figure 4.31**.

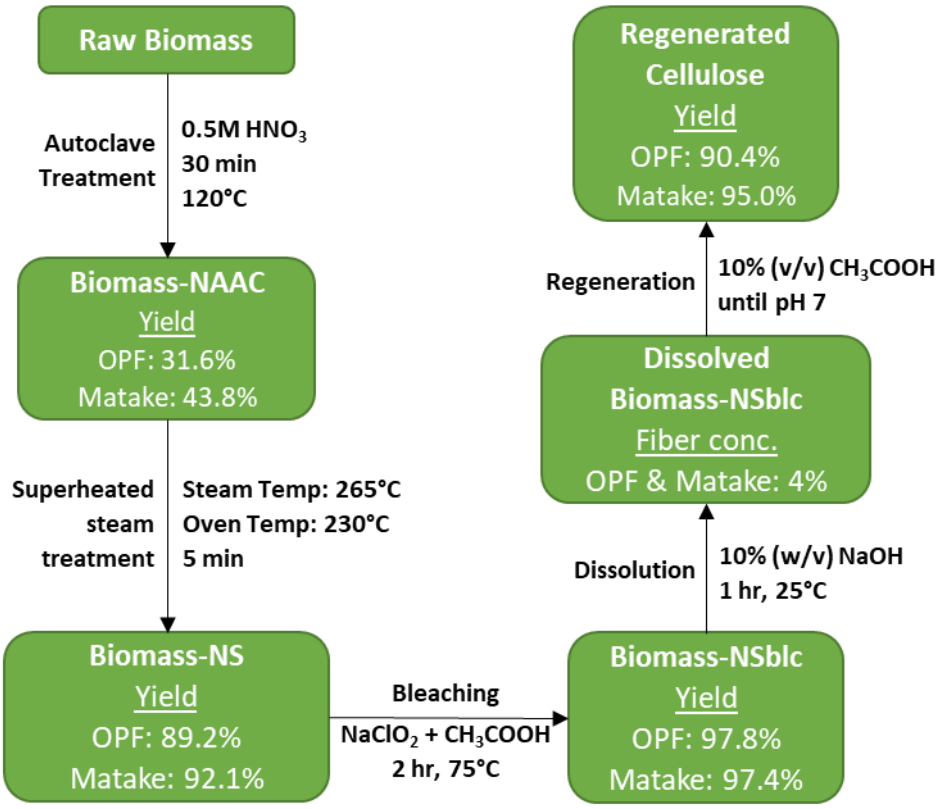

Figure 4.31: Combined treatment, dissolution, and regeneration process flow chart. Yield is calculated based on the previous step biomass initial dry weight.

The efficiency of each process is relatively high, except for the initial autoclave treatment. SHS treatment step yield was higher compared to SHS treatment of sugi wood where the yield reported was around 80% [126]. This shows that the process can be applied to hydrothermally treated biomass to convert it to a soluble cellulose product at room temperature without major yield loss. Regeneration yield was also high, with more than 90% of the fiber dissolved in NaOH solution recovered. The yield is comparable with regeneration yield from cellulose dissolve in an ionic liquid such as

1-butyl-3-methylimidazolium acetate and regenerated using water and ethanol where the yield was above 90% [127]. The loss here could be attributed to other lignocellulosic components removed from the biomass during dissolution.

4.5 Conclusion

Based on the result presented in this chapter, it can be concluded that combined hydrothermal and SHS treatment were able to produce biomass fiber that can be dissolved in NaOH solution. The resulting biomass after SHS treatment was physically similar to biomass before treatment. SEM, TGA, FTIR, and XRD analysis shows that the combined treated biomass was not significantly modified in terms of its surface functional groups and morphology compared to the original hydrothermally treated biomass. The solubility of the biomass was studied, with the biomass able to dissolve in NaOH solution only, and other bases were not able to dissolve the biomass successfully. Reduction of hydrogen bonding might be a contributing factor in increasing dissolution of cellulose in NaOH solution. Regenerated cellulose was successfully produced from the dissolved biomass solution, with properties similar to regenerated cellulose produced from cellulose nanofiber dissolve using LiOH/Urea mixture, based on TGA, FTIR, and XRD analysis. This process can be implemented in the industry as a new, simpler, and easier method to dissolve cellulose and produce regenerated cellulose with easily available chemicals and low energy requirements. Further studies need to be done to determine the mechanism of dissolution and also the reason why SHS treatment was able to modify the biomass to be able to dissolve in NaOH solution at room temperature.

CHAPTER 5

HYDROTHERMAL SURFACE FUNCTIONALIZATION OF OIL PALM BIOCHAR AND OTHER CARBON MATERIAL

5.1 Introduction

Production of carbon material (biochar) from biomass for different types of purposes has gained interest in the sustainable technology development scene due to its simple and low-cost process. A large amount of biomass can be processed in one or two-step with a relatively high yield of 20-40% [128] and only be limited with the size of the reactor used. Previous reports had shown that a large variety of biomass from different sources such as soft/hardwoods [129], fibers [61], shells [130], and even byproducts of fermentation [131] and wastewater treatment processes [132] can be used as feedstock for biochar production. Biochar can be used in a variety of situations mainly in wastewater treatment [133] and soil conditioning [134] due to its inherent adsorptive capabilities. Biochar also indirectly reduced carbon emission by sequestering carbon from the environment and reducing greenhouse gas emission, by converting active carbon that can be used in nature or through human activities into stable form of carbon (biochar) [135].

Due to its advantages, the carbonization of oil palm biomass has gained traction in recent years as a more environmentally friendly method of disposing of abundant amount of biomass produced by the palm oil industry in Malaysia. In 2019 alone, 151.2 million tonnes of fresh fruit bunches were processed [25,136], producing solid and liquid biomass, with oil palm empty fruit bunch (OPEFB) as the largest fraction of solid biomass at about 33.3 million tonnes [137]. The current practice of reusing OPEFB as

mulching and crude compost in the plantation can lead to the leaching of nutrients into the ground soil and proliferation of pests such as rodents and rhinoceros beetle [138,139]. With carbonization, a large amount of OPEFB can be processed at once as reported by Idris et al., with a successful self-sustaining carbonization process, which can be upscaled to 3 tons per run [58,140]. These show the feasibility of OPEFB as biochar feedstock and economy of scale can be applied as the carbonization process can be upscaled as needed. While OPEFB biochar itself has a high higher heating value (HHV) and can be used as fuel, the value of OPEFB biochar can be improved significantly if it can be used as an adsorbent in wastewater treatment applications.

The major problem in utilizing OPEFB biochar as an adsorbent is the relatively low surface area of the biochar without any activation step. It is widely known that the adsorption performance and capacity of carbon material can be significantly improved through the activation process [141,142]. Subjecting biochar to the activation step, either using gaseous agents such as CO_2 or H_2O [28,143] or using chemical agents such as phosphoric acid, zinc chloride and potassium hydroxide [144] will increase the surface area significantly, hence improving its adsorption capability. But activation process usually requires high temperature treatment and high concentration chemicals which increases energy cost and waste material respectively. It is imperative that a method to improve the adsorption performance of biochar using available technology with lower energy requirements and low waste generation needs to be studied.

Surface functionalization has been suggested as another way to improve biochar adsorption performance via the introduction of surface functional groups to the carbon surface of the biochar. While biochar inherently possesses some functional groups such as hydroxyl and carbonyl groups, the amount was small compared to the bulk surface of the biochar. Biochar surface can be functionalized using oxidating chemicals such as nitric acid to increase its oxygen surface functional groups. Even though multiple studies report successful surface functionalization of biochar using nitric acid, the process usually requires a long time [145] and a very high concentration of nitric acid. In addition to that, the functionalization process tends to affect the morphology and pore structure of the carbon material modified, resulting in a reduction in surface area. With this problem in hand, a functionalization process using an autoclave; which was readily available in the palm oil mills as sterilizers, is suggested to accelerate biochar functionalization to improve biochar surface functionalities and subsequently its adsorption performance.

In this study, a simple functionalization process for biochar as an adsorbent from oil palm biomass was proposed through the hydrothermal method using an autoclave. In this system, nitric acid was used as an oxidation agent to functionalize the surface of biochar to increase its oxygen surface functional groups. The autoclave was used as an apparatus to accelerate and increase the efficiency of the functionalization process. This in turn reduces the amount of nitric acid used and the functionalization period. In addition to the increased efficiency, the functionalization process does not significantly change the structure of the biochar, as shown in SEM analysis. Functionalized biochar performance was measured through adsorption of methylene blue dye. Surface functional group changes were also observed through FTIR and energy dispersive X-ray (EDX) analysis.

5.2 Materials and methods

5.2.1 Sample preparation

OPEFB was collected from Seri Palm Oil Mill, Dengkil Selangor. OPEFB sample was dried in an oven for 48 hr before being ground and sieved to about 2mm in size. The moisture content of the biomass was analyzed using a moisture analyzer (Shimadzu, MOC-120H, Japan). Dried, ground OPEFB was then kept in an airtight container at room temperature before further experiment and analysis.

Chemicals for experiments and analysis such as concentrated nitric acid (96%), concentrated hydrochloric acid (36%), methylene blue (MB), copper (II) nitrate trihydrate, cobalt (II) nitrate hexahydrate, nickel (II) nitrate hexahydrate, lead (II) nitrate and standard metal nitrate salt solution (100 ppm) for ICP-AES calibration were sourced from FUJIFILM Wako Pure Chemical Corporation, Osaka, Japan. A stock solution was prepared from pure chemicals and diluted to required concentrations using deionized water. Deionized water (18.25 MΩ.cm) was obtained from a Milli-Direct 16 Filtration system (MilliporeSigma, Massachusetts, USA).

5.2.2 Biomass carbonization

OPEFB was weighted and carbonized using a muffle furnace at 450°C for 30 min at a heating rate of 15°C/min. The muffle furnace was tightly closed during carbonization to create a low oxygen atmosphere without any inert gas. After carbonization has completed, the biochar was left to cool slowly in the muffle furnace for 12 hr. Biochar was then rinsed with 0.1 M hydrochloric acid (HCl) solution to remove any ash and further rinsed with deionized water to remove excess HCl until the rinsing water pH reached 6-7. Rinsed biochar was dried in a drying oven at 75°C for 24 hr and weighed

for yield calculation. Dried biochar (EFB-BC) was kept in the desiccator before hydrothermal functionalization.

5.2.3 Hydrothermal surface functionalization

5.0 g biochar and 100 mL 1.0 M nitric acid (HNO_3) solution were added to a 500 mL Erlenmeyer flask. The flask was shaken to mix the solution and biochar. The flask mouth was then covered with aluminum foil to avoid boil over and autoclaved in an autoclave (ASONE, NC-0170, Osaka Japan) at 132°C and 241 kPa for 60 min. After hydrothermal treatment was completed, the mixture was left to cool to about 60°C before being filtered and rinsed with deionized water until the rinsing water pH reached pH 6-7. Functionalized biochar (EFB-FBC) was then dried in an oven at 75°C for 24 hr and kept in a desiccator for analysis and adsorption experiments.

5.2.4 Adsorption performance determination

Methylene blue solution at different concentrations was prepared by diluting stock MB solution (1000 mg/L) with deionized water to the required concentration. 50 mg of EFB-BC or EFB-FBC was added to 25 mL MB solution (2 g/L adsorbent dosage) and shaken with an orbital shaker at 300 rpm. For the isotherm determination experiment, the initial concentrations used are 125, 150, 175, and 250 mg/L and for the kinetic experiment, the initial concentration is 125 mg/L. The adsorption experiments were performed for 24 hr at 30°C to reach adsorption equilibrium except for the isotherm kinetic experiment. After 24 hr, the mixture was filtered and residual MB concentration was determined. For heavy metal adsorption performance determination, 100 ppm solution of nickel, cobalt, lead and copper nitrate salt was prepared by serial dilution of stock 1000 ppm salt solution. MB adsorption parameters were applied to heavy metal adsorption as well.

Equilibrium adsorption capacity, Q_e, was calculated using the equation:

$$Q_e = (C_0 - C_e)V/m$$

Where C_0 represents the initial MB or heavy metal concentration (mg/L), C_e represents equilibrium concentration (mg/L), V is the solution volume (L) and m is the mass of the adsorbent (g). Q_e value is reported in terms of mass or adsorbate (mg) adsorbed per unit mass of adsorbate (g).

Adsorption kinetics and isotherm were analyzed and fitted to Langmuir isotherm as shown below:

$$Q_e = (K_{ads} \cdot Q_{max} \cdot C_e)/(1 + K_{ads} \cdot C_e)$$

Where K_{ads} is the Langmuir constant related to the heat of adsorption (L/mg) and Q_{max} is the maximum adsorption capacity (mg/g)

The isotherm data were fitted using the linear form of the Langmuir equation:

$$C_e/Q_e = (C_e/Q_{max}) + (1/Q_{max} \cdot K_{ads})$$

By plotting C_e/Q_e vs C_e, the value of K_{ads} and Q_{max} can be determined from the slope and intercept of the line.

For adsorption kinetic analysis, the data were fitted into 3 different kinetic models: pseudo-first-order (PFO), pseudo-second-order (PSO), and intraparticle diffusion (IPD) kinetic model. The equation for each kinetic model is shown below:

PFO kinetic model equation:

$$ln(Q_e - Q_t) = -k_1 t + \ln(Q_e)$$

PSO kinetic model equation:

$$t/Q_t = (1/Q_e) \cdot t + 1/{Q_e}^2 \cdot k_2$$

IPD kinetic model equation:

$$Q_t = k_p t^{1/2}$$

Where t is time, Q_t is amount adsorbed at time t (mg/g) and k_1 (min^{-1}), k_2 (g/mg.min), and k_p ($mg/g.min^{1/2}$) is the adsorption rate constant for PFO, PSO, and IPD kinetic model, respectively.

PFO kinetic model supposes that the adsorption process is controlled by diffusion of adsorbate at the solid-liquid interphase boundary (physisorption), while the PSO model ascribes the adsorption process to be controlled by the reaction of the adsorbate and the surface at the interphase boundary (chemisorption). IPD model presumes that the adsorption process continues in multi-stage diffusion steps throughout the bulk of the adsorbent.

5.3 Analysis

Surface morphology and surface atomic composition of EFB-BC and EFB-FBC were analyzed using JEOL-9000 SEM/EDX analyzer (JEOL, Tokyo, Japan). EDX analysis was done at an accelerating voltage of 15 kV. Surface functional groups were analyzed via Fourier Transform infrared spectroscopy performed on Nicolet iS5 spectrophotometer (ThermoFisher Scientific, Wisconsin, USA). The sample was measured via a KBr pellet in the wavenumber range of 400–4000 cm^{-1}. Thermogravimetric analysis was done to determine the thermal stability of EFB-BC and EFB-FBC using EXSTAR TG/DTA7000 (Hitachi High-Tech, Tokyo, Japan) under N_2 atmosphere from 30–550°C at 10°C/min heating rate. BET surface area, pore diameter, and volume of EFB-BC and EFB-FBC were analyzed using Belsorp Mini-SPRII surface analyzer (MicrotracBEL, Osaka, Japan) using N_2 and CO_2 as adsorbate at 77°K and 298°K, respectively. The sample was dried in a vacuum drying oven at 105°C for 48 hr before surface area analysis. Residual MB concentration was measured spectrophotometrically using Genesys 50 UV-Vis spectrophotometer (ThermoFisher Scientific, Wisconsin, USA). A standard curve of known MB concentration range was prepared to determine a standard curve equation. MB solution absorption at 660 nm was measured and MB concentration was calculated using previously calculated standard curve equation. Residual heavy metal concentration was measured using simultaneous inductively coupled plasma-atomic emission spectroscopy (ICP-AES) system (ICPE-9800, Shimadzu, Japan). Similar standard curve equation preparation was prepared for equilibrium concentration calculation.

5.4 Results and discussions

5.4.1 Carbonization and functionalization yield

OPEFB carbonization yield was calculated to be 25.8% based on OPEFB dry weight. The yield was similar to the carbonization yield reported in the literature, with reported yield value in the range of 20-45% [146,147], with differences in yield value attributed to different carbonization methods and minor biological differences in biomass from different sources. Hydrothermal functionalization treatment was in the range of 95-99%, with yield loss due to losses during sample transfer and rinsing. Very high functionalization yield suggests that hydrothermal treatment only affects the surface of the carbon and does not destroy or change the bulk of the biochar structure.

5.4.2 FTIR analysis

FTIR analysis of EFB-BC and EFB-FBC was done to determine the changes in surface functional groups, especially oxygen functional groups. An increase in oxygen surface functional groups can increase the performance of adsorbent material due to the affinity of the groups towards charged compounds. An abundant amount of research has shown that increasing oxygen surface functional groups will improve the performance of adsorbents in adsorption of heavy metal, dye and other adsorbates through increase hydrogen bonding and complexation between oxygen functional groups and adsorbate molecules, especially heavy metal ions. Increased oxygen surface functional groups also improved hydrophilicity of the biochar, which in turn improves the interaction between adsorbent and adsorbate at the solid-liquid interphase boundary.

FTIR spectra of EFB-BC and EFB-FBC are shown in **Figure 5.1** below.

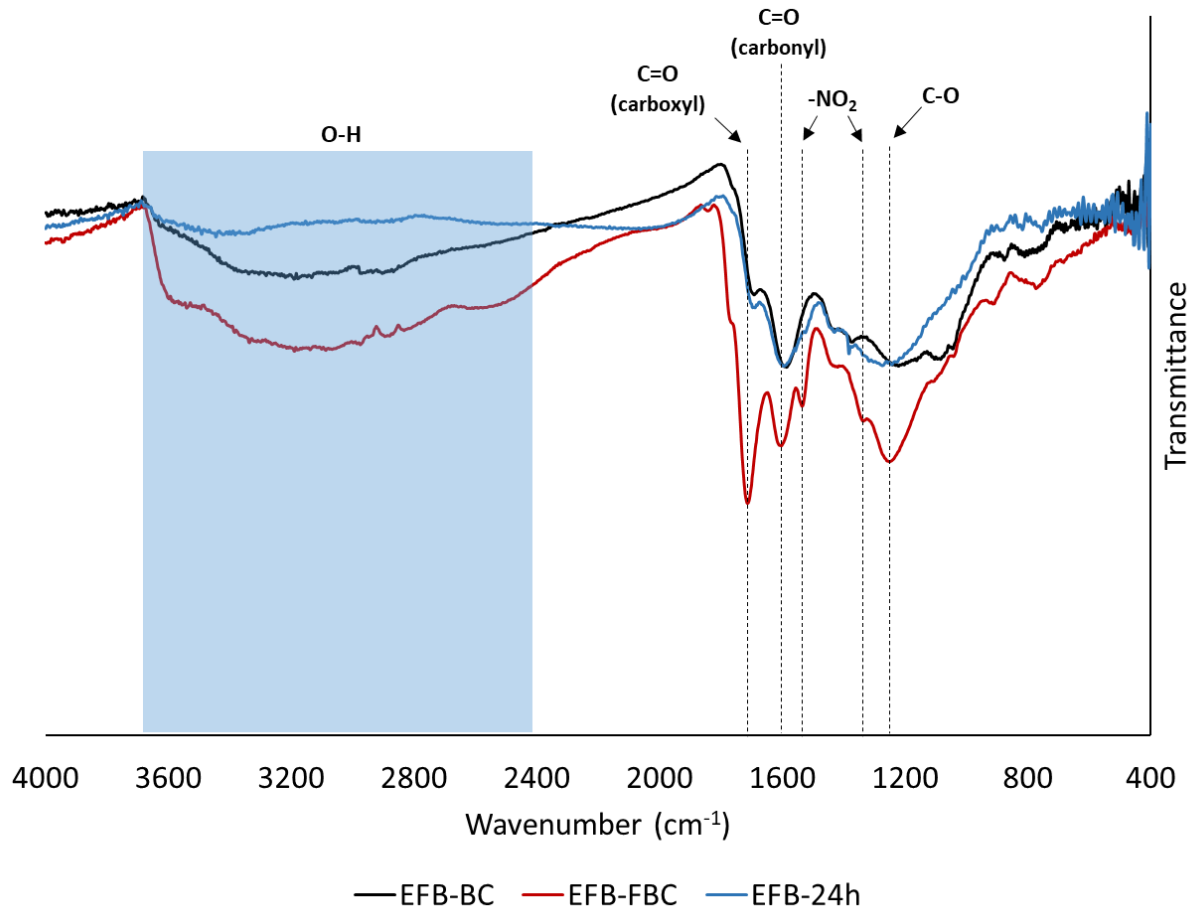

Figure 5.1: FTIR spectra of EFB-BC, EFB-FBC and EFB--24h

From the FTIR spectra, it is apparent that the surface functional groups of the EFB biochar change significantly after hydrothermal treatment. The strong absorbance peak at 1710 cm^{-1} can be attributed to the C=O stretching vibration of carboxylic groups while 1605 cm^{-1} can be assigned to conjugated C=O carbonyl stretching or C=C aromatic stretching vibrations. These peaks are also present in EFB-BC before treatment but at weaker intensity. The peak at 1246 cm^{-1} and broad absorption band in the range of 2400-3500 cm^{-1} can be assigned to aromatic alkoxy stretching and hydroxyl stretching respectively. Alkoxy stretching peak is due to phenolic C-O bonds while broad O-H stretching band is indicative of carboxylic O-H. This suggests that the treatment successfully increase the amount of C=O functional groups on the biochar

surface. In addition to oxygen-containing functional groups, new peaks were present in the EFB-FBC spectra at 1535 and 1339 cm^{-1}, which can be attributed to asymmetric and symmetric vibration of the nitro (-NO_2) group. This indicates that nitric acid also introduces new nitrogen-containing functional groups to the biochar surface. Gokce and Aktas reported similar peaks were detected after treatment of waste tea biochar using nitric acid [148]. Furthermore, the introduction of nitrogen-containing surface groups might open up new avenues of secondary modification with other compounds to either convert current surface groups via reduction or further oxidation or graft other compounds to the functional groups. A review by Liu *et al*. suggests many different methods of modification and grafting methods on biochar surfaces that can be implemented with the right initial surface functional groups [63].

To compare treatment using nitric acid with and without hydrothermal conditions, a sample of EFB-BC was refluxed with 1M nitric acid at 80°C for 24 hr (EFB-24h) and its FTIR spectra were also shown in **Figure 5.1**. Treatment using nitric acid at elevated temperature was not enough to introduce new functional groups to the biochar surface. Some increase in nitro and carboxyl group absorption peak can be seen but significantly less compared to EFB-FBC. This highlights the importance of hydrothermal conditions for a successful functionalization of biochar surface using nitric acid at low concentrations. The significant increase in absorption bands of oxygen-containing functional groups, with the introduction of new peaks indicating the introduction of nitrogen-containing functional groups, shows that the functionalization of biochar surface is successful.

5.4.3 TGA analysis

Thermogravimetric analysis (TGA) of EFB-BC, EFB-FBC, and EFB-24h was done to determine its thermal stability and thermal degradation profile. The thermogravimetric

(TG) and differential thermogravimetric (DTG) curve of all samples is shown in **Figure 5.2**.

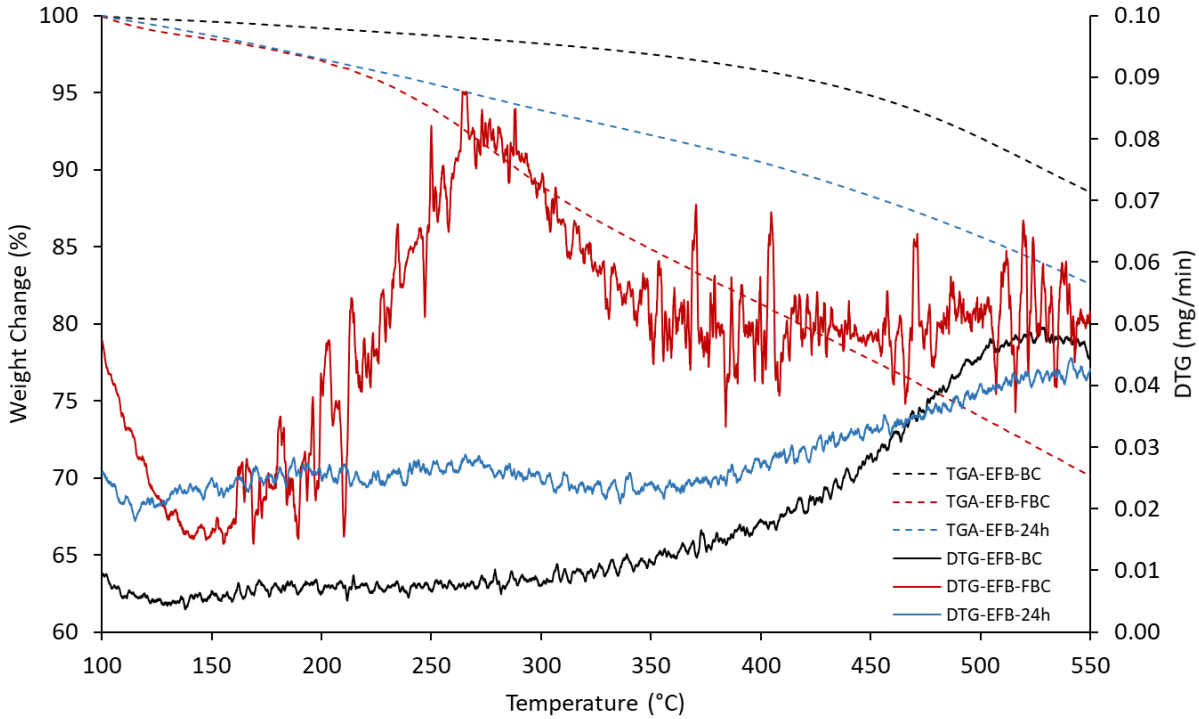

Figure 5.2: TG/DTG curve of EFB-BC, EFB-FBC and EFB-24h

For EFB-BC, degradation starts at around 300°C, with a maximum degradation rate at around 500C. Early-onset of thermal degradation can be attributed to the degradation of recalcitrant lignin that is left from the carbonization and decomposition of relatively unstable chemical structures and functional groups such as methoxy and carbonyl groups. A similar trend of biochar thermal degradation was also reported with biochar derived from various feedstock such as manure, switchgrass, water oak, rice husk, rice bran, and sludge [149,150]. While for EFB-FBC, thermal degradation starts at a lower temperature of around 200°C with a peak degradation rate at 275°C. This can be attributed to the degradation of oxygen functional groups, which are introduced by nitric acid functionalization such as carboxyl and anhydride groups with the evolution of water and carbon dioxide [151]. For EFB-24h, the degradation pattern shown by the EFB-FBC sample is not as obvious. There are more weight changes and a higher degradation rate shown in the DTG curve compared to EFB-BC, but it is not as significant as EFB-FBC. This supports the FTIR findings where nitric acid treatment introduces more carboxyl groups to the biochar surface and the hydrothermal condition is necessary for successful surface functionalization. The TG/DTG curve also shows that EFB-FBC is stable at temperatures up to 200°C before degradation starts, suggesting that the functionalized biochar can be used with wastewater even at relatively high temperatures such as cooling water from power plants.

5.4.4 SEM micrograph

EFB-BC and EFB-FBC SEM micrograph is shown in **Figure 5.3**.

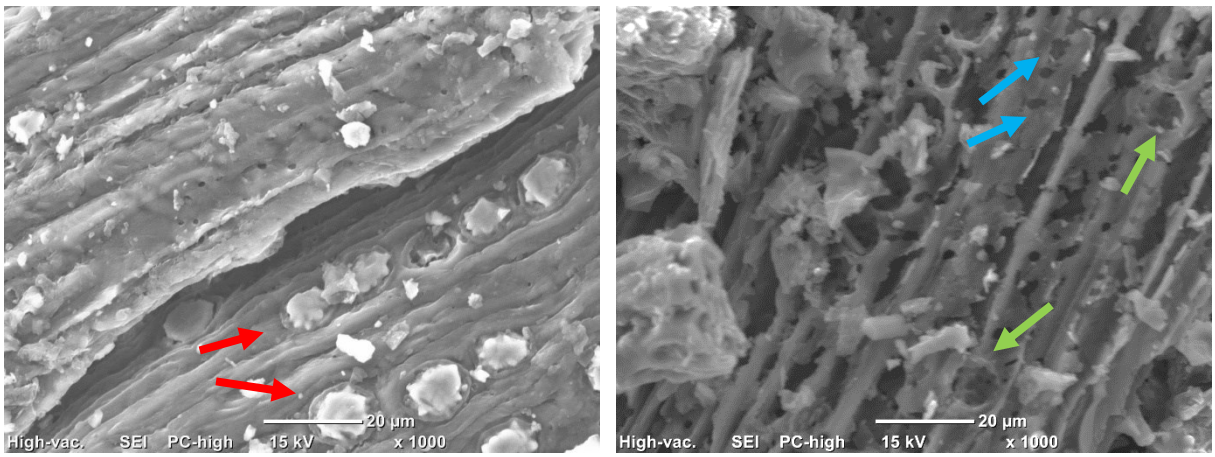

Figure 5.3: SEM micrograph of EFB-BC and EFB-FBC

The structure of EFB-FBC remains similar after hydrothermal treatment, indicating that the treatment does not significantly change the macrostructure of the biochar. There are some changes in the macropores of the biochar, with enlargement of pore and removal of some silica bodies (red arrows →) on the surface, which would improve the diffusion of adsorbate molecules throughout the biochar.

5.4.5 EDX analysis

To confirm the changes in surface functional groups from FTIR, EDX analysis was done to EFB-BC and EFB-FBC to quantify the surface elemental composition of the biochar before and after hydrothermal functionalization treatment. The oxygen atomic percent is shown in **Figure 5.4**.

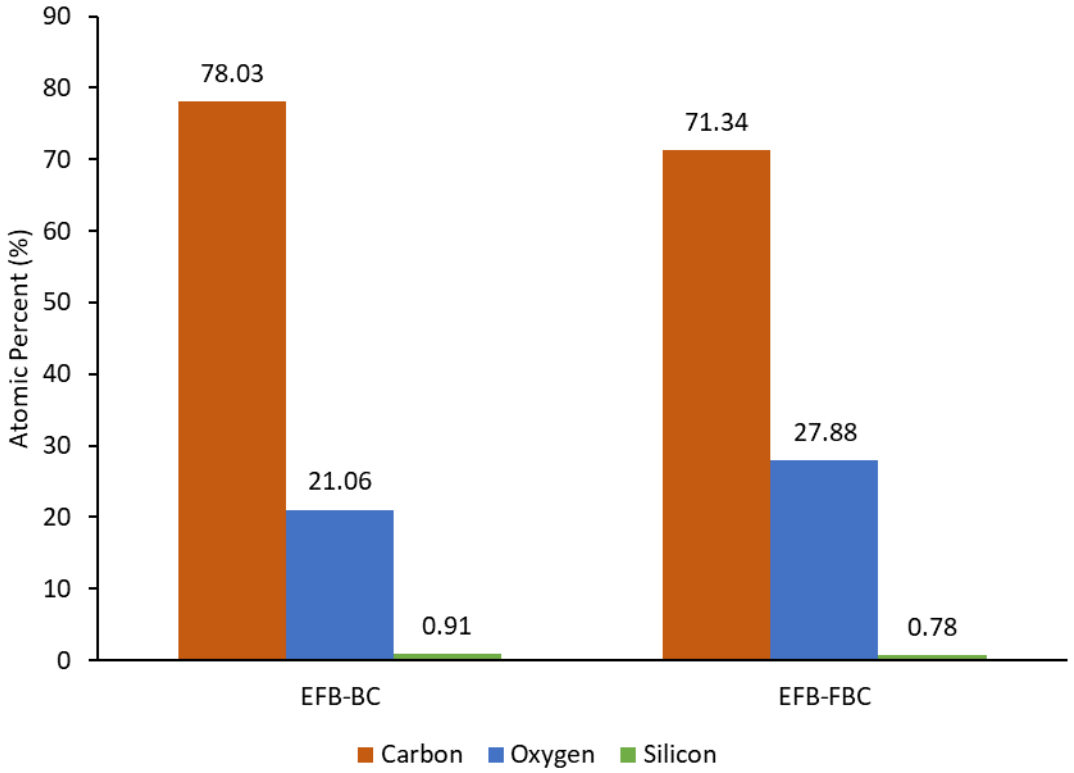

Figure 5.4: Surface atomic composition of EFB-BC and EFB-FBC

From EDX, the amount of atomic oxygen on the surface of the biochar increases from 21% to 28%. This correlates with the changes seen in FTIR spectra of the EFB-FBC. Silicon content also decreases, which supports the observation in the SEM where the hydrothermal treatment removes some of the silica bodies on the biochar surface, opening new pores and increasing diffusion of adsorbate into the internal structure of the biochar.

5.4.6 BET surface area

EFB-BC and EFB-FBC surface area were determined to see whether the hydrothermal functionalization process has any effect on the pore structure and morphology of the biochar. BET surface area (a_{sBET}), total pore volume (V_T), pore diameter (D_P), micropore surface area (a_{mic}) and micropore volume (V_{mic}) values are as shown in **Table 5.1**.

Table 5.1: N_2 and CO_2 adsorption values for EFB-BC and EFB-FBC

	N_2 Adsorption				**CO_2 Adsorption**
	a_{sBET} (m^2/g)	V_T (cm^3/g)	D_P (nm)	a_{mic} (m^2/g)	V_{mic} (cm^3/g)
EFB-BC	3.7855	0.01836	19.401	3.44	0.1396
EFB-FBC	3.0499	0.01476	19.363	2.86	0.1312

BET surface area from N_2 adsorption analysis shows that the functionalization does not affect the pore structures of the biochar appreciably, with surface area values decreasing by about 20%. This is significantly less than what has been reported by other researchers after nitric acid functionalization where surface area values can decrease by up to 96% [148,152]. This signifies a considerable amount of pore destruction and collapses during treatment which can be detrimental to the performance of the biochar or carbon material after modification. Other values also show small changes which indicate that the hydrothermal treatment successfully functionalized the biochar surface without any notable physical difference to the biochar pore structure that may increase or decrease the surface area. In addition to that, this signals the possibility of using this method to functionalize other carbon material without changing the pore structure which may affect its inherent surface area values. This possibility will be explored in the subsequent section.

5.4.7 Adsorption performance

5.4.7.1 Methylene blue adsorption

EFB-FBC adsorption performance and characteristics were determined using methylene blue as synthetic adsorbate and EFB-FBC as a control for comparison. MB was selected as adsorbate due to its prevalent use in research as a model adsorbate and ease of analysis. The adsorption capacity of EFB-FBC increased from 8.70 ± 0.09 mg/g to 62.52 ± 0.48 mg/g even though the surface area value of EFB-BC remains similar after treatment. This suggests that the functionalization process successfully improves the adsorption capacity of the biochar without any changes to its surface area. The increase in oxygen surface functional groups after hydrothermal functionalization treatment increases the electrostatic interaction between the highly electronegative oxygen groups and dye molecules, increasing its affinity and adsorption capacity. This also proves that functionalization of biochar surface is a viable method to improve biochar performance, without resorting to a more energy-intensive activation process.

Adsorption isotherm and kinetic profile of EFB-FBC were done to characterize its adsorption process. The isotherm constants and the linear fit curve is as shown in **Table 5.2** and **Figure 5.5**

Table 5.2: Langmuir adsorption isotherm constants for EFB-FBC adsorption of methylene blue

Q_{max} (mg/g)	K_{ads} (L/mg)	R^2
62.11 ± 0.14	0.9938 ± 0.0036	0.9991

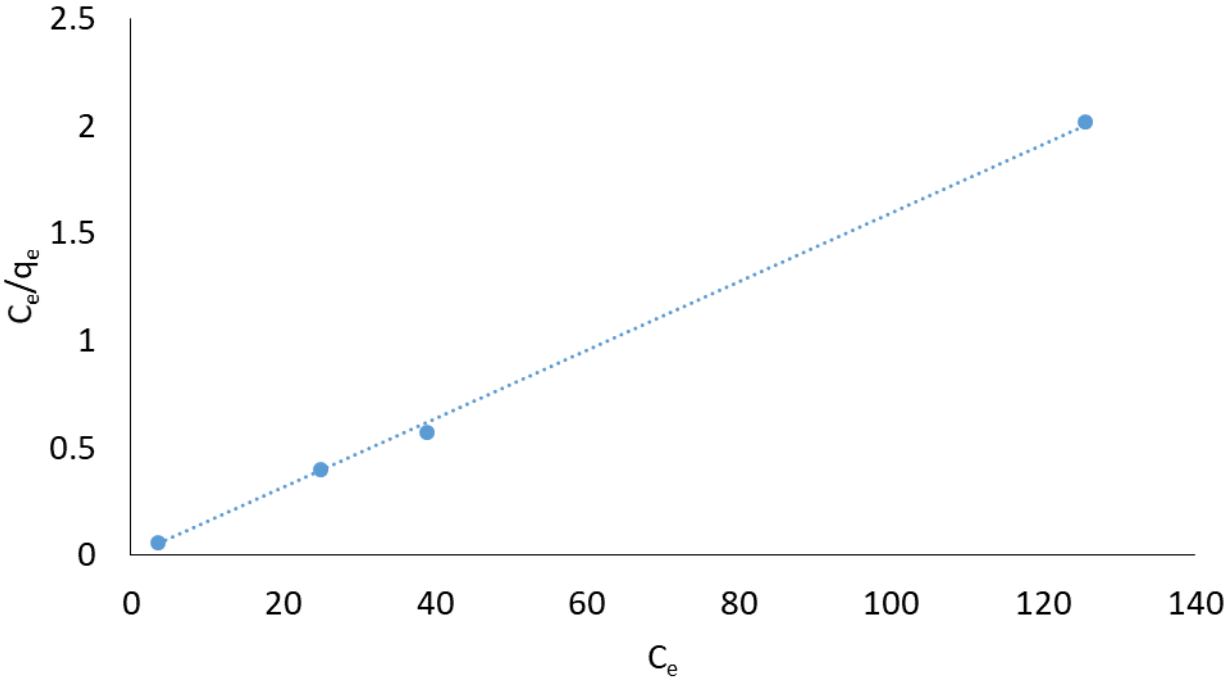

Figure 5.5: Linear fit curve for Langmuir adsorption isotherm of EFB-FBC

The R^2 value of 0.9991 and Q_{max} values closely matching experimental values signify a very well representation of the adsorption process by the model. This suggests that EFB-FBC surface are homogenous adsorption-wise and formation of MB monolayer are the main adsorption process.

Adsorption kinetic profiles of MB adsorption onto EFB-FBC were also analyzed, with data collected being fit into 3 different kinetic models; PSO, PFO, and IPD kinetic models. The adsorption kinetic constants and linear fit curves are shown in **Figure 5.6 - Figure 5.8** and **Table 5.3**.

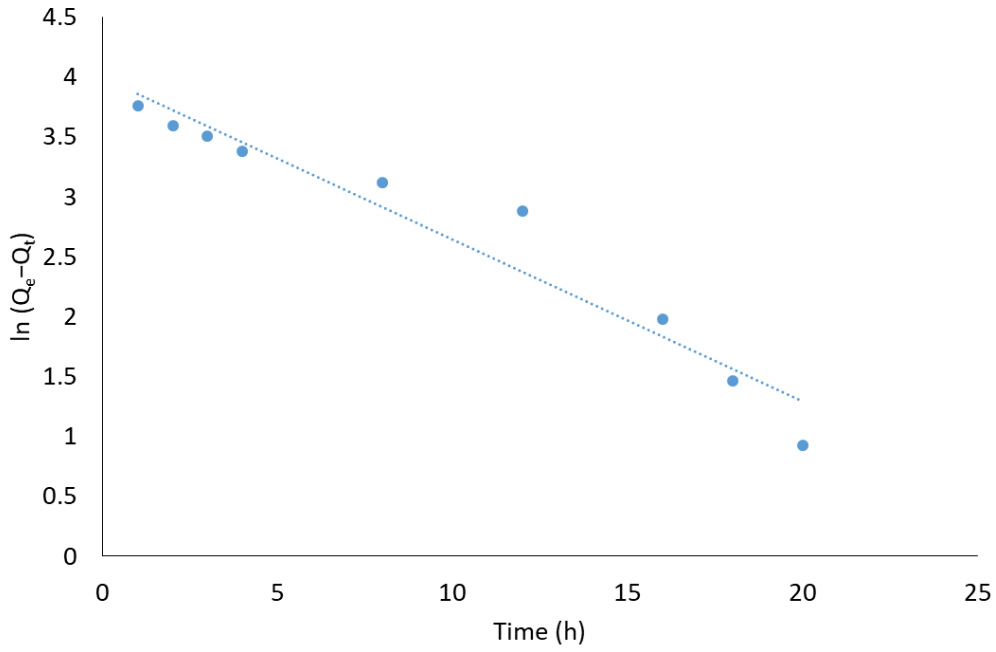

Figure 5.6: Pseudo-first order (PFO) linear fit curve for EFB-FBC

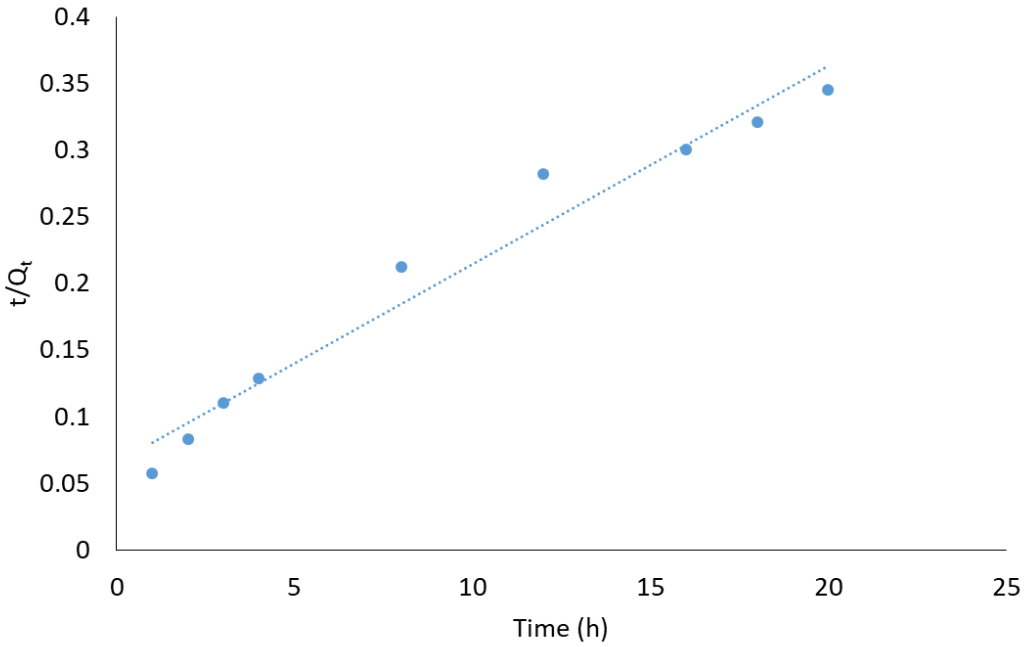

Figure 5.7: Pseudo-second order (PSO) linear fit curve for EFB-FBC

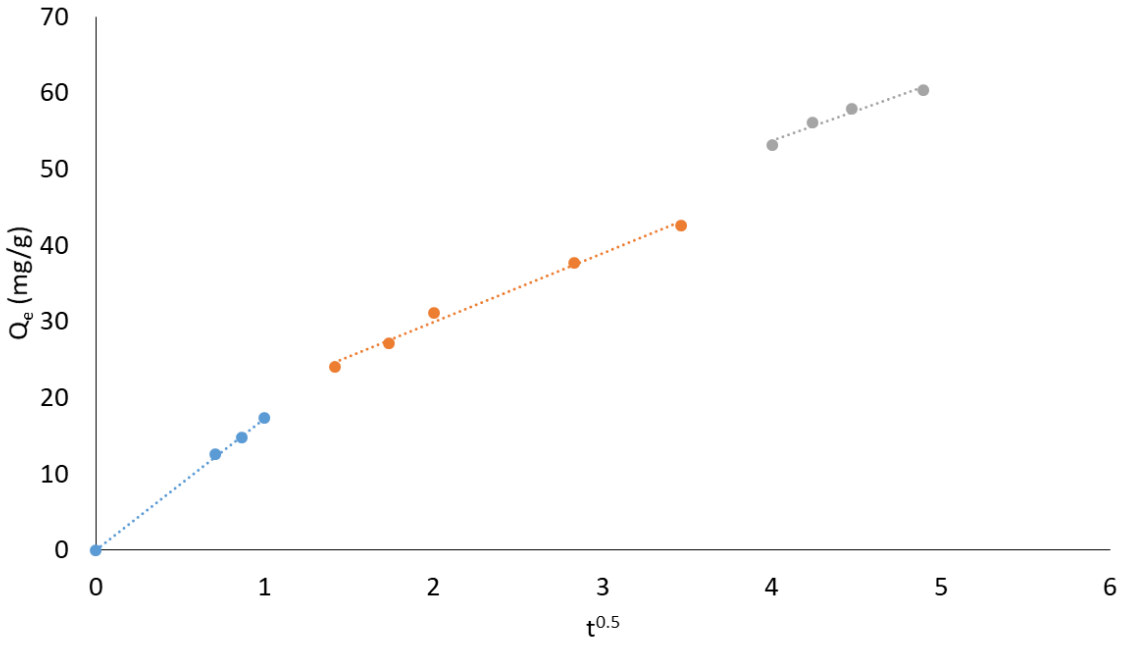

Figure 5.8: Intra-particle diffusion model linear fit curve for EFB-FBC

Table 5.3: Kinetic constants for EFB-FBC adsorption of methylene blue

Model	Constants	
Pseudo-first order	Q_{e1} (mg/g)	42.674 ± 0.316
	k_1 (min^{-1})	0.076 ± 0.006
	R^2	0.9402
Pseudo-second order	Q_{e2} (mg/g)	45.662 ± 0.338
	k_2 (g/mg.min)	0.015 ± 0.003
	R^2	0.9666
Intraparticle diffusion	k_{p1}	17.312 ± 0.140
	R^2_1	0.9991
	k_{p2}	9.007 ± 0.073
	R^2_2	0.9901
	k_{p3}	7.817 ± 0.063
	R^2_3	0.9703

PSO kinetic model represents the adsorption kinetic best with an R^2 value of 0.9666 compared to PFO of 0.9402. This suggests that chemisorption is the main adsorption method, where chemical interaction between EFB-FBC surface and MB dye molecule was dominant. From the linear fit curves, it can be seen that PSO kinetic model cannot fully describe the adsorption kinetics completely. Due to this, the IPD model was applied to the kinetic data and it is clear that the adsorption proceeds as a multiple-layer adsorption process, from the multiple linear it of the curve. It is deduced that the adsorption process can be separated into 3 different stages; (1) the adsorption of MB onto the external surface area (macropore) of EFB-FBC (film diffusion), (2) the diffusion of MB molecule from the external surface into the pores of the EFB-FBC, and (3) the intra particle diffusion of MB molecule in the internal structures of the EFB-FBC. The multi-stage adsorption process was also reported by other researchers on the adsorption of heavy metal ions and dyes on ramie and sludge-based biochar [153,154]. The multi-layer adsorption process can also explain the relatively slow uptake of MB by the EFB-FBC. Since the EFB-FBC has a low surface area with mainly microporous structures, the initial adsorption of MB molecule to the external

macroporous surface area quickly saturates it, which limits the subsequent adsorption stages. When adsorbed MB from the external surfaces diffused into the internal adsorption sites, the external surfaces are freed up and able to accept more MB molecules. This is apparent in the k_p values, which are lower for higher adsorption stages since later stages adsorption process are limited by the diffusion rate of MB between adsorption stages.

5.4.7.2 Heavy metal adsorption

EFB-FC performance on adsorption of heavy metal ions from aqueous solution was also determined to see whether additional oxygen functional groups improve its affinity towards negatively charged heavy metal ions. Tan et al. reported that oxygen functional groups with their electronegative oxygen atoms have a higher affinity towards negatively charged heavy metal ions, which should increase its adsorption capacity [155]. Performance of EFB-FBC was compared with untreated EFB-BC as control. Removal percentages are shown in **Figure 5.9**.

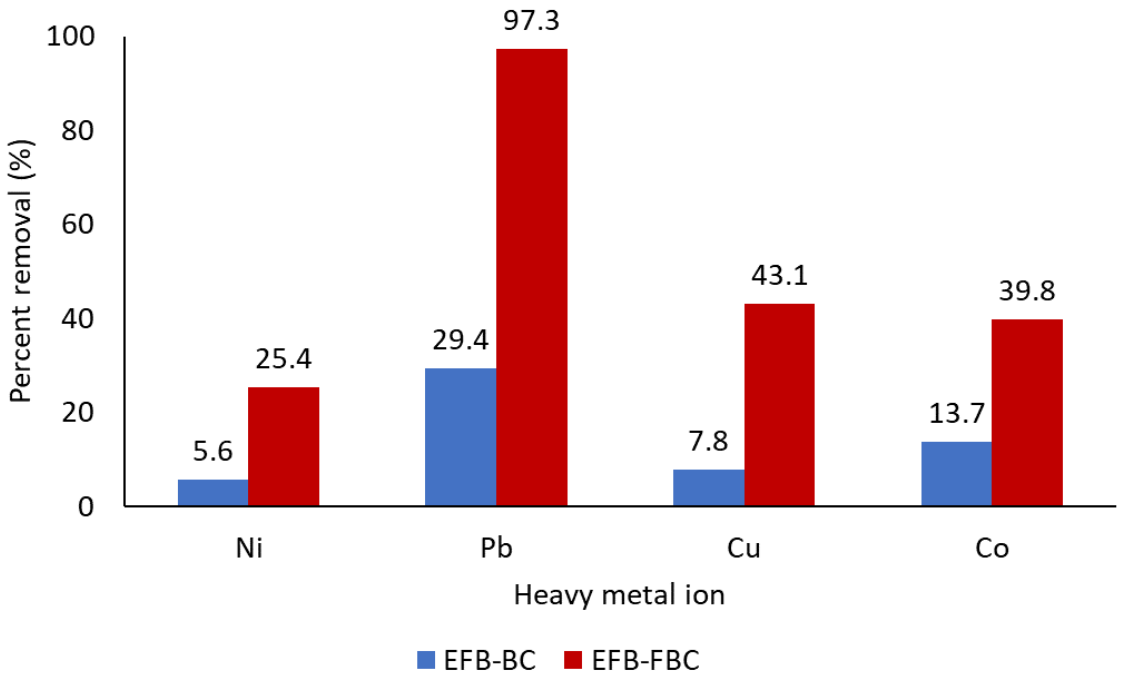

Figure 5.9: Heavy metal removal percentage of EFB-FBC

From **Figure 5.9**, it can be seen that the hydrothermal functionalization treatment increases the performance of EFB-BC in adsorbing all types of heavy metal tested. Improvement to up to 6x in terms of removal percentage suggests that oxygen functional groups increase the affinity of biochar in adsorbing heavy metal ions. This supports the idea of modifying low-performance carbon material to improve or tune its properties for specialized usage, which can in turn increase its value using simple processes at low cost.

5.4.8 Mechanism of hydrothermal functionalization using nitric acid

Previously, oxidation and nitration of carbon materials using nitric acid have been reported but the concentration of nitric acid used was relatively high compared to this study. The temperature used was in the range of 50–140°C but sustained for a long time, up to 5 hr. **Table 5.4** shows the comparison between previously reported nitric acid modification on carbon material and its treatment parameters. Based on the literature, it is clear that functionalization of carbon material using nitric acid has only been done either using a highly concentrated nitric acid solution, use of an extended period of treatment time, the high temperature under reflux, or a combination of those. By using a hydrothermal process via autoclave, the increased pressure of the process was enough to improve the efficiency of the reaction, hence reducing the concentration and time needed to successfully functionalize the biochar surface.

Table 5.4: Comparison of surface functionalization of biochar using nitric acid

Carbon Material	Nitric acid conc. (v/v %)	Treatment Time (min)	Treatment Temp. (°C)	Reference
Biomass-based bagasse biochar	10 - 25	360	60	[156]
Coal based activated carbon	5 - 20	120	100	[157]
Waste tea activated carbon	20 - 80	N/A	90	[148]
Rice husk activated carbon	42 - 71	50 -20	90 - 150	[158]
Activated carbon, Carbon nanotube and graphene oxide	N/A	30	140	[159]
Carbon cloth	68	60	90	[151]
Bagasse activated carbon	32.5	300	60	[160]
Mesoporous carbon	68	120	60	[161]
Oil palm empty fruit bunch biochar	6	60	132	This study

The oxidation mechanism of biochar surface by nitric acid was not clearly explained in previous literature even though similar observation has been reported in terms of FTIR

spectra changes and total surface acid groups. It is suggested that surface oxidation proceeds via the oxidation of aromatic groups in the bulk carbon structure of the biochar. This process is possible due to the inherent presence of some surface groups such as hydroxyl and carbonyl groups that can be further oxidized by nitric acid and other nitrogen-containing species, which might be produced due to the degradation of nitric acids, such as nitrous acid [162]. Multiple processes during carbonization such as depolymerization of cellulose and hemicellulose structure, bond cleavage of lignin structure and subsequent dehydration, decarboxylation, aromatization, and intramolecular condensation between the major component of the biomass and its degradation products result in a complex biochar structure rich with aromatic rings, aliphatic structures, and oxygen-containing functional groups. An excellent review by Liu et al. provides an in-depth explanation and characterization of the lignocellulosic carbonization process [63]. OPEFB carbonization temperature at 450°C allows some functional groups to still be present on the biochar surface, as shown in the FTIR spectra of EFB-BC. A similar trend of functional group presence was also reported by Zhang et al., where they investigate the effect of pyrolysis temperature on the abundance of oxygen functional groups on the surface of barley grass biochar [163]. In addition to that, the functional groups activate the aromatic ring for nitration [164], which explains the nitro group peaks present in the FTIR spectra of the EFB-FBC.

5.4.9 Application on other carbon material

The same hydrothermal treatment was applied to other types of biochar from oil palm biomass, and also on activated carbon to determine the feasibility of the process in functionalizing other carbon materials. After hydrothermal treatment, treated carbon materials were subjected to FTIR analysis to observe any surface functional group change. The FTIR spectra are shown in **Figure 5.10 - Figure 5.12**

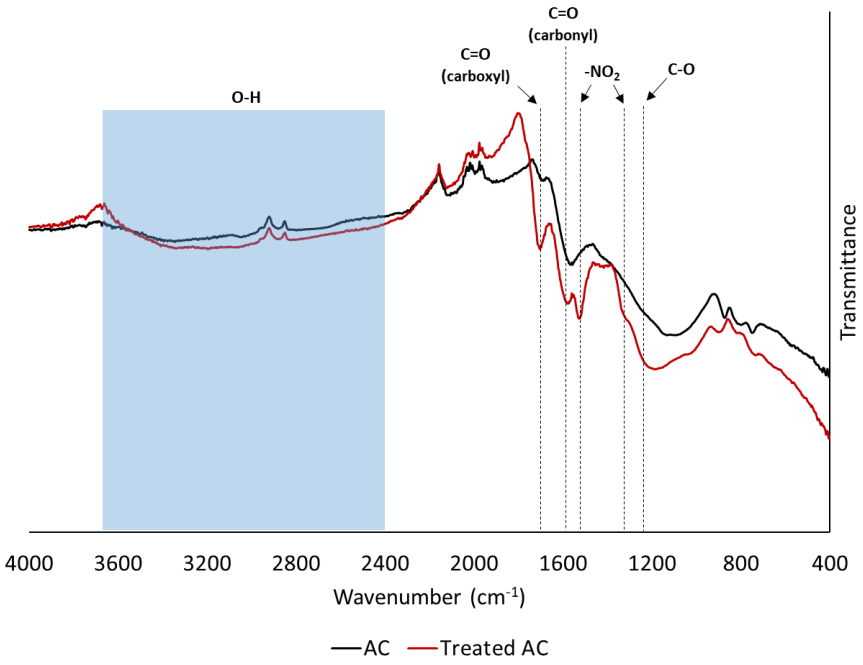

Figure 5.10: FTIR spectra of untreated and treated activated carbon (AC)

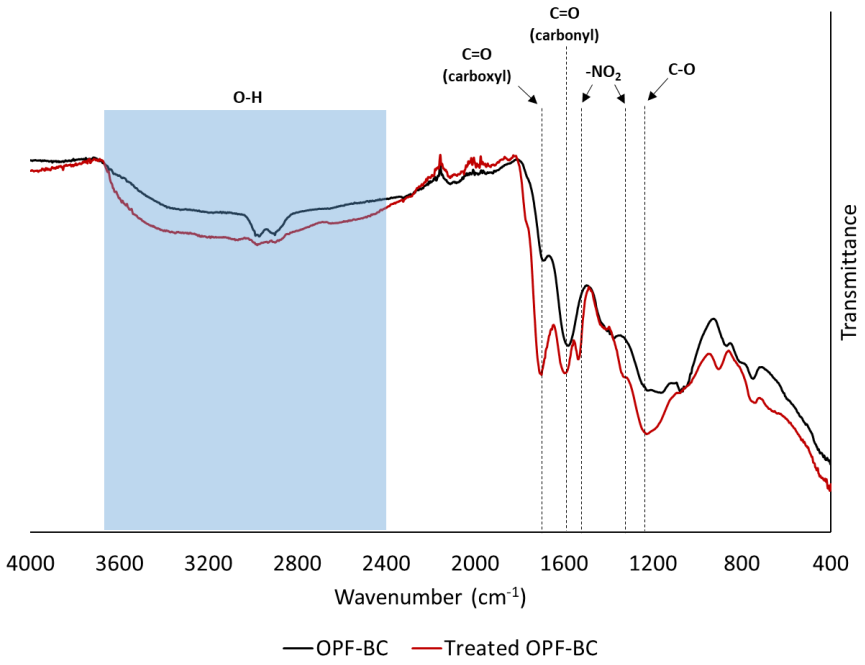

Figure 5.11: FTIR spectra of untreated and treated OPF biochar (OPF-BC)

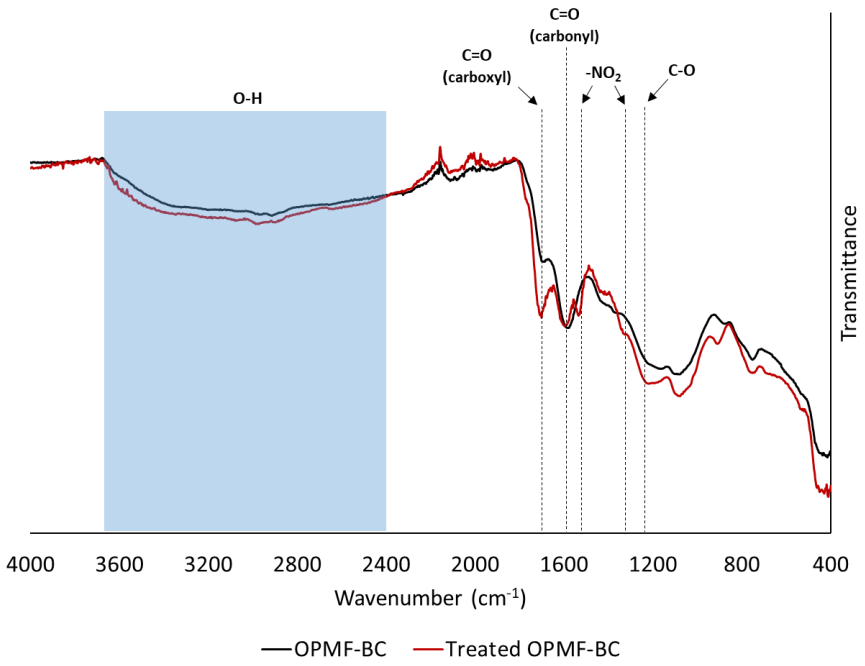

Figure 5.12: FTIR spectra of untreated and treated OPMF biochar (OPMF-BC)

Based on the FTIR spectra of the carbon materials before and after hydrothermal treatment, it is apparent that the process successfully increases surface functional groups of the carbon material surfaces. The process introduces new absorption peaks in the FTIR spectra, such as carbonyl, carboxyl, and nitro group peaks. For activated carbon, OPF-BC and OPMF-BC, the structure is mostly amorphous due to the abundant number of pores in their macrostructure which translates to more surface area available for the reaction that results in significant changes in surface functional groups. With this result, it can be safely concluded that the process can be a feasible way to functionalize carbon material, not just biochar but also activated carbon to improve its performance, or to tune its properties for specialized processes.

5.5 Conclusion

Based on the analysis data of the biochar after treatment, it can be concluded that the proposed hydrothermal functionalization treatment successfully adds new functional oxygen functional groups to the biochar surface. Functional groups such as carboxyl, carbonyl, and nitro groups were detected through FTIR analysis and supported with an increase in oxygen content through EDX analysis. The treatment does not significantly change the pore structure of the biochar, as proven by the BET surface area analysis where surface area, pore diameter, and volume does not significantly change compared to other reported method in the literature. SEM analysis shows some enlargement of macropore, with the removal of silica bodies on the biochar surface, which would help the diffusion of adsorbate into the internal structure of the biochar. Adsorption isotherm and kinetic analysis using methylene blue as synthetic adsorbate suggest Langmuir isotherm, with pseudo-second-order and intraparticle diffusion kinetic model, can explain the adsorption process. EFB-FBC also shows increase performance in removing methylene blue and heavy metal ions, compared

to untreated EFB biochar. Applying the hydrothermal treatment on other carbon material such as oil palm biomass-based biochar and activated carbon suggest that the process can be a feasible way to functionalize carbon material, with an exception on highly structured carbon material such as graphite. With these results, it is conclusive that the hydrothermal process using an autoclave to functionalize carbon material, especially carbon material produced from oil palm biomass can be proposed as a new, simpler method to produce a higher value-added product using currently available resources in the palm oil industry.

CHAPTER 6

CONCLUSION AND RECOMMENDATIONS

6.1 Conclusion

Previous working chapters of this thesis have shown that hydrothermal treatment is a versatile method for biomass treatment and carbon material modification. This study has successfully achieved the following:

1. Removal of lignin from oil palm fronds was successfully achieved with lignin removal of 91.7%. The yield of the process is 60.9% for OPF, which is comparable to other processes reported in the literature while being much simpler and easier. The process produces biomass with relatively high holocellulose content, which is 70.4% cellulose and 20.3% hemicellulose by mass. The treated OPF has good thermal stability and high Segal crystallinity based on TGA, FTIR, and XRD analysis. This suggests high purity cellulose with high crystallinity that can be a good feedstock for biocomposites production. The optimal parameters for OPF lignin removal were found to be 0.5M nitric acid, 30 min, and temperature of 120°C.
2. The hydrothermal lignin removal process was successfully applied to other types of biomass, which are oil palm empty fruit bunch and Matake bamboo. This shows that the process can be applied to other types of biomass to remove lignin without major parameter changes.
3. Combined superheated steam and hydrothermal treatment were successful in producing biomass that can dissolve in NaOH. The method developed was simple, require only two steps with minimal use of reagent. The dissolution process was also easier and faster compared to the cold alkali dissolution process reported in

the literature. Combined treated biomass can be dissolved to produce a stable solution for up to 4% in biomass concentration. Cellulose dissolved in NaOH solution can be readily regenerated through neutralization with acetic acid. It is hypothesized that the change in biomass properties through SHS treatment might be due to a decrease in intra-chain and inter-sheet hydrogen bonding strength which in turn improves the solubility of the cellulose macrostructure in NaOH solution. SEM, TGA, FTIR, and XRD analysis towards combined treated biomass does not show any significant change in the structure and surface functional groups of the biomass that can explain the dissolution property. Combined SHS-hydrothermal treatment was also shown to be a feasible way to treat another type of biomass which is Matake bamboo.

4. A new, simpler, and appropriate method to functionalize biochar from oil palm biomass was successfully developed. Treatment using 1M nitric acid at 132°C for 60 min successfully introduced new surface functional groups on the surface of the biochar. EDX and FTIR analysis show the process added new oxygen surface functional groups such as carboxyl and carbonyl groups. Nitrogen-containing groups in the form of the nitro group were also detected. SEM analysis and BET surface area determination show that the process does not affect the bulk structure and surface area of the biochar. Functionalized biochar performance in removing methylene blue and heavy metal increased significantly compared to untreated biochar. The improvement in performance can be attributed to the increase in affinity towards dye and heavy metal through the increase in electronegative oxygen and nitrogen-containing surface functional groups
5. The hydrothermal functionalization process was determined to be applicable towards other carbon materials such as biochar from OPF and also commercial

activated carbon. FTIR analysis shows a similar increase in oxygen and nitrogen-containing functional groups on the surface of the carbon material. This result suggests that the process can be applied to other carbon materials to improve their performance through functionalization.

Based on the result and analysis shown in this thesis, it is concluded that hydrothermal treatment using nitric acid can be an alternative process for producing value-added products from biomass and its derivatives such as biochar.

6.2 Recommendations

Further studies towards the use of hydrothermally treated biomass as raw material in the production of biocomposite and other biomass-based materials are recommended. Application in the industry includes the use of real-world equipment such as sterilizers as a proof of concept and scale-up feasibility studies should also be considered for future works. Besides that, the mechanism of nitric acid in removing lignin, and its selectivity towards lignin are not fully understood and should be investigated further. The waste from the hydrothermal treatment can be neutralized and used as crude fertilizer, fortified with additional nutrients from the degradation by-products of lignin. For the combined hydrothermal-SHS treatment process, the mechanism of biomass solubility needs to be investigated further to improve the understanding of the dissolution process. Further studies especially in cellulose regeneration methods and production of usable products from dissolved cellulose from this method such as cellulose membranes and films are also recommended.

REFERENCES

1. Sukiran, M.A.; Loh, S.K.; Bakar, N.A. Conversion of pre-treated oil palm empty fruit bunches into bio-oil and bio-char via fast pyrolysis. *J. Oil Palm Res.* **2018**, *30*, 121–129, doi:10.21894/jopr.2017.0006.
2. Khatun, R.; Reza, M.I.H.; Moniruzzaman, M.; Yaakob, Z. Sustainable oil palm industry: The possibilities. *Renew. Sustain. Energy Rev.* **2017**, *76*, 608–619, doi:10.1016/j.rser.2017.03.077.
3. 8 things to know about palm oil | WWF Available online: https://www.wwf.org.uk/updates/8-things-know-about-palm-oil (accessed on May 11, 2021).
4. Tan, Y.D.; Lim, J.S. Feasibility of palm oil mill effluent elimination towards sustainable Malaysian palm oil industry. *Renew. Sustain. Energy Rev.* **2019**, *111*, 507–522, doi:10.1016/j.rser.2019.05.043.
5. Rizal, N.F.A.A.; Ibrahim, M.F.; Zakaria, M.R.; Abd-Aziz, S.; Yee, P.L.; Hassan, M.A. Pre-treatment of Oil Palm Biomass for Fermentable Sugars Production. *Molecules* **2018**, *23*, 1–14, doi:10.3390/molecules23061381.
6. Corporation, M.P. *Sustainable Development Initiatives in Malaysia*; 2010; ISBN 9789832025726.
7. Zainudin, M.H.M.; Ramli, N.; Hassan, M.A.; Shirai, Y.; Tashiro, K.; Sakai, K.; Tashiro, Y. Bacterial community shift for monitoring the co-composting of oil palm empty fruit bunch and palm oil mill effluent anaerobic sludge. *J. Ind. Microbiol. Biotechnol.* **2017**, *44*, 869–877, doi:10.1007/s10295-017-1916-1.
8. Najib, M.A.; Samsu, A.B.; Hock, L.S. Co-Composting of Chipped Oil Palm Frond Enriched With Palm Oil Mill Effluent. **2016**.
9. Razali, W.A.W.; Baharuddin, A.S.; TarmezeeTalib, A.; Sulaiman, A.; Naim, M.N.; Hassan, M.A.; Shirai, Y. Degradation of oil palm empty fruit bunches (OPEFB) fibre during composting process using in-vessel composter. *BioResources* **2012**, *7*, 4786–4805, doi:10.15376/biores.7.4.4786-4805.
10. TDM Bhd bina dua loji biogas Available online: https://www.bharian.com.my/bisnes/korporat/2018/07/449987/tdm-bhd-bina-dua-loji-biogas (accessed on Apr 14, 2021).
11. Biomass - an overview | ScienceDirect Topics Available online: https://www.sciencedirect.com/topics/agricultural-and-biological-sciences/biomass (accessed on Apr 14, 2021).
12. biomass | Definition, Types, & Facts | Britannica Available online: https://www.britannica.com/science/biomass (accessed on Apr 14, 2021).
13. Mckendry, P. Energy production from biomass (part 1): overview of biomass. *Bioresour. Technol.* **2002**, *83*, 37–46.
14. Langholtz, M.; Stokes, B.; Eaton, L. 2016 billion-ton report: Advancing domestic resources for a thriving bioeconomy (Executive Summary). *Ind. Biotechnol.* **2016**, *12*, 282–289, doi:10.1089/ind.2016.29051.doe.

15. U.S. Department of Energy *US Billion Ton Update: Supply for a Bioenergy and Bioprodcts Industry*; Oak Ridge, 2011;

16. GLOBAL BIOENERGY STATISTICS 2020 World Bioenergy Association. **2020**, 3; 23; 49.

17. Pimentel, D. Limits of Biomass Utilization. *Encycl. Phys. Sci. Technol.* 2002, *2*, 1–13.

18. Corley, R.H.V.; Tinker, P.B. *The Oil Palm*; Corley, R.H.V., Tinker, P.B., Eds.; Blackwell Science Ltd: Oxford, UK, 2003; ISBN 9780470750971.

19. FAO *Better Farming Series: The Oil Palm*; 3rd ed.; Food and Agriculture Organization of the United Nations, 1990; ISBN 92-5-100625-3.

20. Khomphet, T.; Eksomtramage, T.; Duangpan, S. Genetic variation of improved oil palm tenera hybrid populations using morphological and SSR markers. *Songklanakarin J. Sci. Technol.* **2018**, *40*, 1329–1335, doi:10.14456/sjst-psu.2018.163.

21. Priambodo, R.; Witarto, A.B.; Salamah, A.; Setiorini; Triyono, D.; Bowolaksono, A. Morphology and protein molecular weight analysis from three variant of oil palm pollen; Dura, Pisifera, and Tenera. *AIP Conf. Proc.* **2017**, *1862*, doi:10.1063/1.4991220.

22. Poku, K. Small-Scale Palm Oil Processing in Africa Available online: http://www.fao.org/docrep/005/y4355e/y4355e03.htm.

23. Malaysian Palm Oil Board *Overview of the Malaysian Oil Palm Industry*; 2020;

24. Oil yield by crop type, 2017 Available online: https://ourworldindata.org/grapher/oil-yield-by-crop (accessed on Mar 26, 2021).

25. Malaysian Palm Oil Board Oil Palm Planted Area 2019 Available online: http://bepi.mpob.gov.my/index.php/en/area/area-2019/oil-palm-planted-area-as-at-dec-2019.html (accessed on Aug 5, 2020).

26. Foong, S.Z.Y.; Andiappan, V.; Foo, D.C.Y.; Ng, D.K.S. Flowsheet Synthesis and Optimisation of Palm Oil Milling Processes with Maximum Oil Recovery. In; Springer, Singapore, 2019; pp. 3–32.

27. Maycock, J.H. Innovations in palm oil mill processing and refining. *Innov. palm oil mill Process. refining.* **1990**, 23–37.

28. Ibrahim, I.; Hassan, M.A.; Abd-Aziz, S.; Shirai, Y.; Andou, Y.; Othman, M.R.; Ali, A.A.M.; Zakaria, M.R. Reduction of residual pollutants from biologically treated palm oil mill effluent final discharge by steam activated bioadsorbent from oil palm biomass. *J. Clean. Prod.* **2017**, *141*, 122–127, doi:10.1016/j.jclepro.2016.09.066.

29. Ali, A.A.M.; Othman, M.R.; Shirai, Y.; Hassan, M.A. Sustainable and integrated palm oil biorefinery concept with value-addition of biomass and zero emission system. *J. Clean. Prod.* **2015**, *91*, 96–99, doi:10.1016/j.jclepro.2014.12.030.

30. Poh, P.E.; Yong, W.J.; Chong, M.F. Palm oil mill effluent (POME)

characteristic in high crop season and the applicability of high-rate anaerobic bioreactors for the treatment of pome. *Ind. Eng. Chem. Res.* **2010**, *49*, 11732–11740, doi:10.1021/ie101486w.

31. Agensi Inovasi Malaysia National Biomass Strategy 2020 for Malaysia v2.0. **2015**, 47.

32. Then, Y.Y.; Ibrahim, N.A.; Zainuddin, N.; Ariffin, H.; Yunus, W.M.Z.W.; Chieng, B.W. The influence of green surface modification of oil palm mesocarp fiber by superheated steam on the mechanical properties and dimensional stability of oil palm mesocarp fiber/poly(butylene succinate) biocomposite. *Int. J. Mol. Sci.* **2014**, *15*, 15344–15357, doi:10.3390/ijms150915344.

33. Baharuddin, A.S.; Wakisaka, M.; Shirai, Y.; Abd-Aziz, S.; Abdul Rahm, N.A.; Hassan, M.A. Co-Composting of Empty Fruit Bunches and Partially Treated Palm Oil Mill Effluents in Pilot Scale. *Int. J. Agric. Res.* **2009**, *4*, 69–78, doi:10.3923/ijar.2009.69.78.

34. Loh, S.K. The potential of the Malaysian oil palm biomass as a renewable energy source. *Energy Convers. Manag.* **2017**, *141*, 285–298, doi:10.1016/j.enconman.2016.08.081.

35. Novianti, S.; Nurdiawati, A.; Zaini, I.N.; Prawisudha, P.; Sumida, H.; Yoshikawa, K. Low-potassium Fuel Production from Empty Fruit Bunches by Hydrothermal Treatment Processing and Water Leaching. *Energy Procedia* **2015**, *75*, 584–589, doi:10.1016/j.egypro.2015.07.460.

36. Adnan, M.F.; Mokhtar, H. Potential of empty fruit bunches (EFB) as a new renewable energy.

37. Abdullah, N.; Sulaiman, F. The Oil Palm Wastes in Malaysia. In *Biomass Now - Sustainable Growth and Use*; Matovic, M.D., Ed.; InTech, 2013; pp. 75–100 ISBN 978-953-51-1105-4,.

38. Ooi, Z.X.; Teoh, Y.P.; Kunasundari, B.; Shuit, S.H. Oil palm frond as a sustainable and promising biomass source in Malaysia: A review. *Environ. Prog. Sustain. Energy* **2017**, *36*, 1864–1874, doi:10.1002/ep.12642.

39. Yunos, N.S.H.M.; Baharuddin, A.S.; Md Yunos, K.F.; Hafid, H.S.; Busu, Z.; Mokhtar, M.N.; Sulaiman, A.; Som, A.M. The physicochemical characteristics of residual oil and fibers from oil palm empty fruit bunches. *BioResources* **2015**, *10*, 14–29, doi:10.15376/biores.10.1.14-29.

40. Aziz, M.; Kurniawan, T.; Oda, T.; Kashiwagi, T. Advanced power generation using biomass wastes from palm oil mills. *Appl. Therm. Eng.* **2017**, *114*, 1378–1386, doi:10.1016/j.applthermaleng.2016.11.031.

41. Shuit, S.H.; Tan, K.T.; Lee, K.T.; Kamaruddin, a. H. Oil palm biomass as a sustainable energy source: A Malaysian case study. *Energy* **2009**, *34*, 1225–1235, doi:10.1016/j.energy.2009.05.008.

42. Susanty, W.; Helwani, Z.; Zulfansyah Torrefaction of oil palm frond: The effect of process condition to calorific value and proximate analysis. *IOP Conf. Ser. Mater. Sci. Eng.* **2018**, *345*, doi:10.1088/1757-899X/345/1/012016.

43. Munawar, S.S.; Subiyanto, B. Characterization of Biomass Pellet Made from

Solid Waste Oil Palm Industry. *Procedia Environ. Sci.* **2014**, *20*, 336–341, doi:10.1016/j.proenv.2014.03.042.

44. Uemura, Y.; Omar, W.N.; Tsutsui, T.; Yusup, S.B. Torrefaction of oil palm wastes. *Fuel* **2011**, *90*, 2585–2591, doi:10.1016/j.fuel.2011.03.021.

45. Uemura, Y.; Saadon, S.; Osman, N.; Mansor, N.; Tanoue, K.I. Torrefaction of oil palm kernel shell in the presence of oxygen and carbon dioxide. *Fuel* **2015**, *144*, 171–179, doi:10.1016/j.fuel.2014.12.050.

46. Hassan, S.; Kee, L.S.; Al-Kayiem, H.H. Experimental study of palm oil mill effluent and oil palm frond waste mixture as an alternative biomass fuel. *J. Eng. Sci. Technol.* **2013**, *8*, 703–712.

47. Saeman, J.F.; Bubl, J.L.; Harris, E.E. Quantitative 1 of Wood and Cellulose. *Ind. Eng. Chem. - Anal. Ed.* **1945**, *17*, 35–37, doi:10.1021/i560137a008.

48. Nik Mahmud, N.A.; Baharuddin, A.S.; Kamal Bahrin, E.; Sulaiman, A.; Naim, M.N.; Zakaria, R.; Hassan, M.A.; Nishida, H.; Shirai, Y. Enzymatic Saccharification of Oil Palm Mesocarp Fiber (OPMF) Treated with Superheated Steam. *BioResources* **2013**, *8*, 1320–1331, doi:10.15376/biores.8.1.1320-1331.

49. Garritano, A.N.; Faber, M. de O.; De Sà, L.R.V.; Ferreira-Leitão, V.S. Palm oil mill effluent (POME) as raw material for biohydrogen and methane production via dark fermentation. *Renew. Sustain. Energy Rev.* **2018**, *92*, 676–684, doi:10.1016/j.rser.2018.04.031.

50. Zahari, M.A.K.M.; Zakaria, M.R.; Ariffin, H.; Mokhtar, M.N.; Salihon, J.; Shirai, Y.; Hassan, M.A. Renewable sugars from oil palm frond juice as an alternative novel fermentation feedstock for value-added products. *Bioresour. Technol.* **2012**, *110*, 566–571, doi:10.1016/j.biortech.2012.01.119.

51. Zakaria, M.R.; Hirata, S.; Fujimoto, S.; Ibrahim, I.; Hassan, A. Soluble inhibitors generated during hydrothermal pretreatment of oil palm mesocarp fiber suppressed the catalytic activity of Acremonium cellulase. *Bioresour. Technol.* **2016**, *200*, 541–547, doi:10.1016/j.biortech.2015.10.075.

52. Hock, L.S.; Baharuddin, A.S.; Ahmad, M.N.; Shah, U.K.; Aini, N.; Rahman, A.; Abd-aziz, S.; Hassan, M.A.; Shirai, Y. Physicochemical Changes in Windrow Co-Composting Process of Oil Palm Mesocarp Fiber and Palm Oil Mill Effluent Anaerobic Sludge. *Aust. J. Basic Appl. Sci.* **2009**, *3*, 2809–2816.

53. Vakili, M.; Rafatullah, M.; Ibrahim, M.H.; Salamatinia, B.; Gholami, Z.; Zwain, H.M. A review on composting of oil palm biomass. *Environ. Dev. Sustain.* **2015**, *17*, 691–709, doi:10.1007/s10668-014-9581-2.

54. Gandahi, A.W.; Hanafi, M.M. Bio-composting Oil Palm Waste for Improvement of Soil Fertility. In; Springer, Cham, 2014; pp. 209–243.

55. Antal, M.J.; Grønli, M. The Art, Science, and Technology of Charcoal Production. *Ind. Eng. Chem. Res.* **2003**, *42*, 1619–1640.

56. Rashid, M.; Chong, W.C.; Ramli, M.; Zainura, Z.N.; Norruwaida, J. Evaluation of particulate emission from a palm oil mill boiler. *Sains Malaysiana* **2013**, *42*, 1289–1292.

57. Hosseini, S.E.; Wahid, M.A. Utilization of palm solid residue as a source of renewable and sustainable energy in Malaysia. *Renew. Sustain. Energy Rev.* **2014**, *40*, 621–632, doi:10.1016/j.rser.2014.07.214.

58. Idris, J.; Shirai, Y.; Andou, Y.; Mohd Ali, A.A.; Othman, M.R.; Ibrahim, I.; Hassan, M.A. Self-sustained carbonization of oil palm biomass produced an acceptable heating value charcoal with low gaseous emission. *J. Clean. Prod.* **2015**, *89*, 257–261, doi:10.1016/j.jclepro.2014.11.016.

59. Kim, S.J.; Jung, S.H.; Kim, J.S. Fast pyrolysis of palm kernel shells: Influence of operation parameters on the bio-oil yield and the yield of phenol and phenolic compounds. *Bioresour. Technol.* **2010**, *101*, 9294–9300, doi:10.1016/j.biortech.2010.06.110.

60. Chen, Y.; Zhang, X.; Chen, W.; Yang, H.; Chen, H. The structure evolution of biochar from biomass pyrolysis and its correlation with gas pollutant adsorption performance. *Bioresour. Technol.* **2017**, *246*, 101–109, doi:10.1016/j.biortech.2017.08.138.

61. Rashidi, N.A.; Yusup, S. A review on recent technological advancement in the activated carbon production from oil palm wastes. *Chem. Eng. J.* **2017**, *314*, 277–290, doi:10.1016/j.cej.2016.11.059.

62. Ibrahim, I.; Tsubota, T.; Hassan, M.A.; Andou, Y. Surface Functionalization of Biochar from Oil Palm Empty Fruit Bunch through Hydrothermal Process. *Processes* **2021**, *9*, 149, doi:10.3390/pr9010149.

63. Liu, W.J.; Jiang, H.; Yu, H.Q. Development of Biochar-Based Functional Materials: Toward a Sustainable Platform Carbon Material. *Chem. Rev.* **2015**, *115*, 12251–12285, doi:10.1021/acs.chemrev.5b00195.

64. Megashah, L.N.; Ariffin, H.; Zakaria, M.R.; Hassan, M.A. Properties of Cellulose Extract from Different Types of Oil Palm Biomass. *IOP Conf. Ser. Mater. Sci. Eng.* **2018**, *368*, doi:10.1088/1757-899X/368/1/012049.

65. Xiang, L.Y.; Mohammed, M.A.; Samsu Baharuddin, A. Characterisation of microcrystalline cellulose from oil palm fibres for food applications. *Carbohydr. Polym.* **2016**, *148*, 11–20, doi:10.1016/j.carbpol.2016.04.055.

66. Lamaming, J.; Hashim, R.; Sulaiman, O.; Leh, C.P.; Sugimoto, T.; Nordin, N.A. Cellulose nanocrystals isolated from oil palm trunk. *Carbohydr. Polym.* **2015**, *127*, 202–208, doi:10.1016/j.carbpol.2015.03.043.

67. Abdullah, M.A.; Nazir, M.S.; Raza, M.R.; Wahjoedi, B.A.; Yussof, A.W. Autoclave and ultra-sonication treatments of oil palm empty fruit bunch fibers for cellulose extraction and its polypropylene composite properties. *J. Clean. Prod.* **2016**, *126*, 686–697, doi:10.1016/j.jclepro.2016.03.107.

68. Nazir, M.S.; Wahjoedi, B.A.; Yussof, A.W.; Abdullah, M.A. Eco-friendly extraction and characterization of cellulose from oil palm empty fruit bunches. *BioResources* **2013**, *8*, 2161–2172, doi:10.15376/biores.8.2.2161-2172.

69. Mohamad Haafiz, M.K.; Eichhorn, S.J.; Hassan, A.; Jawaid, M. Isolation and characterization of microcrystalline cellulose from oil palm biomass residue. *Carbohydr. Polym.* **2013**, *93*, 628–634, doi:10.1016/j.carbpol.2013.01.035.

70. Masran, R.; Bahrin, E.K.; Ibrahim, M.F.; Phang, L.Y.; Abd-Aziz, S. Simultaneous pretreatment and saccharification of oil palm empty fruit bunch using laccase-cellulase cocktail. *Biocatal. Agric. Biotechnol.* **2020**, *29*, 101824, doi:10.1016/j.bcab.2020.101824.

71. Liu, H.; Sun, J.; Chang, J.S.; Shukla, P. Engineering microbes for direct fermentation of cellulose to bioethanol. *Crit. Rev. Biotechnol.* 2018, *38*, 1089–1105.

72. Ilyas, R.A.; Sapuan, S.M.; Kadier, A.; Kalil, M.S.; Ibrahim, R.; Atikah, M.S.N.; Nurazzi, N.M.; Nazrin, A.; Lee, C.H.; Faiz Norrrahim, M.N.; et al. Properties and Characterization of PLA, PHA, and Other Types of Biopolymer Composites. In *Advanced Processing, Properties, and Applications of Starch and Other Bio-Based Polymers*; Elsevier, 2020; pp. 111–138.

73. Norrrahim, M.N.F.; Mohd Kasim, N.A.; Knight, V.F.; Mohamad Misenan, M.S.; Janudin, N.; Ahmad Shah, N.A.; Kasim, N.; Wan Yusoff, W.Y.; Mohd Noor, S.A.; Jamal, S.H.; et al. Nanocellulose: a bioadsorbent for chemical contaminant remediation. *RSC Adv.* **2021**, *11*, 7347–7368, doi:10.1039/d0ra08005e.

74. Arca, H.C.; Mosquera-Giraldo, L.I.; Bi, V.; Xu, D.; Taylor, L.S.; Edgar, K.J. Pharmaceutical Applications of Cellulose Ethers and Cellulose Ether Esters. *Biomacromolecules* **2018**, *19*, 2351–2376, doi:10.1021/acs.biomac.8b00517.

75. Li, M.; Pu, Y.; Ragauskas, A.J. Current understanding of the correlation of lignin structure with biomass recalcitrance. *Front. Chem.* **2016**, *4*, 1–8, doi:10.3389/fchem.2016.00045.

76. Li, X.; Zheng, Y. Biotransformation of lignin: Mechanisms, applications and future work. *Biotechnol. Prog.* **2020**, *36*, 1–21, doi:10.1002/btpr.2922.

77. Sun, X.F.; Sun, R.C.; Tomkinson, J.; Baird, M.S. Degradation of wheat straw lignin and hemicellulosic polymers by a totally chlorine-free method. *Polym. Degrad. Stab.* **2004**, *83*, 47–57, doi:10.1016/S0141-3910(03)00205-2.

78. Zhao, X.; Liu, D. Fractionating pretreatment of sugarcane bagasse by aqueous formic acid with direct recycle of spent liquor to increase cellulose digestibility-the Formiline process. *Bioresour. Technol.* **2012**, *117*, 25–32, doi:10.1016/j.biortech.2012.04.062.

79. Wang, J.; Wang, Q.; Wu, Y.; Bai, F.; Wang, H.; Si, S.; Lu, Y.; Li, X.; Wang, S. Preparation of cellulose nanofibers from bagasse by nitric acid and hydrogen peroxide enables fibrillation via a swelling, hydrolysis, and oxidation cooperative mechanism. *Nanomaterials* **2020**, *10*, 1–15, doi:10.3390/nano10112227.

80. Segal, L.; Creely, J.J.; Martin, A.E.; Conrad, C.M. An Empirical Method for Estimating the Degree of Crystallinity of Native Cellulose Using the X-Ray Diffractometer. *Text. Res. J.* **1959**, *29*, 786–794, doi:10.1177/004051755902901003.

81. Mikulski, D.; Kłosowski, G. Efficiency of dilute sulfuric acid pretreatment of distillery stillage in the production of cellulosic ethanol. *Bioresour. Technol.* **2018**, *268*, 424–433, doi:10.1016/j.biortech.2018.08.005.

82. Jaisamut, K.; Paulová, L.; Patáková, P.; Kotúčová, S.; Rychtera, M. Effect of sodium sulfite on acid pretreatment of wheat straw with respect to its final conversion to ethanol. *Biomass and Bioenergy* **2016**, *95*, 1–7, doi:10.1016/j.biombioe.2016.08.022.

83. Yu, J.; Xu, Z.; Liu, L.; Chen, S.; Wang, S.; Jin, M. Process integration for ethanol production from corn and corn stover as mixed substrates. *Bioresour. Technol.* **2019**, *279*, 10–16, doi:10.1016/j.biortech.2019.01.112.

84. Rezania, S.; Oryani, B.; Cho, J.; Talaiekhozani, A.; Sabbagh, F.; Hashemi, B.; Rupani, P.F.; Mohammadi, A.A. Different pretreatment technologies of lignocellulosic biomass for bioethanol production: An overview. *Energy* **2020**, *199*, 117457, doi:10.1016/j.energy.2020.117457.

85. Rodríguez-Chong, A.; Ramírez, J.A.; Garrote, G.; Vázquez, M. Hydrolysis of sugar cane bagasse using nitric acid: A kinetic assessment. *J. Food Eng.* **2004**, *61*, 143–152, doi:10.1016/S0260-8774(03)00080-3.

86. Hafid, H.S.; Omar, F.N.; Jiangyu, Z.; Wakisaka, M. Enhanced Crystallinity and Thermal Properties of Cellulose from Rice Husk Using Acid Hydrolysis Treatment. *Carbohydr. Polym.* **2021**, *260*, 117789, doi:10.1016/j.carbpol.2021.117789.

87. Gupta, A.; Simmons, W.; Schueneman, G.T.; Hylton, D.; Mintz, E.A. Rheological and thermo-mechanical properties of poly(lactic acid)/lignin-coated cellulose nanocrystal composites. *ACS Sustain. Chem. Eng.* **2017**, *5*, 1711–1720, doi:10.1021/acssuschemeng.6b02458.

88. Wang, X.; Jia, Y.; Liu, Z.; Miao, J. Influence of the lignin content on the properties of poly(lactic acid)/lignin-containing cellulose nanofibrils composite films. *Polymers (Basel).* **2018**, *10*, doi:10.3390/polym10091013.

89. Johar, N.; Ahmad, I.; Dufresne, A. Extraction, preparation and characterization of cellulose fibres and nanocrystals from rice husk. *Ind. Crops Prod.* **2012**, *37*, 93–99, doi:10.1016/j.indcrop.2011.12.016.

90. Nordin, N.; Ariffin, H.; Andou, Y.; Hassan, M.; Shirai, Y.; Nishida, H.; Yunus, W.; Karuppuchamy, S.; Ibrahim, N. Modification of Oil Palm Mesocarp Fiber Characteristics Using Superheated Steam Treatment. *Molecules* **2013**, *18*, 9132–9146, doi:10.3390/molecules18089132.

91. Hospodarova, V.; Singovszka, E.; Stevulova, N. Characterization of Cellulosic Fibers by FTIR Spectroscopy for Their Further Implementation to Building Materials. *Am. J. Anal. Chem.* **2018**, *09*, 303–310, doi:10.4236/ajac.2018.96023.

92. Galiwango, E.; Abdel Rahman, N.S.; Al-Marzouqi, A.H.; Abu-Omar, M.M.; Khaleel, A.A. Isolation and characterization of cellulose and α-cellulose from date palm biomass waste. *Heliyon* **2019**, *5*, e02937, doi:10.1016/j.heliyon.2019.e02937.

93. Khalil, H.P.S.A.; Alwani, M.S.; Ridzuan, R.; Kamarudin, H.; Khairul, A. Chemical composition, morphological characteristics, and cell wall structure of Malaysian oil palm fibers. *Polym. - Plast. Technol. Eng.* **2008**, *47*, 273–280, doi:10.1080/03602550701866840.

94. Zhao, X.; Zhang, L.; Liu, D. Biomass recalcitrance. Part I: the chemical compositions and physical structures affecting the enzymatic hydrolysis of lignocellulose. *Biofuels, Bioprod. Biorefining* **2012**, *6*, 465–482, doi:10.1002/bbb.1331.

95. Nilsson, H.; Galland, S.; Larsson, P.T.; Gamstedt, E.K.; Iversen, T. Compression molded wood pulp biocomposites: A study of hemicellulose influence on cellulose supramolecular structure and material properties. *Cellulose* **2012**, *19*, 751–760, doi:10.1007/s10570-012-9688-2.

96. Norrrahim, M.N.F.; Ariffin, H.; Yasim-Anuar, T.A.T.; Ghaemi, F.; Hassan, M.A.; Ibrahim, N.A.; Ngee, J.L.H.; Yunus, W.M.Z.W. Superheated steam pretreatment of cellulose affects its electrospinnability for microfibrillated cellulose production. *Cellulose* **2018**, *25*, 3853–3859, doi:10.1007/s10570-018-1859-3.

97. Nazmir, M.; Warid, M.; Ariffin, H.; Hassan, M.A. Optimization of Superheated Steam Treatment to Improve. **2016**, *11*, 5780–5796.

98. Yasim-Anuar, T.A.T.; Ariffin, H.; Norrrahim, M.N.F.; Hassan, M.A. Factors affecting spinnability of oil palm mesocarp fiber cellulose solution for the production of microfiber. *BioResources* **2017**, *12*, 715–734, doi:10.15376/biores.12.1.715-734.

99. Patil, S.K.R.; Heltzel, J.; Lund, C.R.F. Comparison of structural features of humins formed catalytically from glucose, fructose, and 5-hydroxymethylfurfuraldehyde. *Energy and Fuels* **2012**, *26*, 5281–5293, doi:10.1021/ef3007454.

100. Aarum, I.; Devle, H.; Ekeberg, D.; Horn, S.J.; Stenstrøm, Y. Characterization of Pseudo-Lignin from Steam Exploded Birch. *ACS Omega* **2018**, *3*, 4924–4931, doi:10.1021/acsomega.8b00381.

101. Adamski, R.; Siuta, D.; Kukfisz, B.; Mitkowski, P.T.; Szaferski, W. Influence of process parameters in superheated steam drying on fire and explosion parameters of woody biomass. *Fuel Process. Technol.* **2021**, *211*, 106597, doi:10.1016/j.fuproc.2020.106597.

102. Megashah, L.N.; Ariffin, H.; Zakaria, M.R.; Hassan, M.A.; Andou, Y.; Padzil, F.N.M. Modification of cellulose degree of polymerization by superheated steam treatment for versatile properties of cellulose nanofibril film. *Cellulose* **2020**, *27*, 7417–7429, doi:10.1007/s10570-020-03296-2.

103. Technical Association of Pulp and Paper Industry T 222 om-98 Acid-insoluble lignin in wood and pulp.

104. Nishida, H.; Gomi, S.; Ariffin, H. Short Bamboo Fibers Prepared by Super-Heated Steam Treatment for Antistatic Bio-composites. *Lignocellulose* **2017**, *6*, 3–14.

105. Poletto, M.; Ornaghi Júnior, H.L.; Zattera, A.J. Native cellulose: Structure, characterization and thermal properties. *Materials (Basel).* **2014**, *7*, 6105–6119, doi:10.3390/ma7096105.

106. Jandura, P.; Kokta, B. V.; Riedl, B. Fibrous long-chain organic acid cellulose

esters and their characterization by diffuse reflectance FTIR spectroscopy, solid-state CP/MAS 13C-NMR, and X-ray diffraction. *J. Appl. Polym. Sci.* **2000**, *78*, 1354–1365, doi:10.1002/1097-4628(20001114)78:7<1354::aid-app60>3.3.co;2-m.

107. Xu, A.; Zhang, Y. Insight into dissolution mechanism of cellulose in [C4mim][CH3COO]/DMSO solvent by 13C NMR spectra. *J. Mol. Struct.* **2015**, *1088*, 101–104, doi:10.1016/j.molstruc.2015.02.031.

108. Gross, A.S.; Chu, J.W. On the molecular origins of biomass recalcitrance: The interaction network and solvation structures of cellulose microfibrils. *J. Phys. Chem. B* **2010**, *114*, 13333–13341, doi:10.1021/jp106452m.

109. Hinterstoisser, B.; Åkerholm, M.; Salmén, L. Load distribution in native cellulose. *Biomacromolecules* **2003**, *4*, 1232–1237, doi:10.1021/bm030017k.

110. Parthasarathi, R.; Bellesia, G.; Chundawat, S.P.S.; Dale, B.E.; Langan, P.; Gnanakaran, S. Insights into hydrogen bonding and stacking interactions in cellulose. *J. Phys. Chem. A* **2011**, *115*, 14191–14202, doi:10.1021/jp203620x.

111. Horii, F.; Hirai, A.; Kitamaru, R. Cross-Polarization/Magic Angle Spinning Study 13 C-NMR. **1984**.

112. Nishiyama, Y.; Sugiyama, J.; Chanzy, H.; Langan, P. Crystal Structure and Hydrogen Bonding System in Cellulose Iα from Synchrotron X-ray and Neutron Fiber Diffraction. *J. Am. Chem. Soc.* **2003**, *125*, 14300–14306, doi:10.1021/ja037055w.

113. Yamashiki, T.; Kamide, K.; Okajima, K.; Kowsaka, K.; Matsui, T.; Fukase, H. Some Characteristic Features of Dilute Aqueous Alkali Solutions of Specific Alkali Concentration (2.5 mol l−1) Which Possess Maximum Solubility Power against Cellulose. *Polym. J.* **1988**, *20*, 447–457, doi:10.1295/polymj.20.447.

114. Medronho, B.; Lindman, B. Brief overview on cellulose dissolution/regeneration interactions and mechanisms. *Adv. Colloid Interface Sci.* **2015**, *222*, 502–508, doi:10.1016/j.cis.2014.05.004.

115. Cai, J.; Zhang, L. Rapid Dissolution of Cellulose in LiOH/Urea and NaOH/Urea Aqueous Solutions. *Macromol. Biosci.* **2005**, *5*, 539–548, doi:10.1002/mabi.200400222.

116. Egal, M.; Budtova, T.; Navard, P. The dissolution of microcrystalline cellulose in sodium hydroxide-urea aqueous solutions. *Cellulose* **2008**, *15*, 361–370, doi:10.1007/s10570-007-9185-1.

117. Isobe, N.; Noguchi, K.; Nishiyama, Y.; Kimura, S.; Wada, M.; Kuga, S. Role of urea in alkaline dissolution of cellulose. *Cellulose* **2013**, *20*, 97–103, doi:10.1007/s10570-012-9800-7.

118. Liu, W.; Budtova, T.; Navard, P. Influence of ZnO on the properties of dilute and semi-dilute cellulose-NaOH-water solutions. *Cellulose* **2011**, *18*, 911–920, doi:10.1007/s10570-011-9552-9.

119. Zhang, L.; Ruan, D.; Gao, S. Dissolution and regeneration of cellulose in NaOH/Thiourea aqueous solution. *J. Polym. Sci. Part B Polym. Phys.* **2002**, *40*, 1521–1529, doi:10.1002/polb.10215.

120. Zhou, J.; Zhang, L. Solubility of cellulose in NaOH Urea.pdf. *Polym. J.* **2000**, *32*, 866–870.

121. Yamashiki, T.; Matsui, T.; Saitoh, M.; Okajima, K.; Kamide, K.; Sawada, T. Characterisation of cellulose treated by the steam explosion method. Part 2. Effect of treatment conditions on changes in morphology, degree of polymerisation, solubility in aqueous sodium hydroxide and supermolecular structure of soft wood pulp during st. *Br. Polym. J.* **1990**, *22*, 121–128, doi:10.1002/pi.4980220205.

122. Cai, J.; Kimura, S.; Wada, M.; Kuga, S.; Zhang, L. Cellulose aerogels from aqueous alkali hydroxide-urea solution. *ChemSusChem* **2008**, *1*, 149–154, doi:10.1002/cssc.200700039.

123. Ebringerová, A.; Heinze, T. Xylan and xylan derivatives - Biopolymers with valuable properties, 1: Naturally occurring xylans structures, isolation procedures and properties. *Macromol. Rapid Commun.* **2000**, *21*, 542–556, doi:10.1002/1521-3927(20000601)21:9<542::AID-MARC542>3.0.CO;2-7.

124. Shafizadeh, F.; Bradbury, A.G.W. Thermal degradation of cellulose in air and nitrogen at low temperatures. *J. Appl. Polym. Sci.* **1979**, *23*, 1431–1442, doi:10.1002/app.1979.070230513.

125. Yang, Y.P.; Zhang, Y.; Lang, Y.X.; Yu, M.H. Structural ATR-IR analysis of cellulose fibers prepared from a NaOH complex aqueous solution. *IOP Conf. Ser. Mater. Sci. Eng.* **2017**, *213*, doi:10.1088/1757-899X/213/1/012039.

126. Sagehashi, M.; Miyasaka, N.; Shishido, H.; Sakoda, A. Superheated steam pyrolysis of biomass elemental components and Sugi (Japanese cedar) for fuels and chemicals. *Bioresour. Technol.* **2006**, *97*, 1272–1283, doi:10.1016/j.biortech.2005.06.002.

127. Liu, Z.; Sun, X.; Hao, M.; Huang, C.; Xue, Z.; Mu, T. Preparation and characterization of regenerated cellulose from ionic liquid using different methods. *Carbohydr. Polym.* **2015**, *117*, 54–62, doi:10.1016/j.carbpol.2014.09.053.

128. Manyà, J.J. Pyrolysis for Biochar Purposes: A Review to Establish Current Knowledge Gaps and Research Needs. *Environ. Sci. Technol.* **2012**, *46*, 7939–7954, doi:10.1021/es301029g.

129. Jiang, S.; Nguyen, T.A.H.; Rudolph, V.; Yang, H.; Zhang, D.; Ok, Y.S.; Huang, L. Characterization of hard- and softwood biochars pyrolyzed at high temperature. *Environ. Geochem. Health* **2017**, *39*, 403–415, doi:10.1007/s10653-016-9873-6.

130. Samsudin, M.H.; Hassan, M.A.; Idris, J.; Ramli, N.; Mohd Yusoff, M.Z.; Ibrahim, I.; Othman, M.R.; Mohd Ali, A.A.; Shirai, Y. A one-step self-sustained low temperature carbonization of coconut shell biomass produced a high specific surface area biochar-derived nano-adsorbent. *Waste Manag. Res. J. a Sustain. Circ. Econ.* **2019**, *37*, 551–555, doi:10.1177/0734242X18823953.

131. Kim, J.A.; Vijayaraghavan, K.; Reddy, D.H.K.; Yun, Y.S. A phosphorus-enriched biochar fertilizer from bio-fermentation waste: A potential alternative source for phosphorus fertilizers. *J. Clean. Prod.* **2018**, *196*, 163–171,

doi:10.1016/j.jclepro.2018.06.004.

132. Liu, Y.; Cheng, H.; He, Y. Application and Mechanism of Sludge-Based Activated Carbon for Phenol and Cyanide Removal from Bio-Treated Effluent of Coking Wastewater. *Processes* **2020**, *8*, 82, doi:10.3390/pr8010082.

133. Inyang, M.; Dickenson, E. The potential role of biochar in the removal of organic and microbial contaminants from potable and reuse water: A review. *Chemosphere* **2015**, *134*, 232–240, doi:10.1016/J.CHEMOSPHERE.2015.03.072.

134. Wang, H.Y.; Chen, P.; Zhu, Y.G.; Cen, K.; Sun, G.X. Simultaneous adsorption and immobilization of As and Cd by birnessite-loaded biochar in water and soil. *Environ. Sci. Pollut. Res.* **2019**, *26*, 8575–8584, doi:10.1007/s11356-019-04315-x.

135. Qambrani, N.A.; Rahman, M.M.; Won, S.; Shim, S.; Ra, C. Biochar properties and eco-friendly applications for climate change mitigation, waste management, and wastewater treatment: A review. *Renew. Sustain. Energy Rev.* **2017**, *79*, 255–273, doi:10.1016/j.rser.2017.05.057.

136. Malaysian Palm Oil Board FFB Yield & Crude Palm Oil Yield of Oil Palm Estates 2019 Available online: http://bepi.mpob.gov.my/index.php/en/yield/yield-2019/yield-2019.html (accessed on Aug 5, 2020).

137. Thoe, J. M. L., Surugau, N., & Chong, H.L.H. Application of Oil Palm Empty Fruit Bunch as Adsorbent : A Review. *Trans. Sci. Technol.* **2019**, *6*, 9–26.

138. Bessou, C.; Verwilghen, A.; Beaudoin-Ollivier, L.; Marichal, R.; Ollivier, J.; Baron, V.; Bonneau, X.; Carron, M.P.; Snoeck, D.; Naim, M.; et al. Agroecological practices in oil palm plantations: Examples from the field. *OCL - Oilseeds fats, Crop. Lipids* **2017**, *24*, doi:10.1051/ocl/2017024.

139. Yoshizaki, T.; Shirai, Y.; Hassan, M.A.; Baharuddin, A.S.; Raja Abdullah, N.M.; Sulaiman, A.; Busu, Z. Improved economic viability of integrated biogas energy and compost production for sustainable palm oil mill management. *J. Clean. Prod.* **2013**, *44*, 1–7, doi:10.1016/j.jclepro.2012.12.007.

140. Idris, J.; Shirai, Y.; Andou, Y.; Mohd Ali, A.A.; Othman, M.R.; Ibrahim, I.; Yamamoto, A.; Yasuda, N.; Hassan, M.A. Successful scaling-up of self-sustained pyrolysis of oil palm biomass under pool-type reactor. *Waste Manag. Res.* **2016**, *34*, 176–180, doi:10.1177/0734242X15616472.

141. Mohamad Nor, N.; Lau, L.C.; Lee, K.T.; Mohamed, A.R. Synthesis of activated carbon from lignocellulosic biomass and its applications in air pollution control—a review. *J. Environ. Chem. Eng.* **2013**, *1*, 658–666, doi:10.1016/j.jece.2013.09.017.

142. Zhang, X.; Gao, B.; Creamer, A.E.; Cao, C.; Li, Y. Adsorption of VOCs onto engineered carbon materials: A review. *J. Hazard. Mater.* **2017**, *338*, 102–123, doi:10.1016/j.jhazmat.2017.05.013.

143. Rashidi, N.A.; Yusup, S.; Ahmad, M.M.; Mohamed, N.M.; Hameed, B.H. Activated Carbon from the Renewable Agricultural Residues Using Single Step

Physical Activation: A Preliminary Analysis. *APCBEE Procedia* **2012**, *3*, 84–92, doi:10.1016/j.apcbee.2012.06.051.

144. Liou, T.-H. Development of mesoporous structure and high adsorption capacity of biomass-based activated carbon by phosphoric acid and zinc chloride activation. *Chem. Eng. J.* **2010**, *158*, 129–142, doi:10.1016/j.cej.2009.12.016.

145. Tan, I.A.W.; Abdullah, M.O.; Lim, L.L.P.; Yeo, T.H.C. Surface Modification and Characterization of Coconut Shell-Based Activated Carbon Subjected to Acidic and Alkaline Treatments. *J. Appl. Sci. Process Eng.* **2017**, *4*, 186–194, doi:10.33736/jaspe.435.2017.

146. Idris, J.; Shirai, Y.; Anduo, Y.; Ali, A.A.M.; Othman, M.R.; Ibrahim, I.; Husen, R.; Hassan, M.A. Improved yield and higher heating value of biochar from oil palm biomass at low retention time under self-sustained carbonization. *J. Clean. Prod.* **2015**, *104*, 475–479, doi:10.1016/j.jclepro.2015.05.023.

147. Claoston, N.; Samsuri, A.W.; Ahmad Husni, M.H.; Mohd Amran, M.S. Effects of pyrolysis temperature on the physicochemical properties of empty fruit bunch and rice husk biochars. *Waste Manag. Res.* **2014**, *32*, 331–339, doi:10.1177/0734242X14525822.

148. Gokce, Y.; Aktas, Z. Nitric acid modification of activated carbon produced from waste tea and adsorption of methylene blue and phenol. *Appl. Surf. Sci.* **2014**, *313*, 352–359, doi:10.1016/j.apsusc.2014.05.214.

149. Li, S.; Chen, G. Thermogravimetric, thermochemical, and infrared spectral characterization of feedstocks and biochar derived at different pyrolysis temperatures. *Waste Manag.* **2018**, *78*, 198–207, doi:10.1016/j.wasman.2018.05.048.

150. Xu, Y.; Chen, B. Investigation of thermodynamic parameters in the pyrolysis conversion of biomass and manure to biochars using thermogravimetric analysis. *Bioresour. Technol.* **2013**, *146*, 485–493, doi:10.1016/j.biortech.2013.07.086.

151. Polovina, M.; Babić, B.; Kaluderović, B.; Dekanski, A. Surface characterization of oxidized activated carbon cloth. *Carbon N. Y.* **1997**, *35*, 1047–1052, doi:10.1016/S0008-6223(97)00057-2.

152. Kasnejad, M.H.; Esfandiari, A.; Kaghazchi, T.; Asasian, N. Effect of pre-oxidation for introduction of nitrogen containing functional groups into the structure of activated carbons and its influence on Cu (II) adsorption. *J. Taiwan Inst. Chem. Eng.* **2012**, *43*, 736–740, doi:10.1016/j.jtice.2012.02.006.

153. Zhou, L.; Liu, Y.; Liu, S.; Yin, Y.; Zeng, G.; Tan, X.; Hu, X.; Hu, X.; Jiang, L.; Ding, Y.; et al. Investigation of the adsorption-reduction mechanisms of hexavalent chromium by ramie biochars of different pyrolytic temperatures. *Bioresour. Technol.* **2016**, *218*, 351–359, doi:10.1016/j.biortech.2016.06.102.

154. Fan, S.; Tang, J.; Wang, Y.; Li, H.; Zhang, H.; Tang, J.; Wang, Z.; Li, X. Biochar prepared from co-pyrolysis of municipal sewage sludge and tea waste for the adsorption of methylene blue from aqueous solutions: Kinetics, isotherm, thermodynamic and mechanism. *J. Mol. Liq.* **2016**, *220*, 432–441, doi:10.1016/j.molliq.2016.04.107.

155. Tan, X.; Liu, Y.; Zeng, G.; Wang, X.; Hu, X.; Gu, Y.; Yang, Z. Application of biochar for the removal of pollutants from aqueous solutions. *Chemosphere* **2015**, *125*, 70–85, doi:10.1016/J.CHEMOSPHERE.2014.12.058.

156. Li, B.; Li, K. Effect of nitric acid pre-oxidation concentration on pore structure and nitrogen/oxygen active decoration sites of ethylenediamine -modified biochar for mercury(II) adsorption and the possible mechanism. *Chemosphere* **2019**, *220*, 28–39, doi:10.1016/j.chemosphere.2018.12.099.

157. Su, P.; Zhang, J.; Tang, J.; Zhang, C. Preparation of nitric acid modified powder activated carbon to remove trace amount of Ni(II) in aqueous solution. *Water Sci. Technol.* **2019**, *80*, 86–97, doi:10.2166/wst.2019.248.

158. Yao, S.; Zhang, J.; Shen, D.; Xiao, R.; Gu, S.; Zhao, M.; Liang, J. Removal of Pb(II) from water by the activated carbon modified by nitric acid under microwave heating. *J. Colloid Interface Sci.* **2016**, *463*, 118–127, doi:10.1016/j.jcis.2015.10.047.

159. Li, Y.; Du, Q.; Liu, T.; Peng, X.; Wang, J.; Sun, J.; Wang, Y.; Wu, S.; Wang, Z.; Xia, Y.; et al. Comparative study of methylene blue dye adsorption onto activated carbon, graphene oxide, and carbon nanotubes. *Chem. Eng. Res. Des.* **2013**, *91*, 361–368, doi:10.1016/j.cherd.2012.07.007.

160. Li, K.; Jiang, Y.; Wang, X.; Bai, D.; Li, H.; Zheng, Z. Effect of nitric acid modification on the lead(II) adsorption of mesoporous biochars with different mesopore size distributions. *Clean Technol. Environ. Policy* **2016**, *18*, 797–805, doi:10.1007/s10098-015-1056-0.

161. Lang, J.W.; Yan, X. Bin; Liu, W.W.; Wang, R.T.; Xue, Q.J. Influence of nitric acid modification of ordered mesoporous carbon materials on their capacitive performances in different aqueous electrolytes. *J. Power Sources* **2012**, *204*, 220–229, doi:10.1016/j.jpowsour.2011.12.044.

162. Thiemann, M.; Scheibler, E.; Wiegand, K.W. Nitric Acid, Nitrous Acid, and Nitrogen Oxides. In *Ullmann's Encyclopedia of Industrial Chemistry*; Wiley-VCH Verlag GmbH & Co. KGaA: Weinheim, Germany, 2012; pp. 177–223.

163. Zhang, Y.; Xu, X.; Zhang, P.; Ling Zhao; Qiu, H.; Cao, X. Pyrolysis-temperature depended quinone and carbonyl groups as the electron accepting sites in barley grass derived biochar. *Chemosphere* **2019**, *232*, 273–280, doi:10.1016/j.chemosphere.2019.05.225.

164. Liljenberg, M.; Stenlid, J.H.; Brinck, T. Mechanism and regioselectivity of electrophilic aromatic nitration in solution: the validity of the transition state approach. *J. Mol. Model.* **2018**, *24*, doi:10.1007/s00894-017-3561-z.

PUBLICATIONS, PATENT AND CONFERENCES ATTENDED

Publication

1. **Izzudin Ibrahim**, Toshiki Tsubota, Mohd Ali Hassan, Yoshito Andou. Surface functionalization of biochar from oil palm empty fruit bunch through hydrothermal process. Published in **Processes. Impact Factor: 2.753**
2. **Izzudin Ibrahim**, Mohd Ali Hassan, Yoshito Andou. Simple hydrothermal lignin removal process for production of cellulose products from oil palm biomass (Drafted Manuscript)
3. **Izzudin Ibrahim** and Yoshito Andou. Combined hydrothermal and superheated steam treatment on biomass for the production of soluble biomass in sodium hydroxide solution (Drafted Manuscript)

Patent

1. Andou. Y, **Ibrahim, I**. Patent Application Number 2021-098297, Application date 2021/06/11 “Method for Producing Alkali-Soluble Cellulose Material from Plant Biomass“ (Patent applied)

Conference

1. **Izzudin Ibrahim** and Yoshito Andou (2019). Modification of Biochar from Oil Palm Fibers for Water Treatment Purposes. *56th Kyushu Branch Chemical Society Meeting*, Kitakyushu International Conference Center, Kokura, Kitakyushu, 13th July, 2019
2. **Izzudin Ibrahim** and Yoshito Andou (2019). Simple Modification of Oil Palm Biochar for Wastewater Treatment Purposes. *7th International Symposium on Applied Engineering and Sciences 2019 (SAES2019).* Universiti Putra Malaysia (UPM), Malaysia. 11th -12th November 2019
3. **Izzudin Ibrahim** and Yoshito Andou (2019). Simple Modification of Biochar from Oil Palm Fibers using Autoclave for Water Treatment Purposes. *18th Asian Chemical Congress (18th ACC) and the 20th General Assembly of the Federation of Asian Chemical Societies (FACS)*, Taipei International Convention Center, Taiwan. 8th -12th December 2019
4. **Izzudin Ibrahim** and Yoshito Andou (2020). Hydrothermal Cellulose Extraction from Oil Palm Frond. *8th International Symposium on Applied Engineering and Sciences (SAES 2020).* Virtual Conference. 12th – 19th December 2020.
5. **Izzudin Ibrahim** and Yoshito Andou (2021). Hydrothermal Cellulose Extraction from Oil Palm Frond. *The 4th International Conference on Materials Engineering and Nanotechnology 2021 (ICMEN 2021).* Virtual Conference. 3rd - 4th April 2021